

Study and prediction of the energy interactions between buildings and the urban climate

by

Bruno Bueno Unzeta

*Industrial Engineer
University of Malaga, 2007*

*Master of Science in Building Technology
Massachusetts Institute of Technology, 2010*

ARCHIVES

Submitted to the Department of Architecture
in Partial Fulfillment of the Requirements for the Degree of

Doctor of Philosophy in Architecture: Building Technology

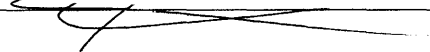
at the

Massachusetts Institute of Technology

September 2012

© 2012 Massachusetts Institute of Technology.
All rights reserved.

Signature of Author:



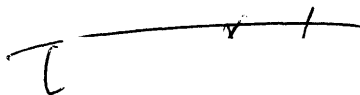
Department of Architecture
June 29, 2012

Certified by:



Leslie K. Norford
Professor of Building Technology
Thesis Supervisor

Accepted by:



Takehiko Nagakura
Associate Professor of Design and Computation
Chair, Departmental Committee on Graduate Students

Thesis Committee:

Leslie K. Norford
Professor of Building Technology
Massachusetts Institute of Technology
Thesis Supervisor

Leon R. Glicksman
Professor of Building Technology and Mechanical Engineering
Massachusetts Institute of Technology
Thesis Reader

Rex E. Britter
Professor Emeritus of Environmental Fluid Dynamics
University of Cambridge
Visiting Scientist
Massachusetts Institute of Technology
Thesis Reader

Study and prediction of the energy interactions between buildings and the urban climate

by

Bruno Bueno Unzeta

Submitted to the Department of Architecture
on June 29, 2012 in Partial Fulfillment of the Requirements
for the Degree of Doctor of Philosophy in Architecture: Building Technology

Abstract

Urbanization produces higher air temperatures in cities than in the undeveloped rural surroundings. This phenomenon is known as the Urban Heat Island (UHI) effect and has been measured in different cities around the world. Conventional building energy programs use standard meteorological databases obtained from measurements at operational weather stations, which are usually located in open areas outside of the city, typically at the airport. Therefore, air temperature measurements may not include the UHI effect.

The UHI effect can have an impact on the energy consumption of buildings, especially residential and naturally ventilated buildings. At the same time, the energy performance of buildings can affect outdoor air temperatures, mainly through the waste heat emissions from outdoor air-conditioning equipment. Consequently, there are situations in which the interactions between the indoor and outdoor environments are reciprocal and thus both domains have to be solved simultaneously.

This thesis presents a study of the energy interactions between buildings and the urban climate through the development and evaluation of a set of models. Based on first principles, these models include three different Urban Canopy and Building Energy Models (UC-BEMs), with different levels of detail and applications, and a novel urban climate prediction tool, the Urban Weather Generator (UWG). Developed at the intersection of building energy and urban climate studies, the research builds on fundamental knowledge in both domains.

The UC-BEMs account for building thermal effects on climatological predictions and have the potential to predict building energy consumption at urban scale. The UC-BEMs can be coupled with mesoscale atmospheric simulations, establishing a multi-scale model approach from the atmosphere down to buildings that can be used to analyze the impact of future climate change scenarios on the urban climate and the energy consumption of buildings.

The UWG calculates site-specific urban climate conditions from measurements at an operational weather station. The model can be used alone or integrated into existing programs in order to account for the UHI effect in building energy simulations. The UWG is evaluated with field data from Toulouse, France, and Basel, Switzerland.

Thesis supervisor: Leslie K. Norford
Title: Professor of Building Technology

Acknowledgements

Essential founding for this research was provided by the Singapore National Research Foundation through the Singapore-MIT Alliance for Research and Technology (SMART) Center for Environmental Sensing and Modeling (CENSAM). The MIT/Masdar Institute of Science and Technology Collaborative Research Program and the MIT Energy Initiative have also contributed to make this research possible.

Among the people who have advised me during my Ph.D. program, I would like to give a special thanks to my advisor, Prof. Les Norford. I will always be grateful for the trust he has placed on me from the beginning and for the great value he has always attached to my work. I hope we will keep collaborating in the future.

I would like to acknowledge the invaluable contribution of Prof. Rex Britter, whose expertise in the meteorological field solved many of the questions arisen in the exploration of urban climate studies.

I would also like to thank Prof. Leon Glicksman for his commitment, guidance, and insights as a member of my committee. This thesis has very much improved as a result of our discussions.

I would like to acknowledge the group of meteorologists of the GAME/CNRM (Météo-France, CNRS). As a part of my doctoral research, I worked for nine months in France with this extraordinary group of researchers, and I am very grateful for how they welcomed and supported me during that period. I want to give a very special thanks to my college and friend, Dr. Grégoire Pigeon, with whom I have worked very closely during the last three years and whose effort is also part of this thesis. Also, I would also like to acknowledge Dr. Julia Hidalgo, with whom I have intensely collaborated during the last year. Dr. Valery Masson and Colette Marchadier made possible my stay at the CNRM.

I would also like to acknowledge the following people: Dr. Afroditi Synnefa from NKUA (Greece) for providing the data for the Egaleo case study; Dr. Roland Vogt from the University of Basel (Switzerland) for sharing the field data from the experiment BUBBLE; and Dr. Alberto Martilli from the Ciemat (Spain) for his advice.

I am grateful for all the support I have received from the entire Building Technology community at MIT: students, faculty, and staff. I am honored to be part of a group that uniquely combines academic excellence and interpersonal skills. Some of my lab-mates have already become friends.

I would like to thank all the people close to me for their affection: my family in Spain, especially my mother, my father, my sister Cecilia, and my brother Gonzalo; and my friends here, in Spain, and around the world, particularly my friends Tito and Luis.

Especially, I would like to give my thanks to my wife Kasia whose patient love enabled me to complete this work.

Table of Contents

- 1 Introduction** **13**
- 1.1 Context 13
- 1.2 Needs 15
 - 1.2.1 Building energy engineering 15
 - 1.2.2 Urban climatology 15
- 1.3 Research goals 17
- 1.4 Methodology 17
- 1.5 Thesis structure and scope 18

- 2 The Coupled Scheme between EnergyPlus and the TEB scheme** **23**
- 2.1 Overview 23
- 2.2 Urban climate and building energy modeling 23
 - 2.2.1 The Town Energy Balance (TEB) model 23
 - 2.2.2 Building parametrizations 24
 - 2.2.3 EnergyPlus 24
- 2.3 Model description 25
 - 2.3.1 Definition of a reference building in EnergyPlus 25
 - 2.3.2 Exchanged information 26
 - 2.3.3 Iterative coupling method 28
- 2.4 Model evaluation 28
 - 2.4.1 Observations from the CAPITOUL experiment 28
 - 2.4.2 Characterization of the dense urban center of Toulouse 30
 - 2.4.3 Model verification 31
 - 2.4.4 Comparison with field data from Toulouse, France 33
- 2.5 Application 35
 - 2.5.1 Differences between an ideal and a realistic simulation of an HVAC system 35
 - 2.5.2 Effect of waste heat on outdoor air temperatures 37
 - 2.5.3 Effect of shading devices on energy consumption and HVAC waste heat emissions 37
 - 2.5.4 Effect of economizers on energy consumption and HVAC waste heat emissions . 37
 - 2.5.5 Effect of heat recovery on energy consumption and HVAC waste heat emissions . 38

- 3 The building energy model integrated in the TEB scheme** **41**
- 3.1 Overview 41
- 3.2 Model description 42
 - 3.2.1 Objective and main features 42

TABLE OF CONTENTS

3.2.2	Geometry and building definition	43
3.2.3	Heat balance method	43
3.2.4	Windows and solar heat transmission	44
3.2.5	Passive building systems	45
3.2.6	HVAC system	45
3.3	Model evaluation	49
3.3.1	Modeling assumptions	49
3.3.2	Model verification	52
3.3.3	Comparison with field data from Toulouse, France	55
3.3.4	Comparison with field data from Athens, Greece	56
4	The RC model for the analysis of the energy interactions between buildings and the urban climate	59
4.1	Overview	59
4.2	Model description	59
4.2.1	Physics	60
4.2.2	Assumptions	61
4.2.3	State-space formulation	62
4.2.4	Heat fluxes	63
4.2.5	Boundary conditions, inputs and outputs	63
4.3	Model evaluation	63
4.3.1	Building energy demand	64
4.3.2	HVAC waste heat emissions	66
4.3.3	Urban air temperatures	66
4.4	Impact of the UHI effect on the energy performance of buildings	68
4.5	Impact of the energy performance of buildings on the outdoor environment	70
4.5.1	Effect of the indoor environment without waste heat emissions	71
4.5.2	Effect of waste heat emissions	72
5	The Urban Boundary-Layer model	77
5.1	Overview	77
5.2	Model description	78
5.2.1	Urban Boundary-Layer Model	79
5.2.2	Vertical Diffusion Model	81
5.3	Model evaluation	81
5.3.1	Comparison with mesoscale atmospheric simulations	81
5.3.2	Comparison with field data from Basel, Switzerland, and Toulouse, France	86
6	The Urban Weather Generator	91
6.1	Overview	91
6.2	Model description	91
6.2.1	Rural Station Model	93
6.2.2	Urban Canopy and Building Energy Model	93
6.3	Model evaluation	96
6.3.1	Comparison with field data from Basel, Switzerland	96

6.3.2	Comparison with field data from Toulouse, France	99
6.3.3	Sensitivity analysis	101
6.3.4	Heat flux comparison	103
7	Summary of contributions and future work	107
7.1	Urban canopy and building energy models	107
7.2	Urban climate prediction tool	109
A	Nomenclature	113
B	Building Energy Model in TEB	117
B.1	Heat balance method	117
B.2	Solar heat transmission	118
B.3	Natural ventilation	118
B.4	Cooling system	119
B.5	Autosize function	120
C	Vertical Diffusion Model	121
D	Urban Weather Generator	123
D.1	Outdoor radiant heat transfer	123
D.2	Solar radiation received by walls and roofs	123
	References	125

Chapter 1

Introduction

1.1 Context

This research is motivated by the environmental and societal challenges we face in the context of an increasing global population, global warming, and energy scarcity. In particular, it aims to be a step toward the improvement of the sustainability of urban areas, where more than half of the global population currently lives [P.R.B., 2011].

Urban areas are affected by an increase in air temperature relative to the surrounding rural areas, a phenomenon known as the Urban Heat Island (UHI) effect. The UHI effect has been documented based on meteorological experiments carried out in different cities around the world [Roth, 2007; Hicks et al., 2010; Lee and Baik, 2010; Zhou and Shepherd, 2010; Houet and Pigeon, 2011]. Fig. 1.1 shows the average diurnal cycle of urban and rural air temperature measured in Basel (Switzerland) during the summer of 2002 [Rotach et al., 2005]. The UHI effect has a characteristic diurnal pattern [Oke, 1987], being more intense at late afternoon and night. In the morning, the urban-rural temperature difference can be negative, what is called the Urban Cool Island effect.

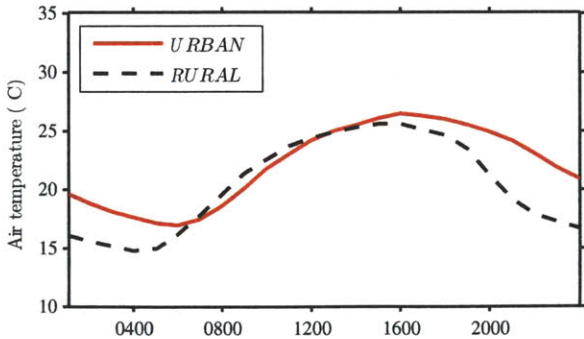


Figure 1.1 – Monthly-average diurnal cycle of urban and rural air temperatures measured in Basel, Switzerland, between June 10 and July 10, 2002, during the experiment BUBBLE [Rotach et al., 2005].

The observed UHI effect can be explained by the different morphology of the urban terrain relative to the rural terrain. The effective albedo tends to be higher due to the inter-reflections between urban surfaces. Additionally, the urban terrain delays the diurnal cycle of air temperature due to the fact that

there is more surface exposed to the environment, increasing the effective thermal inertia [Erell and Williamson, 2007]. Furthermore, urban surface roughness decreases the mean wind velocity and reduces the convective heat removal. Added to this is the heat gain due to anthropogenic sources [Sailor, 2011] and the lower evaporation due to the reduction of vegetated areas. To analyze the UHI effect, it is useful to differentiate between its mesoscale component, produced by the aggregated effect of the city on the urban boundary layer [Kuttler, 2008], and its canopy-scale component due to the urban canyon effect (Fig. 1.2).

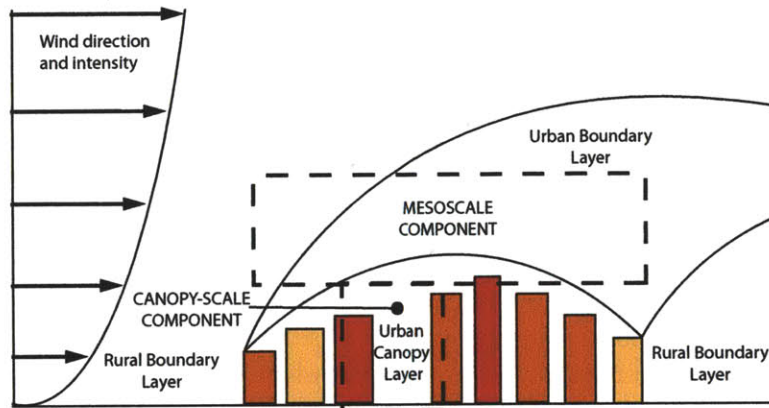


Figure 1.2 – Representation of a city and the components of the UHI effect: mesoscale and canopy-scale.

The UHI effect can have an impact on the energy consumption of buildings, especially residential and/or naturally ventilated buildings. It increases their cooling energy consumption in summer [Assimakopoulos et al., 2007; Santamouris et al., 2001] but can also reduce their heating energy consumption in winter [Memon et al., 2011]. In temperate climates, urban design strategies that combine building energy efficiency and urban climate considerations can optimize the energy demand of urban areas. In hot climates, the operation of residential air-conditioning (AC) systems is a significant percent of a city’s total energy consumption and peak power demand [Rhodes et al., 2011]. Furthermore, AC systems are responsible for waste heat emissions that contribute to the UHI effect, and their use is expected to increase in the following years as a consequence of global-scale climate warming [Adnot, 2003] and improving economies in developing countries.

This research has been developed at the intersection between building energy and urban climate studies. Building energy engineering focuses on the indoor environment but requires weather information as boundary conditions for its calculations. On the other hand, urban climatologists are interested in phenomena such as the UHI effect, which is partially caused by building energy operation. The combination of these two scientific communities can benefit from complementary expertise.

Urban planning also has a crucial role to play for improving urban sustainability. Urban planners have already started to incorporate energy efficiency strategies into the design process of urban areas [Mackey et al., 2012]. However, these initiatives are still tepid or purely experimental. This can be explained by the fact that there has not yet been established a clear and trustworthy relationship between urban design alternatives and their energy performance. This research is presented as a step toward developing a solid knowledge of the physical principles that make some design alternatives more sustainable than others. The ultimate goal is to be able to integrate building energy consumption and urban-scale climate warming considerations into the decision-making process of urban design and operation.

1.2 Needs

1.2.1 Building energy engineering

Building energy simulation programs use standard meteorological databases obtained from measurements at operational weather stations for annual energy calculations. Operational weather stations are usually located in open areas, without nearby obstructions, and outside the city, typically at the airport. Therefore, air temperature measurements might not include the UHI effect.

Crawley [2008] studies the impact of the UHI effect on a small office building by assuming typical diurnal cycles of urban-rural temperature difference. His study suggests that the UHI effect modifies the energy consumption of office buildings between 5% and 10% (increasing their cooling energy demand in summer and decreasing their heating energy demand in winter). A study carried out in this thesis predicts a similar impact of the UHI effect on commercial buildings (i.e. office buildings) and concludes that these buildings are less affected than residential buildings by this phenomenon because their energy performance is usually dominated by internal heat gains. The study shows that the energy demand of residential buildings can be modified by 20% for a typical 4 K daily-maximum UHI effect.

At the same time as the UHI effect modifies the indoor energy operation, the energy performance of buildings can have an impact on outdoor air temperatures, mainly through the waste heat emissions from outdoor AC equipment. Consequently, there are situations in which the interactions between the indoor and outdoor environments are reciprocal and thus both domains have to be solved simultaneously.

This thesis proposes an Urban Weather Generator (UWG) to calculate urban air temperatures using meteorological information measured at an operational weather station and accounting for the reciprocal interactions between building and the urban climate. Other studies that calculate urban weather information through meteorological modeling can be found in the literature. Erell and Williamson [2006] presented a rural-to-urban weather transformation (the CAT model) based on the urban canopy model LUMPS [Grimmond and Oke, 2002] and the CTTC model [Swaid and Hoffman, 1990], which requires the calibration of empirical parameters at the location of analysis. Oxizidis et al. [2008] proposed a computationally expensive method of generating urban weather files by coupling EnergyPlus [Crawley et al., 2001] with Computational Fluid Dynamics (CFD) and mesoscale atmospheric simulations. The UWG overcomes the limitations of previous models.

In urban planning, there is also a demand for building stock models to assist with the implementation of policy. Swan and Ugursal [2009] review the various modeling techniques used to estimate the energy consumption at neighborhood or city scale. The top-down approach utilizes historic aggregate energy data, deriving the energy consumption of building stocks as a function of top-level variables such as macroeconomic indicators, energy price, and general climate. Bottom-up models account for the energy consumption of individual end-users and extrapolate it to represent an urban area based on the representative weight of the modeled sample. A number of physically-based bottom-up models can be found in the literature [Kavgic et al., 2010]. However, none of these models specifically accounts for the interactions between buildings and the urban environment. The Urban Canopy and Building Energy Models (UC-BEMs) presented in this thesis overcome this limitation and have the potential to become fully-operative building stock models.

1.2.2 Urban climatology

Different research groups are interested in predicting future climate change scenarios and their implications in the urban climate and the energy consumption of buildings [CNRM-GAME, 2010]. This requires

a multi-scale model approach from the atmosphere down to buildings.

Urban Canopy Models (UCMs) have been developed to represent urbanized surfaces in atmospheric numerical simulations and are being used as urban-climate prediction tools. The Town Energy Balance (TEB) scheme [Masson, 2000] is a well-established example of a physically-based UCM [Masson and Grimmond, 2002; Lemonsu et al., 2004; Pigeon et al., 2008]. The TEB scheme is based on a two-dimensional approximation of an urban canyon (Fig. 1.3) formed by three generic surfaces: a wall, a road, and a roof. The urban canyon air is represented as a well-mixed thermal zone that exchanges heat with the generic wall, the generic road, and the atmosphere above the urban canopy layer. The generic roof exchanges heat directly with the atmosphere. Further developments of the TEB scheme divide the urban canyon in multiple horizontal layers [Hamdi and Masson, 2008].

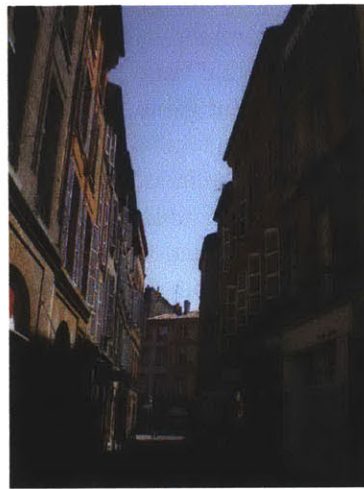


Figure 1.3 – Image of a typical urban canyon in Toulouse (France).

Previous versions of the TEB model implement a simple representation of building energy processes, which did not include important features such as internal heat gains or infiltration. In order to improve the representation of buildings in TEB, this thesis proposes two different approaches.

The first approach is to couple EnergyPlus with TEB. The Coupled Scheme (CS) presented in this thesis makes it possible to analyze the effect on urban climate of all building parameters included in a detailed building model. It also enables the identification of building configurations whose analysis and design are more sensitive to urban climate conditions. Furthermore, taking advantage of the previous evaluations of EnergyPlus, the CS can be used in the evaluation process of new models. However, the scheme requires a number of iterations between EnergyPlus and TEB, which makes it unsuitable for coupling with atmospheric models.

The second approach is to develop a new building energy model integrated in the urban canopy model. This is the method used by Kikegawa et al. [2003] and Salamanca et al. [2010]. They developed simplified building energy models that are able to capture the main heat transfer processes that occur inside buildings and to calculate building energy demand and waste heat emissions from AC systems [Kondo and Kikegawa, 2003; Salamanca and Martilli, 2010; Kikegawa et al., 2006; Ihara et al., 2008]. However, their models do not include active and passive building systems, which are sometimes necessary to get a good estimation of building energy consumption. Furthermore, active and passive system

models allow for an evaluation of the impact of energy efficiency strategies on climate. The new building energy model integrated in TEB overcomes the limitations of previous models.

UCMs can be coupled with a mesoscale atmospheric model (on-line approach) or forced with meteorological information above the urban canopy layer (off-line approach) [Masson and Seity, 2009]. The off-line approach takes advantage of the low computational cost of UCMs in order to effectively perform parametric analyses of urban design criteria. However, this approach generally assumes that forcing conditions (i.e. boundary conditions) are not affected by changes in the urban surface, which is a restrictive assumption if one is interested in contrasted scenarios of urban heat fluxes. Furthermore, forcing meteorological information above the urban canopy layer is only available through short-term experiments, a few permanent urban stations, and mesoscale simulation results. This limits the use of UCM by other communities, such as building engineers and urban planners, who may be interested in urban climate prediction but do not have access to this type of information. On the other hand, meteorological information can be easily found in weather data files obtained from measurements at operational weather stations located in open areas outside the city.

The atmospheric component of the UWG, developed in this thesis, calculates air temperatures above the urban canopy layer from measurements at an operational weather station. Previous studies also aimed to estimate the mesoscale UHI effect. Based on similarity theory, Hidalgo et al. [2009] developed a correlation for the daytime UHI effect at mesoscale level. Previously, Lu et al. [1997] had proposed an equivalent correlation for the nighttime case. The main limitation of these models is that they assume the urban boundary layer is at steady state and not dominated by a geostrophic wind (i.e. calm conditions).

1.3 Research goals

The general objective of this thesis is to integrate building energy and urban climate studies, building on fundamental knowledge in both domains. The specific goals are the following:

- Account for building thermal effects in climatological predictions, including the effect of active and passive building systems.
- Develop physically-based bottom-up models to predict building energy consumption at neighborhood or urban scale, specifically accounting for the energy interactions between buildings and the urban environment.
- Understand the dominant mechanisms of interactions between the energy performance of buildings and the urban climate.
- Identify building configurations whose energy performance is sensitive to the UHI effect.
- Develop a methodology to predict the UHI effect, both at mesoscale and canopy-scale levels, by using standard meteorological databases measured at operational weather stations.

1.4 Methodology

Mirzaei and Haghghat [2010] review the existing approaches to study the UHI effect. Microscale CFD models are capable of obtaining accurate information about the canopy-scale UHI distribution at a particular location [Santiago and Martilli, 2010]. However, due to their high computational cost, their scope

must be spatially and temporary limited; thus, these models cannot be applied to annual energy calculations and to analyses at a larger scale than a few blocks. Furthermore, the accuracy of CFD simulations strongly depends on the supplied boundary conditions, for which detailed information in most cases is not available, and on the treatment of the turbulence closure and radiation. In summary, although CFD simulations can be very useful for specific studies, especially involving air velocity distribution, a very high computational cost is paid for a gain in accuracy that is not guaranteed.

Mesoscale models are considered the state-of-the-art in atmospheric weather prediction, used as operational tools [Lafore et al., 1998]. These models represent the urban canopy as an aerodynamic roughness for which correlations act as a bridge between the surface and the first atmospheric layer. The latest generation of mesoscale models is coupled with UCMs, improving the representation of the thermal effect of urban areas on the atmosphere. However, their application to urban climate predictions, for which the temporal scale of interest ranges between few days to one year or even a century, is affected by the same limitations as microscale CFD models.

This research is based on the energy balance approach, which is the one used in building energy and urban canopy models. This thesis shows that this methodology is capable of providing estimates of the UHI effect within an acceptable accuracy range, both at mesoscale and at canopy-scale, and of building energy consumption at urban scale. The advantages are its simplicity and low computational cost. Simple models make the underlying physics easy to understand, test and improve. Fast models allow for parametric studies of greater spatial and temporal scales. The main limitation of the energy balance approach is that the air velocity field is not specifically solved and its effect is represented by correlations. This is particularly important for the heat exchange between the urban canyon air and the atmosphere above it, which is calculated from a formulation based on exchange velocities [Bentham and Britter, 2003].

The models developed in this thesis are evaluated by comparison with both more sophisticated models whose validations have been reported in the literature and field data from experiments. The models that have been used in the evaluation process are EnergyPlus [Crawley et al., 2001], the TEB model [Masson, 2000], and a combination of the two (the CS presented in chapter 2) [Bueno et al., 2011]. The thesis also uses mesoscale simulation results obtained by climatologists of the CNRM-GAME (France) with the model Meso-NH [Lafore et al., 1998]. Field data corresponds to the experiment BUBBLE, carried out in Basel, Switzerland, in 2002 [Rotach et al., 2005]; the experiment CAPITOU, carried out in Toulouse, France, between 2004 and 2005 [Masson et al., 2008]; and an experiment carried out in Athens, Greece, in 2009 [Synnefa et al., 2010].

1.5 Thesis structure and scope

The core of the thesis is divided into two parts and five chapters, which correspond to the five publications that have come out of this research: three published and two in the process of being published [Bueno et al. 2011; 2012; 2012a; 2012b; 2012c]. The first part is devoted to UC-BEMs, which are used to represent building thermal effects on climatological predictions and have the potential to predict building energy consumption at urban scale. The second part is devoted to a novel urban climate prediction tool, the UWG, which predicts urban air temperatures, both at mesoscale and canopy-scale, from measurements at operational weather stations.

Chapter 2 presents the CS between EnergyPlus and TEB. The CS combines models that are well-accepted and evaluated within their respective scientific communities, building engineering and urban

climatology. This makes the CS a very useful tool to evaluate other UC-BEMs (chapters 3 and 4). The CS allows an analysis of the effect on climate of sophisticated building and building system configurations (those included in EnergyPlus), as well as an evaluation of their sensitivity to urban climate conditions. In this chapter, the CS is evaluated by using field data from Toulouse, France. The comparison includes electricity and natural gas energy consumption of buildings, building façade temperatures, and urban canyon air temperatures. As application examples of the CS, the chapter analyzes the effect of different building and HVAC system configurations on building energy consumption, waste heat released from HVAC systems, and outdoor air temperatures for the case study of Toulouse. Three different energy efficiency strategies are considered: shading devices, economizers, and heat recovery.

Chapter 3 presents the building energy model (BEM) that has been integrated in the TEB scheme. The advantage of this model with respect to the CS presented in chapter 2 is that it can be coupled with mesoscale atmospheric simulations. The CS required a number of iterations between EnergyPlus and TEB, which makes it computationally unsuitable for atmospheric coupling. The development of BEM-TEB is framed in the Project Muscade [CNRM-GAME, 2010] in order to represent future scenarios of urban climate and building energy consumption in French cities. Compared to previous UC-BEMs [Kikegawa et al., 2003; Salamanca et al., 2010], BEM-TEB accounts for the dependence of the system capacity and efficiency on indoor and outdoor air temperatures and solves the dehumidification of the air passing through the system. Furthermore, it includes specific models for passive systems, such as window shading devices and natural ventilation. BEM-TEB has satisfactorily passed different evaluation processes, including testing its modeling assumptions, verifying that the chosen equations are solved correctly, and comparing the model with field data from Toulouse, France, and Athens, Greece.

Chapter 4 presents another UC-BEM based on a space-state solution of the thermal network that represents the fundamental physical relations between buildings and the urban environment. The RC model is a complement to the more detailed models previously presented (chapters 2 and 3). Its advantages are its simplicity and computational efficiency. The model allows for faster parametric analyses and makes it possible to easily evaluate modeling hypotheses. In this chapter, the RC model is evaluated against the CS for different building configurations and seasons. The model is then used in a series of parametric analyses to investigate the impact of the UHI effect on the energy consumption of buildings in configurations that are parameterized in terms of internal heat gains, construction, geometry, glazing ratio, and infiltration level. The RC model is also used to investigate the dominant mechanisms by which the indoor environment affects outdoor air temperatures. Parameters such as indoor air temperatures, exfiltration heat, and waste heat from HVAC systems are analyzed. The conclusions obtained by this study can be applied to a wide range of urban configurations.

Chapter 5 presents a methodology to calculate air temperatures above the urban canopy layer from meteorological data measured at an operational weather station. This provides the boundary conditions required by UCMs used off-line (without being coupled with a mesoscale model). The proposed scheme is composed of two modules: a Vertical Diffusion Model (VDM) to calculate vertical profiles of air temperature at the weather station and an Urban Boundary-Layer (UBL) model to calculate air temperatures above the urban canopy layer. The VDM-UBL scheme is proposed as an alternative to mesoscale atmospheric simulations and makes it possible to include the coupled effect between the urban canopy layer and the urban boundary layer in urban climate predictions. In this chapter, the VDM-UBL scheme is evaluated against mesoscale atmospheric simulations and field data from Basel, Switzerland, and Toulouse, France.

Chapter 6 is devoted to the UWG scheme. The UWG is composed of the VDM-UBL scheme presented in chapter 5, a Rural Station Model that calculates sensible heat fluxes at the weather station, and

a UC-BEM based on those presented in chapters 3 and 4. The computational cost of the UWG is intentionally kept at the same order of magnitude as annual building energy simulations, and it specifically accounts for the energy interactions between buildings and the urban climate. In this chapter, the UWG is also evaluated against field data from Basel, Switzerland, and Toulouse, France.

Finally, chapter 7 provides a summary of contributions, comments on the limitations of the models, and outlines the prospects for future work.

Urban canopy and building energy models

Chapter 2

The Coupled Scheme between EnergyPlus and the TEB scheme

2.1 Overview

This chapter presents a Coupled Scheme (CS) between a detailed building energy simulation model, EnergyPlus [Crawley et al., 2001], and an urban canopy model, the Town Energy Balance (TEB) [Masson, 2000]. The CS combines models that have already been extensively used and evaluated and are well-known and accepted within their respective scientific communities, building engineering and urban climatology. This makes the CS a very useful tool to evaluate new Urban Canopy and Building Energy Models (UC-BEMs), such as those presented in chapters 3 and 4. It also allows an analysis of the effect on climate of sophisticated building configurations (those included in EnergyPlus), as well as an evaluation of their sensitivity to urban climate conditions.

In this chapter, first, an overview of building energy modeling as related to urban climate studies is presented. Then, the CS is described. An evaluation of the model is carried out by using field data from the experiment CAPITOUL [Masson et al., 2008] conducted in Toulouse, France. As examples of possible applications of the CS, the scheme is used to study the impact of different building and HVAC system configurations on the energy consumption of buildings, HVAC waste heat emissions, and outdoor air temperatures. Three different energy efficiency strategies are evaluated: shading devices, economizers, and heat recovery.

2.2 Urban climate and building energy modeling

2.2.1 The Town Energy Balance (TEB) model

The TEB model [Masson, 2000] is a physically-based urban canopy model initially developed to represent urbanized surfaces in atmospheric numerical simulations. The TEB model has been evaluated with observations in various urban sites and weather conditions [Masson and Grimmond, 2002; Lemonsu et al., 2004; Offerle et al., 2005; Pigeon et al., 2008]. This model considers a two-dimensional approximation of an urban canyon formed by three generic surfaces: a wall, a road, and a roof. It calculates the climate conditions, the drag force, and heat fluxes of a town or neighborhood formed by identical urban canyons, where all orientations are possible and all exist with the same probability.

The TEB model is based on the energy balance approach. The urban canyon air is represented as a well-mixed thermal zone that exchanges heat with the generic wall, the generic road, and the atmosphere above the urban canopy layer. The generic roof exchanges heat directly with the atmosphere. Further developments of the TEB scheme divide the urban canyon in multiple horizontal layers [Hamdi and Masson, 2008].

Prior to the integration of the building energy model presented in chapter 3, the TEB model implemented a simple representation of building energy processes by solving a transient heat conduction equation through a multi-layered wall and roof. The force-restore method was applied to calculate indoor conditions from the contributions of the different building surfaces. Further developments of the TEB model included a minimum threshold to calculate the heating loads of the building associated with transmission through building surfaces [Pigeon et al., 2008]. Other phenomena, such as transmission through windows, internal heat gains and infiltration, and the calculation of cooling loads, were not yet included.

2.2.2 Building parametrizations

Building parametrizations are simplified building energy models that are integrated in urban canopy models. Their mission is to account for building effects such as the waste heat emissions from AC systems on the urban climate, and to be able to represent the impact of the urban climate on the building energy performance of urban areas. The first building parametrization is developed by Kikegawa et al. [2003]. In addition to solving the diffusion equation for walls, this model takes into account the internal sources of heat, solar radiation transmitted through windows, and the energy loads due to ventilation. Applying sensible and latent energy balances, the model calculates the energy demand required to maintain certain indoor conditions.

Salamanca et al. [2010] developed another building parametrization, but this time coupled with a multi-layer urban canopy model [Martilli et al., 2002]. This building parametrization allows the definition of multiple-story buildings and incorporates a more detailed treatment of windows, including the calculation of the transmitted solar radiation as a function of the angle of incidence. A range of comfort conditions and a maximum capacity of the HVAC system can also be specified in this model.

The building energy models of Kikegawa and Salamanca are able to capture the main heat transfer processes that occur inside buildings [Salamanca et al., 2010]. They are also able to predict the energy demand of a basic building configuration and to estimate the energy consumption and waste heat emissions of an HVAC system [Ihara et al., 2008; Salamanca and Martilli, 2010].

2.2.3 EnergyPlus

One industry-standard building simulation model, EnergyPlus [Crawley et al., 2001], calculates the energy demand of a building by applying a heat balance method [DOE, 2010a], somewhat similar to that used in the above-mentioned building parametrizations. It also implements detailed models for external heat transfer calculations such as convection, solar radiation (including shadows and reflections), and longwave radiation exchange with the sky. EnergyPlus has been extensively evaluated according to building simulation standards [DOE, 2010b,c].

One difference with respect to building parametrizations is that EnergyPlus can calculate the energy consumption of a specific HVAC system by solving the sensible and latent energy transformations of a working fluid (air or water) when this passes through the different HVAC components (coils, fans,

heating and cooling plant equipment, economizers, cooling towers, etc.). Examples of specific HVAC systems are variable-air-volume, fan-coils, or chilled ceilings with dedicated outdoor air systems.

This detailed definition is intended to capture the real performance of HVAC systems that supply energy to cover the energy demand of the building and to counteract thermal losses through the system. The capacity of the system depends on the conditions inside and outside the building, and there are situations where the system is not able to supply the required energy, affecting the resulting indoor conditions. Cooling-system efficiency (as measured by the coefficient of performance (COP), the dimensionless ratio of thermal output to fuel input) also depends on the conditions inside and outside the building and on the part load ratio of the cooling plant. The latter takes into account the loss of efficiency when the cooling plant is not working at its maximum capacity.

In an ideal building energy model, the indoor air humidity is assumed constant and the latent energy supplied or removed by the HVAC system is directly equal to the latent energy demand of the building. On the contrary, a detailed definition solves for the dehumidification of the air passing through a cooling system. In many HVAC system configurations, the indoor air humidity is not controlled in the same way as the air temperature, so the calculation of the air humidity requires a psychrometric model of the air crossing the system. This capability allows a better estimation of building energy consumption and associated waste heat emissions.

Another difference between detailed building simulation models and building parametrizations is the capability of modeling building demand reduction strategies or passive systems. Passive systems take advantage of the sun, the wind and environmental conditions to reduce or eliminate the need for HVAC systems. Accurate simulation of their effect is sometimes crucial in predicting the overall energy performance of buildings and consequently the heat released from buildings into the environment. Examples of passive systems are shading devices, double-skin façades, natural ventilation, heat storage devices, evaporative cooling, earth tubes for pre-heating or pre-cooling ventilation air, and cool or green roofs.

Finally, detailed building simulation models can make daylighting calculations and include them in the thermal energy balance of buildings. Lights can contribute significantly to building energy end-use, both directly and by adding heating loads, which affect the eventual waste heat released from HVAC systems.

2.3 Model description

The CS combines EnergyPlus and the TEB model to calculate the energy performance of buildings and the urban climate around the buildings, taking into account the reciprocal interactions between the two. The latest version of the CS uses EnergyPlus 5.0 and the TEB model integrated in SURFEX 6.1.

2.3.1 Definition of a reference building in EnergyPlus

In the TEB model, the morphology of urban areas is represented by three parameters: the average building height (h_{bld}); the horizontal building density (ρ_{bld}), defined as the building plan area divided by the plan area of the urban site; and the vertical-to-horizontal urban ratio (VH_{urb}), defined as the exterior vertical building area divided by the plan area of the urban site. The model approximates any urban layout by a homogeneous and regular urban morphology through this parameterization. Although the TEB model has been evaluated in different and not necessarily regular urban areas, the effect of heterogeneities in this approximation has not been formally tested yet.

The CS uses the same urban morphology parameterization as the TEB model, including the concept of an average-oriented urban canyon [Masson, 2000]. The reference building in EnergyPlus is specified from TEB urban morphology parameters by assuming a regular layout of square-plan buildings (Fig. 2.1). The geometric relationship can be expressed as:

$$\rho_{bld} = a^2 / (a/2 + b/2)^2, \quad (2.1)$$

$$VH_{urb} = 4ah_{bld} / (a/2 + b/2)^2, \quad (2.2)$$

where a is the side of the square-plan building and b is the side of the square formed by the projection of the surrounding buildings façades on the ground (Fig. 2.2). The geometric unit of the urban grid used to derive Eqs. 2.1 and 2.2 is indicated with a broken-dash line in both Figs. 2.1 and 2.2.

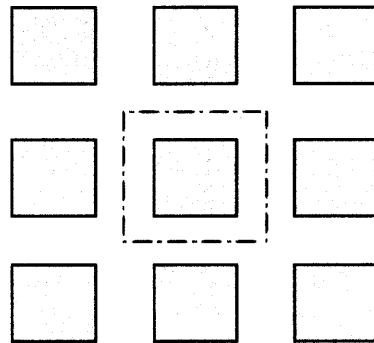


Figure 2.1 – Plan view of an urban area composed of a homogeneous grid of square-plan buildings. The geometric unit of the grid is indicated with a broken-dash line.

The reference building is composed of a single zone with an internal thermal mass representing intermediate floor constructions. Windows are defined such that their vertical dimension matches the vertical dimension of building façades, and their horizontal dimension is a fraction of the horizontal dimension of building façades according to the glazing ratio. Surrounding buildings are represented by shadowing surfaces. The solar radiation received by the four vertical surfaces of the reference building approaches the solar radiation received by walls in the average-oriented canyon calculated by the TEB model. A closer agreement to the average-oriented canyon approach can be achieved by rotating the building 45° with respect to the north-south axis (Fig. 2.2).

2.3.2 Exchanged information

Both EnergyPlus and the TEB model are able to calculate exterior wall and roof surface temperatures. In the CS, these surface temperatures are calculated by TEB and then used in EnergyPlus as boundary conditions. One of the reasons for this choice is that EnergyPlus simplifies the calculation of longwave radiation between a building surface and the surrounding urban surfaces, assuming that the latter are at the outdoor air temperature. Wall convective heat transfer correlations (CHTC) also differ between the

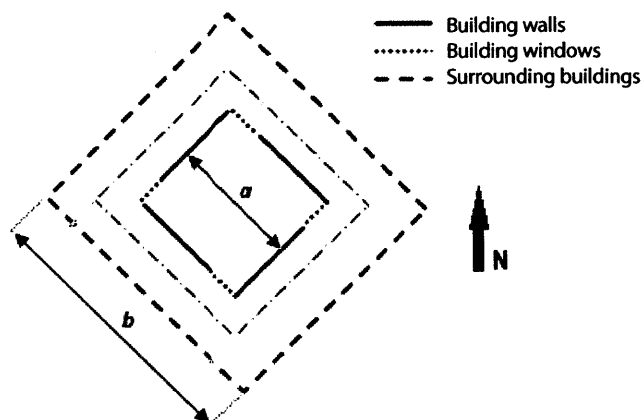


Figure 2.2 – Plan view of the reference building defined in EnergyPlus, indicating building walls, building windows and surrounding buildings. The building is rotated 45° with respect to the north-south axis. The geometric unit of the grid is indicated with a broken-dash line. The dimension parameters a and b are calculated from TEB’s morphology parameters.

two models. Palyvos [2008] presented a literature review of CHTC applied to building surfaces, and proposed a generic correlation more similar to the one used in TEB [Masson, 2000] than to that used in EnergyPlus [DOE, 2010a].

The original version of the TEB model is only able to calculate surface temperatures associated with the fraction of façades covered by walls, neglecting the effect of windows in the outdoor energy balance. Window surface temperatures can be significantly different from wall surface temperatures and are more affected by the indoor environment. The CS uses an adapted version of TEB that is able to use the window temperatures calculated by EnergyPlus in its outdoor energy balance according to the glazing ratio of building façades. Solar reflections, convective and radiative heat exchanges are modified in TEB accordingly.

EnergyPlus also calculates the waste heat released from HVAC systems. In vapor-compression refrigeration cycles (the most common cooling systems), waste heat emissions (Q_{waste}) can be calculated by adding the heat exchanged between the HVAC system and the building (Q_{exch}) and the energy consumption of the HVAC system (Q_{HVAC}), $Q_{waste} = Q_{HVAC} + Q_{exch}$. In fuel-combustion heating systems, waste heat emissions correspond to the combustion gases exhausted from chimneys and are calculated as $Q_{waste} = Q_{HVAC} - Q_{exch}$. The energy exchanged between the HVAC system and the building and the energy consumed by the system are calculated by EnergyPlus taking into account the interactions among system, building, and environment.

In reality, outdoor HVAC equipment can be located on the façade or the roof of buildings. If located on the roof, waste heat emissions can have no effect on urban canyon air temperatures or an indirect effect through air recirculation from the roof to the urban canyon. This version of the CS assumes that all waste heat is released from building façades, which represents a typical situation in which window or small split AC units are used. The calculated waste heat emissions are included in the outdoor energy balance of TEB as a wall-distributed energy source.

Future developments of the CS should also include the heat flux associated with the exfiltrated and exhausted air. Chapter 4 shows that the exfiltration heat flux can have a noticeable effect on urban air

temperatures in winter. This effect is not accounted for in this chapter.

2.3.3 Iterative coupling method

The CS uses an iterative method to calculate the interactions between EnergyPlus and the TEB model. The iterative coupling process starts from a preliminary TEB simulation using off-line meteorological forcing information [Masson and Grimmond, 2002]. The wall temperatures, roof temperatures, and urban canyon climate conditions calculated by TEB are supplied as boundary conditions to an EnergyPlus simulation. Then, window temperatures and HVAC waste heat emissions calculated by EnergyPlus are used in a new iteration of TEB. This process (Fig. 2.3) is repeated until a convergence criterion is satisfied. In the present study, convergence was assumed to be reached when the average canyon temperature difference between iterations fell below 0.05 °C. This was typically achieved after two or three iterations.

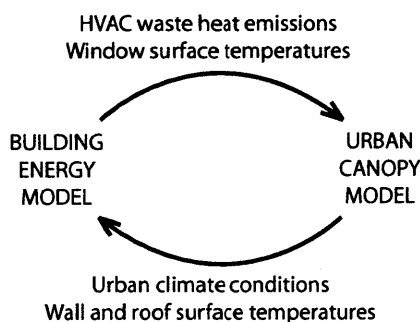


Figure 2.3 – Iterative method of the CS. The building energy model (EnergyPlus) calculates window temperatures and waste heat release from HVAC systems. The urban canopy model (TEB) calculates wall and roof surface temperatures, as well as climate conditions inside the urban canyon. Both models iterate until a convergence criterion is satisfied.

2.4 Model evaluation

The CS is intentionally composed of well-established models and therefore relies on their respective previous evaluations. Additionally, this section uses field data from the experiment CAPITOU, carried out in Toulouse, France, from February 2004 to March 2005 [Masson et al., 2008], to verify that the iterative procedure of the CS is correctly implemented and to carry out a first evaluation of the model.

2.4.1 Observations from the CAPITOU experiment

Weather information at the top of urban canyons is used as boundary conditions in urban canopy models, such as the TEB model. During the CAPITOU experiment, meteorological measurements were taken from an instrumented tower in the dense urban center of Toulouse at 27.5 m above the average building height and 47.5 m above the ground. In the same area, urban air temperatures were measured inside urban canyons. Instruments were placed in locations where air temperature could be representative of a larger scale than the street around them [Oke, 2004].

Surface temperatures of building façades were measured with infrared radiometers for different urban canyon orientations. The results are the area-weighted façade temperature resulting from the surface temperatures of the wall and the windows included in the view angle of the sensor. In addition, traffic heat release over a 500-m radius circle area around the instrumented tower was estimated by using automatic counters [Pigeon et al., 2008]. Anthropogenic heat from traffic is an input of the TEB model and the CS.

A city-scale inventory of electricity and natural gas energy consumption of buildings was also conducted during the experiment [Pigeon et al., 2007]. This is used to evaluate the capacity of the CS to predict heating energy consumption in winter. As it is explained below, electricity consumption data in summer suggests that AC systems are not widely used in Toulouse, so this case study is not suitable to compare cooling energy consumption. On the other hand, summer electricity consumption data is used to estimate building internal heat gains, which are an input of the model.

In climatology, anthropogenic heat flux refers to the energy input of an urban area that can be computed to human activity. It is therefore composed of traffic heat and building internal heat gains, which are inputs of the model, and energy consumption of HVAC systems, which is dynamically calculated by the model. This is different from the waste heat flux released by outdoor HVAC equipment, which includes internal heat gains and HVAC energy consumption, but also heat gains through the building enclosure. During the CAPITOUL experiment, anthropogenic heat flux data was obtained from the residual of the surface energy balance (SEB) equation [Pigeon et al., 2007] and is compared with the CS simulations.

2.4.2 Characterization of the dense urban center of Toulouse

Table 2.1 presents the set-up of the original TEB model and the CS according to the reported information from the experiment. The thermal properties of construction materials used in this study are specified in Table 2.2. A number of modeling assumptions were made given the lack of detailed information about the buildings of the site. In the comparison between TEB simulations and CAPITOU observations carried out by Pigeon et al. [2008], walls and roof were assumed to have no insulation. However, preliminary comparisons between simulation results and observations showed that both TEB and EnergyPlus consistently overpredict exterior wall temperatures in winter when no insulation is considered in the walls and roof. Furthermore, it is reasonable to think that many of the buildings in Toulouse are provided with some kind of insulation to reduce heating energy consumption in winter. This can be a simple air-cavity or an insulation material installed after a rehabilitation process. Based on a comparison between calculated and observed wall surface temperatures in winter (section 2.4.3), an interior insulation layer 0.3-m thick was assumed in this study.

Figure 2.4 represents the daily-average observations of electricity consumption of buildings and outdoor air temperatures during two months in summer. As can be seen, variations of air temperature do not have a noticeable impact on electricity consumption, which presents a typical-week profile. This fact suggests that AC systems are not extensively used in Toulouse during the summer and that the electricity consumption of buildings is dominated by the use of domestic electricity devices. This conclusion is used to obtain an average internal heat gain value of 5.8 W m^{-2} (building floor area) to be used in the model. This value typically corresponds to the residential sector, which represents the majority of the buildings of the urban area under study.

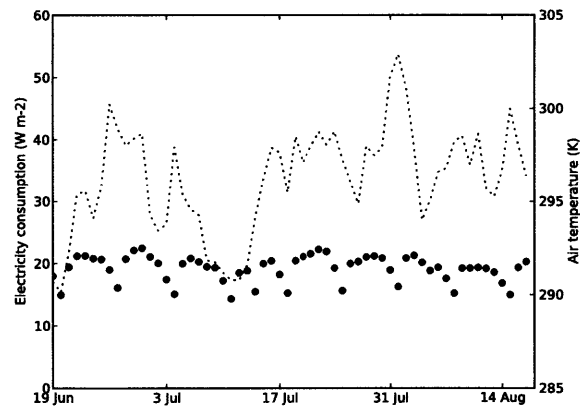


Figure 2.4 – Daily-average observations of electricity consumption per unit of urban area (thick points) and urban canyon air temperature (thin points) between 19 June 2004 and 17 August 2004. The urban area corresponds to the dense urban center of Toulouse.

Infiltration level in buildings is an important source of modeling uncertainty, above all in the residential sector. Our analysis uses a generic infiltration/ventilation air flowrate value of 0.5 ACH (room air volume changes per hour). Finally, it is also assumed that 60% of heating systems are fueled by natural gas and 40% are electric. This assumption is revisited in section 2.4.4.

Table 2.1 – Simulation parameters used for the evaluation of the CS with field data from the experiment CAPI-TOUL conducted in Toulouse (France). The terms urb and fl indicate unit of urban area and floor area, respectively.

Parameter	Settings
Urban parameters	
Location	Toulouse
Latitude	43.48°
Longitude	1.3°
Average building height	20 m
Horizontal building density	0.68
Vertical-to-horizontal urban area ratio	1.05
Roughness length	2 m
Anthropogenic heat from traffic	8.0 W m ⁻² urb [Pigeon et al., 2007]
Wall and roof construction	Brick - 30 cm Insulation - 3 cm
Wall and roof albedo	0.32
Road construction	Asphalt - 5 cm Stones - 20 cm Gravel and soil
Road albedo	0.08
Building parameters	
Building floor construction	Concrete - 20 cm
Glazing ratio	0.3
Window construction	Double-pane clear glass
Internal heat gains	Residential: 5.8 W m ⁻² fl Latent fraction: 0.2 Radiant fraction: 0.2 Electric fraction: 0.7 Schedule: weekdays, 1; weekend, 0.71.
Infiltration/ventilation air flowrate	0.5 ACH
Cooling system	None
Heating system	Gas furnace
Heating efficiency	0.9
Thermal set points	19 °C - No max.
Fraction of gas heating systems	60%
Fraction of electric heating systems	40%

Table 2.2 – Thermal properties of construction materials used in the simulations.

Material	Thermal conductivity W m ⁻¹ K ⁻¹	Volumetric heat capacity J m ⁻³ K ⁻¹
Brick and tiles	1.15	1.6e6
Concrete	0.93	1.5e6
Wood	0.93	1.2e6
Insulation	0.03	5.2e4
Asphalt	0.74	1.9e6
Stones	2.1	2.0e6
Gravel and soil	0.40	1.4e6

2.4.3 Model verification

This section presents a comparison between the façade temperatures and urban canyon air temperatures calculated by the CS and by the TEB model and those observed during the CAPITOUL experiment. The

objective is to explain the effect of windows in the outdoor energy balance and to show that the iterative procedure of the CS is well implemented. Due to the lack of AC systems in this case study, outdoor air temperatures are expected to be very similar between the CS and the TEB model. A more detailed analysis of urban air temperatures is presented in chapter 6.

Façade temperatures

Figure 2.5 presents a comparison between the measured façade surface temperatures, the wall temperatures calculated by the original TEB, and the window and façade temperatures calculated by the CS for winter and for summer.

Exterior window surface temperatures have a very different behavior with respect to exterior wall surface temperatures between winter and summer. Apart from thermal inertia and solar considerations, window surface temperatures are more affected by the indoor environment than exterior wall surface temperatures, because windows are less insulated. In winter, indoor air temperatures are significantly higher than outdoor air temperatures; thus, window surface temperatures are in general higher than exterior wall surface temperatures (Fig. 2.5 left). In summer, the difference between indoor and outdoor air temperatures is lower than in winter, and wall and window surface temperatures are similar. In Fig. 2.5 (right), window temperatures are slightly higher than wall temperatures during the night, which is related to the fact that the indoor air is not conditioned (no cooling system).

For this particular case study, the façade temperatures calculated by the CS are similar to those predicted by the TEB model, although the latter excludes windows. In both cases, the error compared to observations is small (about 1 K), which justifies the assumptions relative to wall construction made in this comparison.

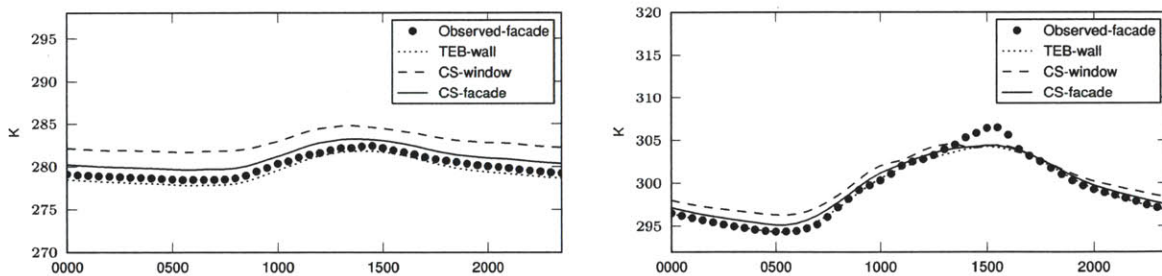


Figure 2.5 – Monthly-average diurnal cycle of façade temperature from observations, calculated by TEB, and calculated by the CS for winter, January 16, 2005 - February 15, 2005 (left); and for summer, July 16, 2004 - August 15, 2004 (right). The urban area corresponds to the dense urban center of Toulouse.

Outdoor air temperatures

Figure 2.6 compares the measured urban canyon air temperatures with the air temperatures calculated by TEB and by the CS for winter and for summer. Both models predict very similar outdoor air temperatures. In winter, waste heat emissions due to indoor air heating are small, and the difference in outdoor air temperatures are given by the higher window surface temperatures calculated by the CS. In summer,

windows and walls have similar surface temperatures, and there are no waste heat emissions associated with cooling systems. This comparison shows a reasonably good agreement between the simulation results and observations with errors smaller than 1 K.

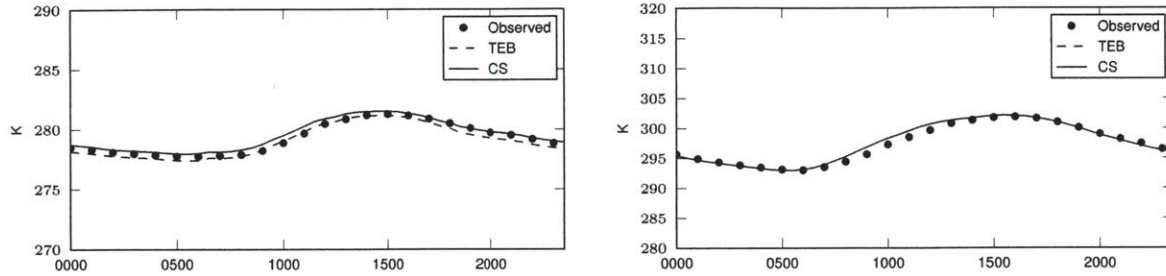


Figure 2.6 – Monthly-average diurnal cycle of urban canyon air temperature from observations, calculated by TEB, and calculated by the CS for winter, January 16, 2005 - February 15, 2005 (left); and for summer, July 16, 2004 - August 15, 2004 (right). The urban area corresponds to the dense urban center of Toulouse.

2.4.4 Comparison with field data from Toulouse, France

Heating energy consumption

In this section, the capacity of the CS to predict heating energy consumption is tested by using electricity and natural gas consumption data obtained during the experiment.

Figure 2.7 shows the daily-average electricity and natural gas consumption for two months in winter. Observations are compared with the simulation results of the TEB model and the CS. The original TEB, which does not account for heat losses due to windows and infiltration, underestimates the heating energy consumption of buildings. Electricity and natural gas consumption computed as root-mean-square error (RMSE) and mean-bias error (MBE) between the CS and observations are presented in Table 2.3. Given the modeling hypothesis indicated in section 2.4.2, the CS is able to capture the variations of electricity and gas consumption during the winter with RMSE and MBE lower than 7 W m^{-2} per unit of urban area, where the average electricity and gas consumption for the same period is 30.8 W m^{-2} and 19.0 W m^{-2} , respectively. The underestimation in gas consumption can be related to uses of gas other than for indoor air heating, such as cooking and domestic hot water. Independent of the estimate of the fraction of houses with gas heat, the prediction of the sum of electricity and gas consumption agrees relatively well with observations.

Table 2.3 – Root-mean-square error (RMSE) and mean-bias error (MBE) between the daily-average electricity and gas consumption per unit of urban area calculated by the CS and observed from December 19, 2004, to February 17, 2005. The reference value (REF) is the average energy consumption for the considered time period.

	RMSE	MBE	REF
Electricity consumption W m^{-2} urb	3.8	-0.7	30.8
Natural gas consumption W m^{-2} urb	6.6	-4.2	19.0

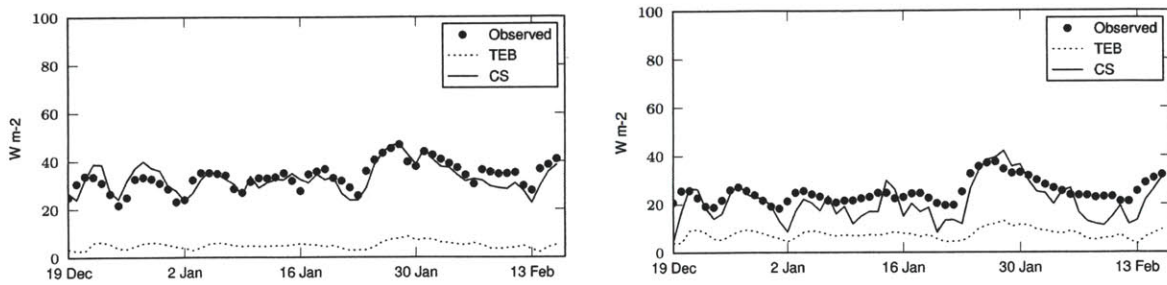


Figure 2.7 – Daily-average electricity (left) and natural gas (right) consumption per unit of urban area from observations, calculated by TEB, and calculated by the CS between December 19, 2004, and February 17, 2005. The urban area corresponds to the dense urban center of Toulouse.

Anthropogenic heat fluxes

An additional comparison is carried out by using the anthropogenic heat flux data obtained during the experiment. Daily-average values of anthropogenic heat fluxes are represented for two months in winter and two months in summer (Fig. 2.8). Observations are available for a certain number of days [Pigeon et al., 2007]. In winter, the original TEB accounts for anthropogenic heat fluxes due to traffic and building heating, without including other building energy uses. As a result, overall anthropogenic heat fluxes are underpredicted. In summer, assuming that a negligible number of cooling systems operate in the urban area, anthropogenic heat fluxes are dominated by the internal heat gains calculated in section 2.4.2. The relatively good agreement reinforces the validity of the assumptions made in this evaluation of the CS.

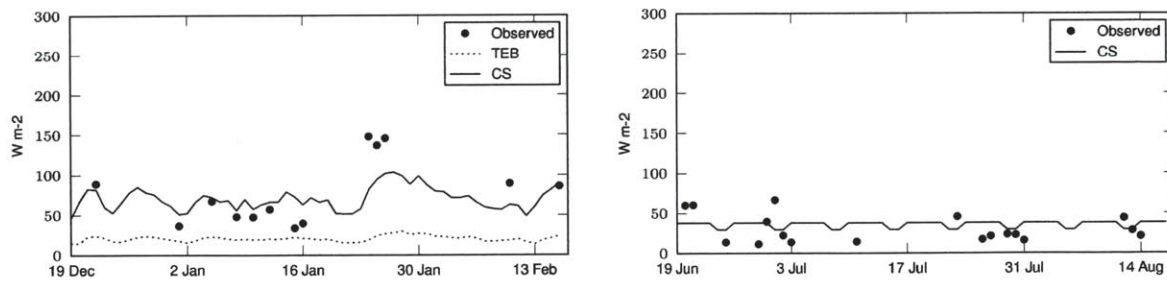


Figure 2.8 – Daily-average anthropogenic heat per unit of urban area from observations, calculated by TEB, and calculated by the CS between December 19, 2004, and February 17, 2005 (left); and from observations and calculated by the CS between June 19, 2004, and August 17, 2004 (right). In summer, the predicted anthropogenic heat fluxes are entirely based on the inputs of the model justified in section 2.4.2. The urban area corresponds to the dense urban center of Toulouse.

2.5 Application

In section 2.4.2, observations indicated that AC systems are not used in the urban center of Toulouse, so waste heat emissions do not contribute significantly to urban heating. This situation is expected to change in the following years as a consequence of global-scale and urban-scale climate warming [Adnot, 2003].

This section presents examples of the kind of analyses that can be carried out with the CS. In particular, the CS is used to analyze different scenarios of buildings and HVAC systems in Toulouse, including the presence of cooling systems and the waste heat emissions associated with them. Table 2.4 summarizes the new modeling parameters used in this analysis (other parameters are defined in Table 2.1).

Table 2.4 – CS simulation set-up used in the application examples. Other parameters are defined in Table 2.1.

Parameter	Settings
Infiltration air flowrate	0.1 ACH
Internal gains	Residential: $5.8 \text{ W m}^{-2} \text{ fl}$ Commercial: $29.0 \text{ W m}^{-2} \text{ fl}$
Solar protections	Residential: exterior window shades are deployed if beam plus diffuse solar radiation incident on the window exceeds 100 W m^{-2} . Commercial: white painted metal blinds are controlled to block beam solar radiation on windows.
HVAC system	All-air unitary system [DOE, 2010a]
Outdoor air flowrate	Residential: 0.4 ACH Commercial: 0.6 ACH
Thermal set points	$19 \text{ }^\circ\text{C} - 24 \text{ }^\circ\text{C}$
Schedule	Operative 24 hours
Cooling system	Single speed fan on the air side, with evaporating refrigerant in the coils.
Nominal COP	2.5
Economizer	Set the outdoor air flowrate at maximum (5 times the minimum) if the outdoor air temperature is lower than $24 \text{ }^\circ\text{C}$ and higher than $19 \text{ }^\circ\text{C}$.
Heating system	Gas furnace
Heating efficiency	0.9
Heat recovery	Type: sensible; efficiency: 0.7

2.5.1 Differences between an ideal and a realistic simulation of an HVAC system

The contribution of a detailed definition of HVAC systems with respect to an ideal representation was highlighted in section 2.2.3. Here, the detailed definition will be referred to as a real HVAC simulation, in contrast to an ideal HVAC simulation. Fig. 2.9 shows the difference in HVAC waste heat emissions between a real and an ideal HVAC simulation for summer, which ranges between 7% and 13%. Two different building uses are represented: residential and commercial (Table 2.4). Different levels of waste heat emissions are predicted for the residential and the commercial buildings, around 60 W m^{-2} and 190 W m^{-2} , respectively, averaged on the urban area. A similar study carried out by Salamanca and Martilli [2010] predicted waste heat emissions in Basel (Switzerland) at summertime that ranged between 90 W m^{-2} and 160 W m^{-2} .

The differences between the real and the ideal HVAC simulations are mainly related to the dehumidification of the air passing through the system, when this is cooled to meet the sensible energy demand of the building. The waste heat flux associated to the latent heat exchanged between the HVAC system and the building is accounted for in the real simulation but not in the ideal one.

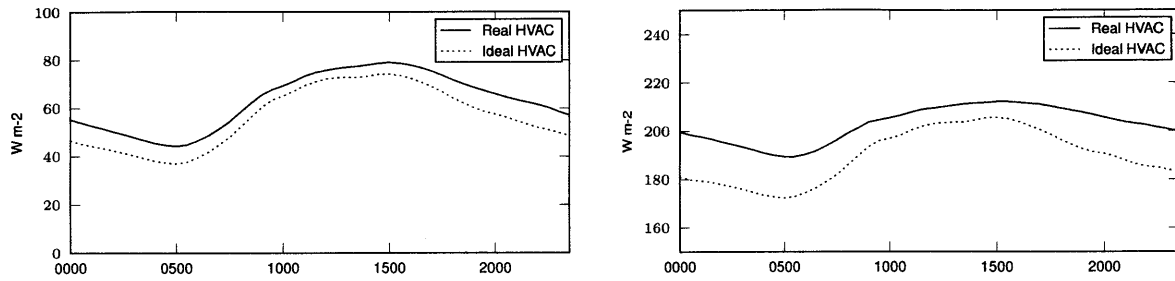


Figure 2.9 – Monthly-average diurnal cycle of HVAC waste heat emissions per unit of façade area from a real and an ideal HVAC simulation of a residential (left) and a commercial building (right) for summer, July 16, 2004 - August 15, 2004. In this case study, units of façade area and urban area are equivalent because $VH_{urb} \sim 1$. The urban area corresponds to the dense urban center of Toulouse.

The fact that the evolution of waste heat during the day is less dynamic in the real case than in the ideal case can be explained by the limited capacity of the real HVAC system. During the peak hours of the warmest days, the system may not be able to provide the required energy and its energy consumption decreases with respect to the ideal simulation.

A statistical analysis of this comparison for the whole cooling period (cooling energy consumption is positive) indicates that the average waste heat difference between the real and the ideal HVAC simulation ranges between 2.4 and 9.1 W m^{-2} of urban area, with maximum differences of 23.4 W m^{-2} and 46.9 W m^{-2} for the residential and the commercial cases, respectively. This analysis corresponds to the simplest representation of a realistic HVAC system. Other common HVAC system configurations have associated energy losses (e.g. reheat systems) that would lead to greater differences between the real and the ideal simulation.

2.5.2 Effect of waste heat on outdoor air temperatures

Figure 2.10 compares the calculated outdoor air temperatures for summer with and without waste heat from HVAC systems. For the residential case, which is associated with low energy consumption and waste heat emissions, the average increase in outdoor air temperature is 0.8 K. In the commercial case, the average increase in the outdoor air temperature is 2.8 K. Similar values of air temperature increase due to HVAC systems have been reported previously [Kikegawa et al., 2003; Ohashi et al., 2007; Hamilton et al., 2009]. A comprehensive parametric analysis of the impact of waste heat emissions on outdoor air temperatures is presented in chapter 4.

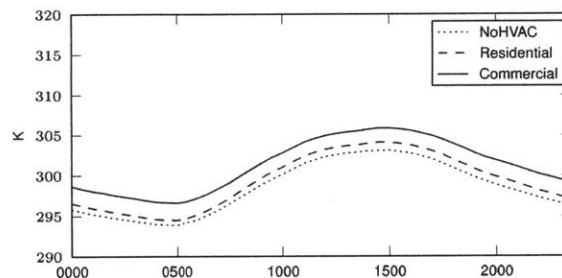


Figure 2.10 – Monthly-average diurnal cycle of urban canyon air temperature from a CS simulation of a residential and a commercial building in summer, assuming waste heat emissions from HVAC systems are released into the urban environment. The urban area corresponds to the dense urban center of Toulouse.

2.5.3 Effect of shading devices on energy consumption and HVAC waste heat emissions

Shading devices are passive systems that reduce the transmitted solar radiation into the building. Ideally, these devices should block direct solar radiation in the cooling period (summer), but allow the transmission of diffuse solar radiation for daylight purposes. They should also allow solar heat transmission in the heating period (winter) provided that there are no glare issues. In this analysis, two different shading devices typically used for residential and for commercial buildings in Toulouse are considered (Table 2.4).

Table 2.5 presents the annual cooling energy savings and average waste heat reduction associated with the use of shading devices in summer for residential and commercial buildings. Residential buildings, whose cooling loads are more sensitive to the transmitted solar radiation due to the low internal heat gains, can achieve reductions in energy savings and waste heat emissions of 21% and 29%, respectively, by using shading devices. Having a similar absolute value of waste heat reduction (similar impact on the outdoor environment), commercial buildings present lower relative values of energy consumption and waste heat reduction than residential buildings (around 5%).

2.5.4 Effect of economizers on energy consumption and HVAC waste heat emissions

An economizer allows more than the minimum outdoor airflow to enter the building when the outdoor temperature is favorable (cooler than indoors in summer). This reduces the consumption of the cooling

Table 2.5 – Annual energy savings and average waste heat reduction associated with the use of shading devices, economizers, and heat recovery systems. Energy savings and waste heat reductions are referred to the cooling system for shading devices and economizers and to the heating system for the heat recovery.

		Annual energy savings per unit of building plan area		Average waste heat reduction per unit of façade area (~ urban area)	
		Absolute (kW h m ⁻²)	Relative (%)	Absolute (W m ⁻²)	Relative (%)
Shading devices (Cooling)	Residential	24.0	20.50	8.5	28.83
	Commercial	26.5	5.60	10.2	5.06
Economizers (Cooling)	Residential	8.7	7.44	3.3	14.80
	Commercial	27.1	3.60	4.3	3.21
Heat recovery (Heating)	Residential	153.8	49.57	3.1	60.02

plant and its waste heat emissions but penalizes the electricity consumption of fans. The application of economizers can be useful in commercial buildings when outdoor air temperatures are below the cooling set point and buildings still have cooling energy demand due to internal heat gains. In residential buildings, the same effect is usually achieved by means of natural ventilation (opening the windows), which does not require the electricity consumption of a fan. The effectiveness of these strategies is very sensitive to increases in outdoor air temperatures, which reduce the amount of time they can operate. For the purposes of this analysis, an economizer is also applied to the residential case instead of a natural ventilation system. The main difference is the outdoor airflow passing through the building, which is constant for an economizer and variable for a natural ventilation system. The results of this analysis provide an upper limit for natural ventilation potential.

Table 2.4 presents the modeling parameters of the economizer considered in this study. Energy savings and waste heat reduction are achieved when outdoor air temperatures are within the minimum and the maximum temperature thresholds of the economizer. This occurs during the warmest days in late spring and fall and during the coolest days in early summer and fall. For the warmest days in summer (from mid-July), the economizer cannot operate and there are no associated reductions in waste heat.

Table 2.5 presents the annual cooling energy savings and average waste heat reduction associated with the use of economizers for residential and commercial buildings in Toulouse. Residential buildings can achieve reductions in energy consumption and waste heat emissions of 7% and 15%, respectively. Commercial buildings can save around 3% in both energy consumption and waste heat emissions by using economizers. In both cases, the effect of waste heat reduction on the outdoor environment is negligible.

2.5.5 Effect of heat recovery on energy consumption and HVAC waste heat emissions

A heat exchanger located between the exhaust air coming from the building and the ventilation air coming from outdoors reduces ventilation heat losses, which are an important fraction of the heating energy demand of buildings in winter. Although not included in this analysis, heat recovery systems also reduce the exfiltration heat flux, which can have an effect on outdoor air temperatures in winter (see chapter 4). In summer, the temperature difference between indoor and outdoor conditions is lower than in winter and heat recovery systems are less effective. Due to the close interaction with the outdoor environment, heat recovery systems are also sensitive to the UHI effect.

Table 2.4 presents the parameters of the heat recovery system considered in this analysis. Table 2.5

presents the annual heating energy savings and average HVAC waste heat reduction associated with the use of heat recovery systems for residential buildings in Toulouse. Reductions in energy consumption and waste heat emissions of 50% and 60%, respectively, can be achieved by this strategy. However, due to the low waste heat emissions associated with fuel-combustion heating systems, the effect of heat recovery systems on the outdoor environment is negligible. This analysis does not include commercial buildings because their heating energy consumption is very small in this case.

Chapter 3

The building energy model integrated in the TEB scheme

3.1 Overview

This chapter presents a Building Energy Model (BEM) integrated in the Town Energy Balance (TEB) scheme [Masson, 2000]. BEM-TEB is therefore an improvement of TEB, which allows a better representation of the effect of buildings on the urban climate. The advantage of this model with respect to the Coupled Scheme (CS) presented in chapter 2 is that it can be coupled with mesoscale atmospheric simulations. The CS required a number of iterations between EnergyPlus and TEB, which makes it computationally unsuitable for atmospheric coupling.

The development of BEM-TEB is framed in the Project Muscade [CNRM-GAME, 2010] in order to represent future scenarios of urban climate and building energy consumption in French cities. BEM-TEB proposes a physically-based (bottom-up) approach to estimate building energy consumption at city scale (~ 10 km) with a resolution of a neighborhood (~ 100 m). Modeling building energy consumption at urban scale has the advantage of building aggregation but requires taking into account the energy interactions between buildings and the urban environment. Building aggregation allows the simplification of the building thermal definition. The underlying assumption is that the average building of a certain urban area is more homogeneous and generic than each particular building. Compared to previous urban canopy and building energy models [Kikegawa et al., 2003; Salamanca et al., 2010], BEM-TEB includes specific models for active and passive building systems. As described in section 2.2.3, the possibility to model specific active and passive building systems allows a better estimation of building energy consumption and associated waste heat emissions.

The chapter is divided in two main sections. In the first one, the underlying physics of the model are presented in detail. In the second section, the model is evaluated at three levels: modeling assumptions; model verification, based on a comparison with the CS; and model validation, based on a comparison with field data from the experiment CAPITOUL [Masson et al., 2008] (Toulouse, France) and an experiment carried out in Athens, Greece [Synnefa et al., 2010].

3.2 Model description

3.2.1 Objective and main features

BEM-TEM constitutes a new version of the urban canopy model TEB, in which the energy effects of buildings on the urban climate are better represented. The new version of the model makes it possible to calculate building energy consumption at city or neighborhood scale. Previous versions of the TEB model (without being coupled with EnergyPlus) could not calculate cooling energy consumption and waste heat emissions associated with HVAC systems.

BEM calculates the energy demand of a building by applying a heat balance method. It considers a single thermal zone and represents the thermal inertia of intermediate building levels by a generic thermal mass. The model accounts for solar radiation through windows, heat conduction through the enclosure, internal heat gains, infiltration, and ventilation (Fig. 3.1).

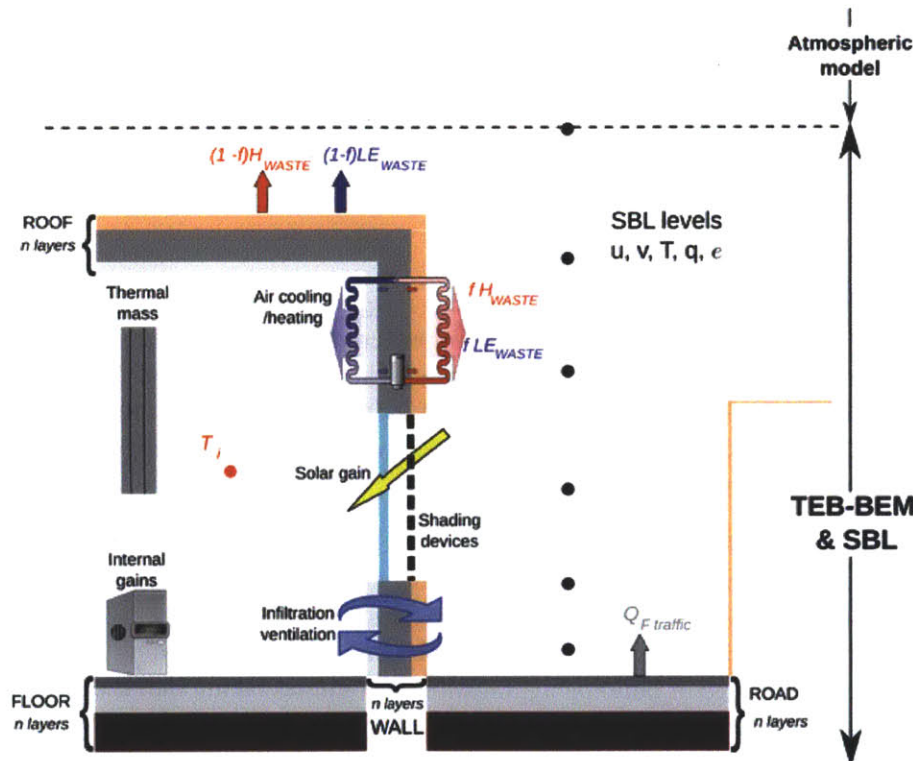


Figure 3.1 – Diagram of a building and an urban canyon. The main physical processes included in BEM-TEB are represented: heat storage and conduction of construction materials, waste heat from HVAC systems, solar radiation through windows, internal heat gains, infiltration, and ventilation. The diagram also represents the multi-layer version of the TEB scheme [Hamdi and Masson, 2008] and the possibility of coupling it with a mesoscale atmospheric model. *Diagram elaborated by G. Pigeon.*

BEM includes specific models for active and passive building systems. It considers the dependence of the cooling system efficiency on indoor and outdoor temperatures and solves the dehumidification of the air passing through the system. The model implements simple representations of window shades and natural ventilation.

The model has been kept as simple as possible, while maintaining the required features of a compre-

hensive building energy model. Multizone building calculations have been intentionally avoided, as part of an overall goal to sacrifice computational efficiency only for a significant gain in accuracy.

3.2.2 Geometry and building definition

BEM uses the same geometric principles as the TEB model and the CS, described in section 2.3.1. These geometric principles imply that the building enclosure is defined as an average-oriented façade and a flat roof, and that the glazing-to-façade ratio is assumed uniform for all the urban area under study. In addition, the following is assumed to define buildings in BEM:

- Single thermal zone: BEM assumes that all buildings in a particular urban area have the same indoor air temperature and humidity. This approach is justified if the objective is to calculate the overall energy consumption of a building (or neighborhood), rather than the energy performance of a specific building zone.
- Internal thermal mass: In the single-zone approach, an internal thermal mass represents the thermal inertia of the construction materials inside a building (e.g. separation between building levels). The transmitted solar radiation and the radiant fraction of internal heat gains are perfectly absorbed by the internal thermal mass and then released into the indoor environment.

3.2.3 Heat balance method

BEM uses a heat balance method to calculate indoor thermal conditions and building energy demand. An energy balance is applied to each indoor surface (is: wall, window, floor, roof, and internal mass), accounting for conduction, convection, and radiation heat components, viz.

$$Q_{cd} + Q_{cv} + \sum_{is} Q_{rd} = 0. \quad (3.1)$$

The convection and radiation terms are calculated from a standard heat transfer coefficient formulation, $Q = h\Delta T$ (see appendix B). Convective heat transfer coefficients depend on the relative position between the surface and the indoor air. Radiative heat transfer coefficients are obtained from linearization of the Stefan-Boltzmann equation, assuming only one bounce of radiative heat fluxes between surfaces. The transient heat conduction through massive building elements (walls, floor, roof, and internal mass) is calculated using TEB routines, which are based on the finite difference method.

To calculate the dynamic evolution of indoor air temperature between a cooling and a heating thermal set point, BEM solves a sensible heat balance at the indoor air. The sensible heat balance is composed of the convective heat fluxes from indoor surfaces, the convective fraction of internal heat gains, the infiltration sensible heat flux, and the sensible heat flux supplied by the HVAC system.

$$\begin{aligned} V_{bld} \rho c_v \frac{dT_{in}}{dt} = & \sum_{is} A_{is} h_{cv,is} (T_{is} - T_{in}) \\ & + Q_{ig} (1 - f_{rd}) (1 - f_{lat}) \\ & + \dot{V}_{inf} \rho c_p (T_{urb} - T_{in}) \\ & + \dot{m}_{sys} c_p (T_{sys} - T_{in}), \end{aligned} \quad (3.2)$$

where T_{in} is the indoor air temperature; V_{bld} , ρ , c_v , and c_p are the volume, density, and specific heat at constant volume and pressure of the indoor air, respectively; A_{is} is the area of the indoor surface; Q_{ig}

represents the internal heat gains; f_{lat} is the latent fraction of internal heat gains; f_{rd} is the radiant fraction of sensible internal heat gains; \dot{V}_{inf} is the infiltration air flowrate; T_{urb} is the outdoor air temperature; and \dot{m}_{sys} and T_{sys} are the mass flowrate and temperature of the air supplied by the HVAC system.

A latent heat balance is also solved to calculate the dynamic evolution of indoor air humidity. The latent heat balance is composed of the latent fraction of internal heat gains, the infiltration latent heat flux, and the latent heat flux supplied by the HVAC system.

$$V_{bld}\rho l_v \frac{dq_{in}}{dt} = Q_{ig}f_{lat} + \dot{V}_{inf}\rho l_v (q_{urb} - q_{in}) + \dot{m}_{sys}l_v (q_{sys} - q_{in}), \quad (3.3)$$

where l_v is the water condensation heat, and q_{in} , q_{urb} , and q_{sys} are the specific humidity of the indoor air, of the outdoor air, and of the air supplied by the HVAC system, respectively.

The building energy demand is calculated by applying the same sensible and latent heat balances at the indoor air, but assuming that this is at set point conditions. The specific humidity set point used for latent energy demand calculations is obtained from the relative humidity set point and the cooling or the heating temperature set point, which are provided by the user.

$$Q_{dem,sens} = \sum_{is} Q_{cv,is} + Q_{ig,sens} + Q_{inf/vent,sens}, \quad (3.4)$$

$$Q_{dem,lat} = Q_{ig,lat} + Q_{inf/vent,lat}. \quad (3.5)$$

3.2.4 Windows and solar heat transmission

Window effects have been introduced in the outdoor energy balance of the TEB model. The external surfaces of windows participate in the outdoor energy balance in the same manner as other urban surfaces (walls, road, garden, etc.). Window surfaces are semi-transparent and therefore have three optical properties (albedo, absorptivity, and transmittance). Two coupled surface energy balances are solved to calculate the internal and external surface temperatures of windows. Each surface energy balance accounts for the convective and radiative heat fluxes reaching the surface and the steady-state heat conduction through the window.

Building energy models usually consider the dependence of the solar heat transmitted through windows on the angle of incidence of the sun. However, simulations with EnergyPlus for different window orientations show that for an average-oriented canyon, the solar transmittance of windows (τ_{win}) can be approximated by a uniform value of 0.75 times the solar heat gain coefficient (SHGC) (see appendix B). The SHGC can be found in window catalogues and represents the fraction of incoming solar radiation that participates in the indoor energy balance. The solar heat transmitted through windows ($Q_{sol,win}$) is then calculated as:

$$Q_{sol,win} = Q_{sol,w} \tau_{win} GR, \quad (3.6)$$

where $Q_{sol,w}$ is the solar radiation reaching the building façade and GR is the glazing ratio.

The solar absorptivity of windows is calculated as a function of the U-factor and the SHGC, by using the equations proposed in EnergyPlus documentation [DOE, 2010a]. The U-factor can also be found in window catalogues and measures the window conductance, including the convective and longwave heat transfer coefficients at both sides of the window.

The window albedo is calculated so that the three optical properties (albedo, absorptivity, and transmittance) sum to unity. Then, the model uses an area-averaged façade albedo to calculate solar reflections by weighting the albedo of walls and windows with the glazing ratio of buildings.

3.2.5 Passive building systems

Section 2.2.3 highlighted the importance of considering passive building systems in energy simulation both at building scale and at urban scale. Passive systems may affect drastically the building energy performance, reducing or eliminating the need of HVAC systems; and they are among the strategies to improve the sustainability of urban areas.

Natural ventilation

In residential buildings in summer (especially when an active cooling system is not available), occupants usually open their windows to naturally ventilate indoor spaces. To represent this situation, BEM includes a natural ventilation module, which modifies the indoor air energy balance (Eqs. 3.2 and 3.3) by including an outdoor air flowrate term, similarly to the infiltration term. If the conditions are favorable for natural ventilation, the HVAC system is assumed to be turned off at least during one hour. The natural ventilation air flowrate is calculated from a correlation that depends on the outdoor air velocity, the indoor and outdoor air temperatures, and the geometry of buildings and windows (see appendix B).

Window shades

BEM also includes a simplified model to account for window shadowing devices. If the solar radiation reaching the window is above a predefined threshold, the model considers that shades are placed outside and in front of the windows. These shades are characterized by a predefined transmittance. The model reduces the solar radiation reaching the windows by changing its optical properties. The solar radiation that is not reflected, absorbed, or transmitted by the windows is assumed to be converted into a sensible heat flux toward the urban canyon.

3.2.6 HVAC system

Ideal and realistic definitions of an HVAC system

BEM includes both an ideal and a realistic definition of an HVAC system (see section 2.5.1). In the ideal definition, the system capacity is infinite, and the system supplies the exact amount of energy required to maintain indoor thermal and humidity set points. On the contrary, the realistic definition considers a finite capacity that can be provided by the user or calculated by the *autosize* function.

In the case of a cooling system, the realistic definition also takes into account the dependence of the system capacity and efficiency on outdoor and indoor conditions. Furthermore, the system efficiency is affected by part-load performance, when the system does not work at its nominal capacity. The realistic definition of the cooling system solves for the dehumidification of the air passing through the cooling coil. In most HVAC system configurations, the indoor air humidity is not controlled in the same way as the air temperature, so the calculation of the air humidity requires a psychrometric model of the air crossing the system. Fig. 3.2 represents a psychrometric chart of humid air and the significant points of the HVAC model for a cooling situation (summer).

Mixing conditions

To calculate the supply air conditions and the energy consumption of the HVAC system, the model first calculates the mixing conditions of the air recirculated from the building and the outdoor air required for

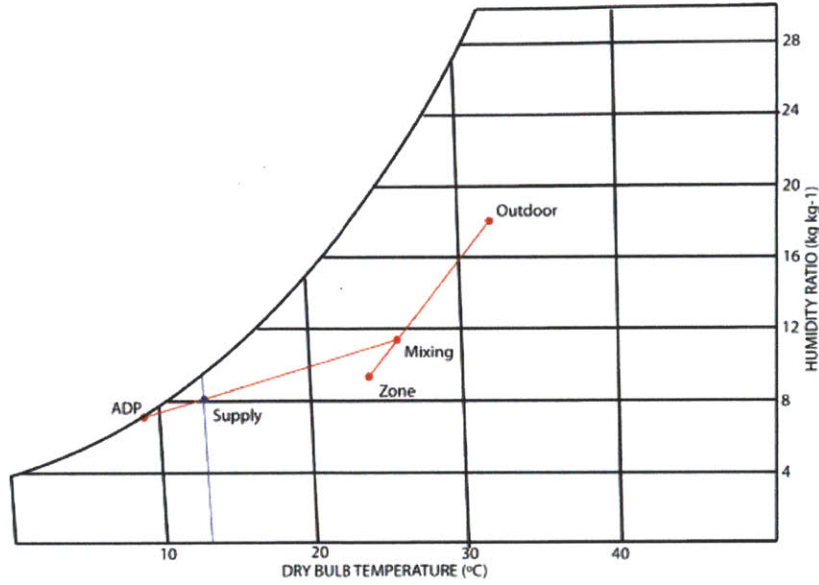


Figure 3.2 – Psychrometric chart of humid air. The significant points of the HVAC system model for a cooling situation are represented. Zone conditions refer to the temperature and humidity of the indoor air. Recirculated air from the zone is mixed with outdoor air before entering the cooling coil (mixing conditions). The air leaves the cooling coil at supply conditions. The apparatus dewpoint (ADP) is an input of the model and represents the temperature of the air leaving the cooling coil if this would be saturated.

ventilation. This calculation is the same for both the cooling and the heating system models. The mixing ratio (X_{mix}) is calculated as $X_{\text{mix}} = \dot{V}_{\text{vent}}\rho / \dot{m}_{\text{sys}}$, where \dot{m}_{sys} is the supply air mass flowrate and \dot{V}_{vent} is the ventilation air volume flowrate, which are given by the user (or calculated by the *autosize* function in the case of the air mass flowrate). Then, the mixing air temperature and humidity are calculated from the building air temperature and the outdoor air temperature as follows:

$$T_{\text{mix}} = X_{\text{mix}}T_{\text{urb}} + (1 - X_{\text{mix}})T_{\text{in}}, \quad (3.7)$$

and

$$q_{\text{mix}} = X_{\text{mix}}q_{\text{urb}} + (1 - X_{\text{mix}})q_{\text{in}}. \quad (3.8)$$

Cooling system

In the ideal cooling system model, the energy consumption is calculated by adding the sensible and the latent energy demand of the building and dividing by the system coefficient of performance (COP), $Q_{\text{HVAC,cool}} = Q_{\text{dem,cool}}/\text{COP}$. The supply conditions are then calculated to meet the building energy demand:

$$T_{\text{sys}} = T_{\text{mix}} - H_{\text{dem,cool}} / (\dot{m}_{\text{sys}}c_p), \quad (3.9)$$

and

$$q_{\text{sys}} = q_{\text{mix}} - LE_{\text{dem,cool}} / (\dot{m}_{\text{sys}}l_v), \quad (3.10)$$

where $H_{\text{dem,cool}}$ and $LE_{\text{dem,cool}}$ are the sensible and latent cooling demand of the building.

In the realistic cooling system model, the model solves a psychrometric model based on the apparatus dewpoint (ADP) temperature. The current version of BEM considers a constant-volume direct-expansion cooling system without reheat, but other system configurations can be added in future versions of the model. At each time step, the supply air temperature and humidity are calculated by satisfying two conditions. First, the supply point in the psychrometric chart (Fig. 3.2) must fall on the line connecting the mixing point and the ADP point. Second, the supply temperature should meet the sensible energy demand of the building (Eq. 3.9). If the energy demand of the building is greater than the system capacity, the system capacity is used to calculate the supply temperature.

The system capacity ($Q_{\text{cap,sys}}$) is calculated from the nominal system capacity multiplied by a coefficient that depends on outdoor and indoor conditions (see appendix B). The electricity consumption of the cooling coil ($Q_{\text{HVAC,sys}}$) is calculated by the following expression:

$$Q_{\text{HVAC,sys}} = Q_{\text{cap,sys}} \text{PLR} f_{\text{PLR}} / \text{COP}, \quad (3.11)$$

where PLR is the part-load ratio, calculated as the fraction between the energy supplied and the system capacity, and f_{PLR} is a coefficient that depends on the PLR and accounts for the loss of the system efficiency due to part-load performance. The actual COP of the system is calculated from the nominal COP (provided by the user) multiplied by a coefficient that depends on outdoor and indoor conditions (see appendix B).

Heating system

The current version of BEM considers a fuel-combustion heating system. Other heating systems, such as heat pumps, can be added in future versions of the model. The supply air temperature of the heating system is calculated to meet the sensible heating energy demand of the building (Eq. 3.12). If the energy demand of the building is greater than the system's heating capacity, the heating capacity is used to calculate the supply temperature.

$$T_{\text{sys}} = T_{\text{mix}} + H_{\text{dem,heat}} / (\dot{m}_{\text{sys}} c_p). \quad (3.12)$$

The heating system model assumes that the indoor air humidity is not controlled and that the supply air humidity is the same as the mixing humidity (Eq. 3.8). The energy consumption of the heating system is calculated from the thermal energy exchanged between the heating system and the indoor air ($Q_{\text{exch,heat}}$) divided by a constant efficiency (η_{heat}), provided by the user.

$$Q_{\text{HVAC,heat}} = Q_{\text{exch,heat}} / \eta_{\text{heat}}. \quad (3.13)$$

Fan electricity consumption

The fan electricity consumption is calculated from the following correlation extracted from EnergyPlus documentation [DOE, 2010a]:

$$P_{\text{fan}} = \dot{m}_{\text{sys}} \Delta P_{\text{fan}} \eta_{\text{fan}} / \rho, \quad (3.14)$$

where ΔP_{fan} is the fan design pressure increase, predefined as 600 Pa; and η_{fan} is the fan total efficiency, predefined as 0.7. These predefined values are the same as the default values used in EnergyPlus.

Waste heat emissions

The waste heat released into the environment by a cooling system is given by:

$$Q_{\text{waste,cool}} = Q_{\text{exch,cool}} + Q_{\text{HVAC,cool}}, \quad (3.15)$$

where $Q_{\text{exch,cool}}$ is the thermal energy exchanged between the cooling system and the indoor air, and $Q_{\text{HVAC,cool}}$ is the energy consumption of the cooling system (e.g. electricity). The user can specify the sensible-latent split of the waste heat produced by the cooling system, depending on whether the system is air-condensed, water-condensed, or both.

For the heating system, the waste heat flux is related to the energy contained in the combustion gases and is given by:

$$Q_{\text{waste,heat}} = Q_{\text{HVAC,heat}} - Q_{\text{exch,heat}}, \quad (3.16)$$

where $Q_{\text{HVAC,heat}}$ is the energy consumption of the heating system (e.g. gas).

The heat flux associated with the exfiltrated and exhausted air is added to the waste heat flux from HVAC systems, assuming that the air leaves the buildings at indoor air temperature.

Autosize function

For the realistic model of an HVAC system, BEM requires information about the size of the system. The parameters that determine the size of a system are the rated cooling capacity and the maximum heating capacity. For a constant-volume cooling system, the model also requires its design mass flowrate. This information can be provided to the model manually, or it can be automatically calculated by the *autosize* function.

The *autosize* function first calculates the maximum heating capacity by applying a sensible heat balance at the indoor air (Eq. 3.4), assuming steady-state heat conduction through the enclosure. An equivalent outdoor air temperature is calculated as the average between the design minimum air temperature (provided by the user) and a generic sky temperature (253 K). The required air flowrate is then obtained from Eq. 3.17, assuming a supply air temperature of 323 K.

$$\dot{m}_{\text{sys, rat}} = \frac{Q_{\text{heat, max}}}{c_p (T_{\text{supply}} - T_{\text{heat, target}})}. \quad (3.17)$$

To calculate the rated cooling capacity, the model dynamically simulates the building during four days, between July 12 and July 15. The rated cooling capacity corresponds to the maximum cooling energy required to maintain indoor set point conditions for the last day of simulation. This dynamic simulation uses a predefined diurnal cycle of outdoor air temperature and incoming solar radiation (see appendix B). Incoming solar radiation depends on the specific location of the urban area, using the solar zenith angle calculated by the TEB model. Outdoor air humidity, air velocity, and air pressure are considered constant during this simulation.

Once the rated cooling capacity is calculated, the required air flowrate is obtained assuming a supply air temperature of 287 K. The rated air flowrate is the maximum of those calculated for cooling and for heating conditions.

3.3 Model evaluation

3.3.1 Modeling assumptions

A methodology is proposed to evaluate BEM assumptions. Two models of the same building with different levels of detail are compared by simulating them with EnergyPlus. The first model, which is referred as the detailed model (DM), includes the exact geometry of the building enclosure, defines each building level as a separate thermal zone, and introduces internal heat gains in terms of people, lighting, and equipment. The second model, which is referred as the simplified model (SM), maintains the assumptions of BEM. It considers a square-base building defined as a single thermal zone with internal mass, somewhat similar to the reference building of the CS described in section 2.3.1. The building height, vertical-to-horizontal building area ratio, roof-to-horizontal building area ratio, glazing ratio, construction configuration of the enclosure (materials and layers), total internal heat gains, and infiltration air flowrate are the same as the DM (Table 3.1).

To avoid orientation-specific results, DM is simulated for eight different orientations, every 45°, and SM is simulated for two different orientations, rotated 45° between each other. Then, the averaged results from each set of simulations are compared.

Table 3.1 – Simulation parameters used in the comparison between the simplified EnergyPlus model and the detailed EnergyPlus model of a residential Haussmannian building. The thermal properties of construction materials are summarized in Table 2.2. The term fl indicates unit of floor area.

Parameter	Settings
Vertical-to-horizontal building area ratio	3.14
Building height	21.50 m
Length of the side of the square building plan	27.36 m
Roof-to-horizontal building area ratio	0.69
Internal heat gains	5.58 W m ⁻² fl
Radiant fraction of internal heat gains	0.40
Latent fraction of internal heat gains	0.20
Window solar heat gain coefficient (SHGC)	0.60
Window U-factor	4.95 W m ⁻² K ⁻¹
Glazing ratio	0.2
Floor height	2.90 m
Infiltration	0.11 ACH
Ventilation	0.43 ACH
Thermal set points	19 °C - 24 °C
Internal mass-to-horizontal building area ratio	12.83
Internal thermal mass construction	Concrete - 10 cm
Wall construction	Main façade: Stone - 38 cm Side walls: Brick - 22 cm
Roof construction	Slate, wood, air cavity

The results presented in this section were obtained in collaboration with K. Zibouche from CSTB (Paris, France) and G. Pigeon from CNRM-GAME (Toulouse, France). The case study corresponds to a Haussmannian building in Paris (Fig. 3.3). Fig. 3.4 and 3.5 represent the daily-average and monthly-average diurnal cycles, respectively, of heating energy demand in winter and cooling energy demand in summer calculated by the simplified and the detailed EnergyPlus models. Differences in heating and cooling energy demands, computed as root-mean-square error (RMSE) and mean-bias error (MBE) between the SM and the DM, are presented in Table 3.2. The RMSE of heating energy demand is

0.9 W m^{-2} of floor area, where the average heating energy demand calculated by the DM for the same period is 19.5 W m^{-2} . The RMSE of cooling energy demand is 1.4 W m^{-2} , where the average for the same period is 9.1 W m^{-2} . In this case, the MBE is 0.9 W m^{-2} , which indicates that the SM overestimates the cooling energy demand.

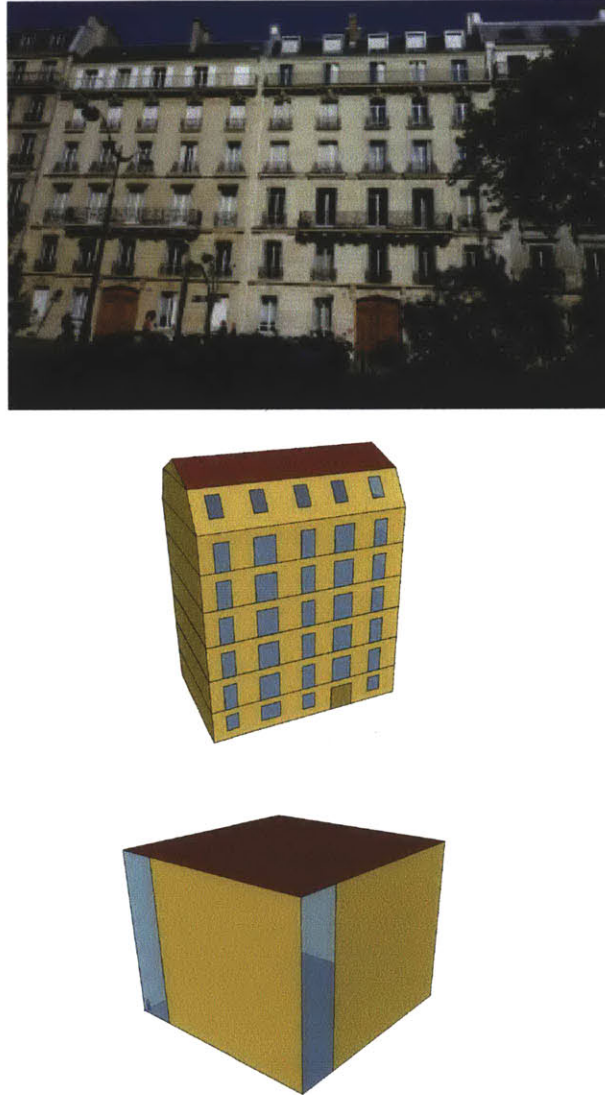


Figure 3.3 – Image of a Haussmannian building in Paris (top). Representation of the detailed model defined in EnergyPlus (middle). Representation of the simplified model defined in EnergyPlus (bottom).

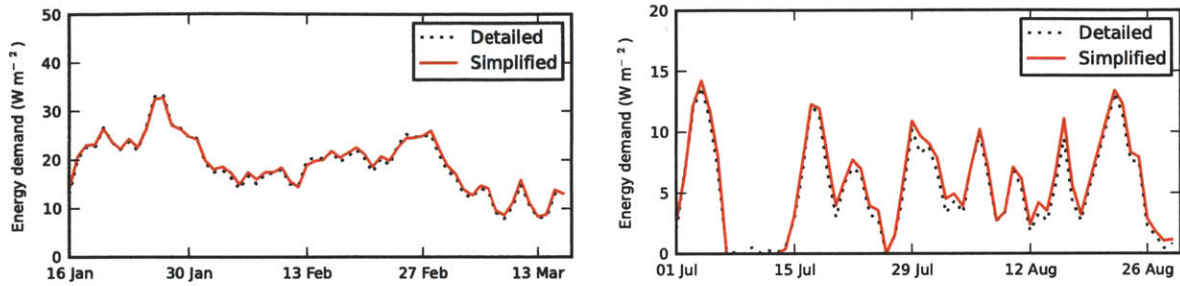


Figure 3.4 – Heating (left) and cooling (right) energy demand per unit of floor area for winter and summer calculated by the simplified and the detailed EnergyPlus models of a Haussmannian building in Paris.

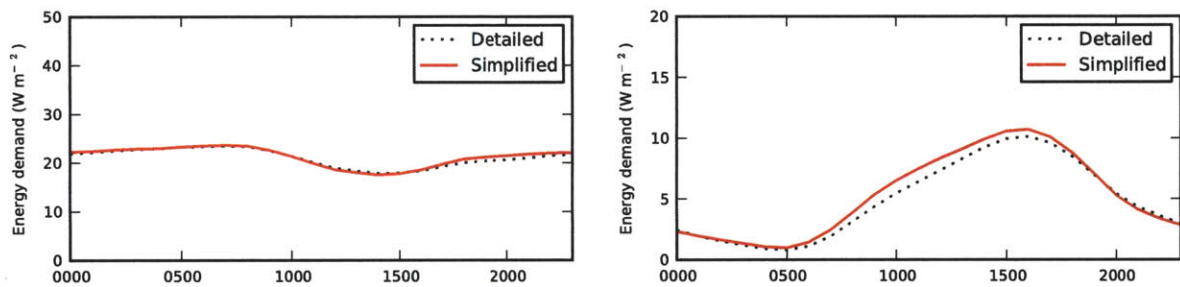


Figure 3.5 – Monthly-average diurnal cycles of heating energy demand between January 16 and February 15, 2005 (left), and cooling energy demand between July 1 and July 30, 2004 (right), per unit of floor area calculated by the simplified and the detailed EnergyPlus models of a Haussmannian building in Paris.

Table 3.2 – Root-mean-square error (RMSE), mean-bias error (MBE), and reference value (REF) of the variables compared in each of the three evaluation sections. The reference value of energy and heat fluxes is the average of the energy and heat fluxes for the considered time period. The terms urb and fl indicate unit of urban area and floor area, respectively.

	RMSE	MBE	REF
modeling assumptions (Simplified-Detailed)			
Heating energy demand ($\text{W m}^{-2} \text{ fl}$)	0.9	0.4	19.5
Cooling energy demand ($\text{W m}^{-2} \text{ fl}$)	1.4	0.9	9.1
Model verification (CS-BEM)			
Heating energy demand ($\text{W m}^{-2} \text{ fl}$)	0.8	0.3	5.6
Cooling energy demand ($\text{W m}^{-2} \text{ fl}$)	1.1	-0.4	6.0
Cooling energy consumption ($\text{W m}^{-2} \text{ fl}$)	0.7	0.5	3.0
Waste heat emissions ($\text{W m}^{-2} \text{ urb}$)	9.8	6.0	50.2
Model validation (BEM-Observations)			
Case study: Toulouse, France			
Simulation period: Dec 19–Feb 17, 2005			
Electricity consumption ($\text{W m}^{-2} \text{ urb}$)	5.1	-2.8	30.8
Gas consumption ($\text{W m}^{-2} \text{ urb}$)	7.4	-6.0	19.0
Case study: Athens, Greece			
Simulation period: Jun 30–Aug 29, 2009			
Indoor air temperature (K)	1.1	0.1	

3.3.2 Model verification

To check that the chosen equations are solved correctly, BEM-TEB is compared to the CS between EnergyPlus and TEB (chapter 2). The case study corresponds to the residential urban center of Toulouse, which was characterized in section 2.4.2. To be able to compare cooling energy consumption between the two models, this study assumes that AC systems are widely used in the urban area. The input parameters are summarized in Table 3.3.

Figures 3.6 and 3.7 represent the daily-average and monthly-average diurnal cycles, respectively, of heating energy demand in winter and cooling energy demand in summer calculated by BEM and the CS. Scores for this comparison are presented in Table 3.2. The RMSE of heating and cooling energy demand ranges between 0.8 and 1.1 W m^{-2} of floor area, where the average heating and cooling energy demand calculated by the CS is around 6 W m^{-2} for the same period. As can be seen, BEM slightly overestimates cooling energy demand in summer (negative MBE) and underestimates heating energy demand in winter (positive MBE) compared to the CS. This can be explained by the fact that the solar radiation model of the TEB scheme tends to overestimate the solar radiation reaching building façades as compared with the CS.

Figure 3.8 compares the daily-average cooling energy consumption and waste heat emissions of the HVAC system calculated by BEM and the CS. The RMSE of cooling energy consumption is 0.7 W m^{-2} of floor area (Table 3.2), where the average cooling energy consumption calculated by the CS is 3 W m^{-2} for the same period. A relative error of 20 % in building energy consumption is acceptable given the state-of-the-art of urban canopy models. Grimmond et al. [2011] show that the surface heat flux error of urban canopy models is usually greater than 20 %. A similar order of magnitude difference is encountered for the waste heat emissions calculated by both models. The RMSE of waste heat emissions is 9.8 W m^{-2} of urban area, where the average waste heat fluxes for the same period is 50.2 W m^{-2} .

Table 3.3 – Simulation parameters used in the evaluation of BEM-TEB for the case study of the residential urban center of Toulouse, France. In the comparison between BEM-TEB and the CS, the study assumes that AC systems are used in this urban area. In the comparison between BEM-TEB and observations, the study represents the actual situation in which AC systems are not widely used in the urban area. The thermal properties of construction materials are indicated in Table 2.2.

Parameter	Settings
Urban parameters	
Location	Toulouse
Latitude	43.48°
Longitude	1.3°
Average building height	20 m
Building density	0.68
Vertical-to-horizontal urban area ratio	1.05
Roughness length	2.0 m
Anthropogenic heat from traffic	8.0 W m ⁻² urb
Wall and roof construction	Brick - 30 cm Insulation - 3 cm
Wall and roof albedo	0.32
Road construction	Asphalt - 5 cm Stones - 20 cm Gravel and soil
Road albedo	0.08
Version of the TEB scheme	Single-layer
Building parameters	
Building floor construction	Concrete - 20 cm
Glazing ratio	0.3
Window construction	Double-pane clear glass
Internal heat gains	Residential (see Table 2.1)
Infiltration/ventilation air flowrate	0.5 ACH
Thermal set points	19 °C - 24 °C
Cooling system	Section 3.3.2: Single speed fan on the air side, with evaporating refrigerant in the coils. Section 3.3.3: None
Nominal COP	2.5
Heating system	Gas furnace
Heating efficiency	0.9
Fraction of gas heating systems	60%
Fraction of electric heating systems	40%

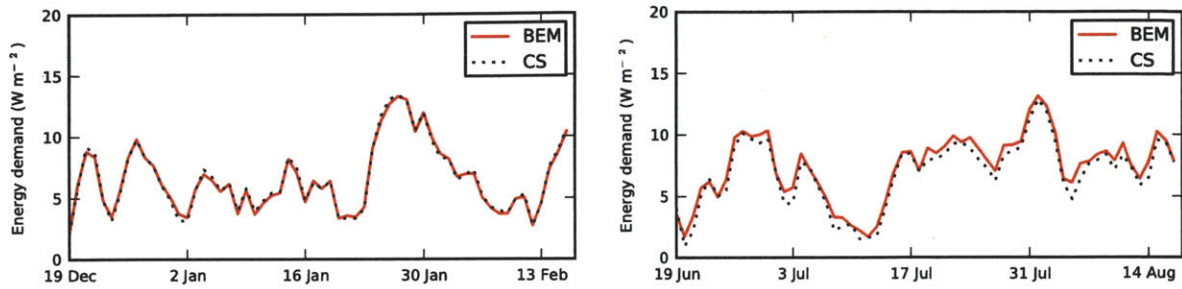


Figure 3.6 – Daily-average heating (left) and cooling (right) energy demand per unit of floor area for winter and summer calculated by the CS and by BEM-TEB for the dense urban center of Toulouse.

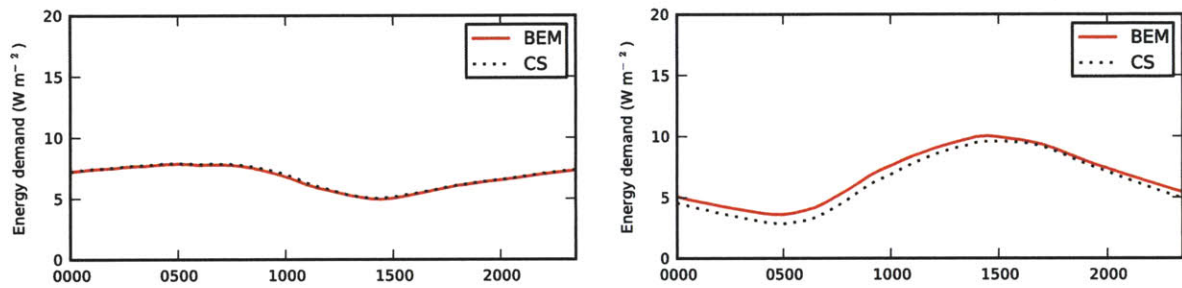


Figure 3.7 – Monthly- diurnal cycles of heating energy demand between January 1 and January 30, 2005 (left), and cooling energy demand between July 1 and July 30, 2004 (right), per unit of floor area calculated by the CS and by BEM-TEB for the dense urban center of Toulouse.

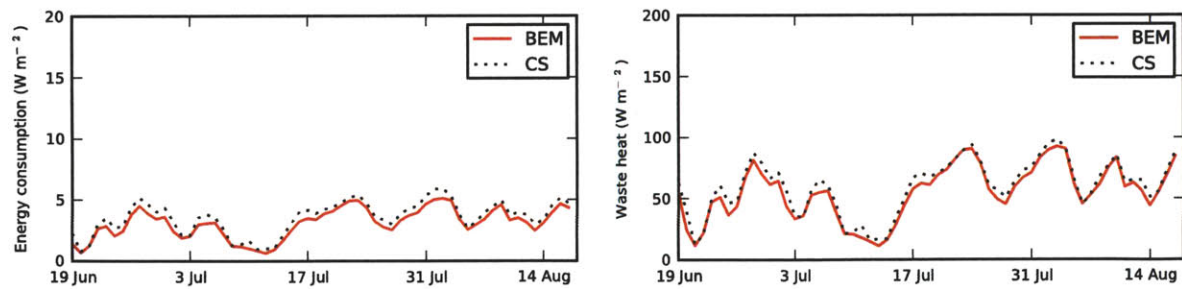


Figure 3.8 – Daily-average cooling energy consumption per unit of floor area (left) and waste heat emissions per unit of urban area (right) calculated by the CS and by BEM-TEB for the dense urban center of Toulouse.

3.3.3 Comparison with field data from Toulouse, France

Field data from the CAPITOUL experiment is used to evaluate BEM-TEB in winter. The case study of Toulouse was used in the previous section and characterized in section 2.4.2. The characterization of the site includes the justification of modeling assumptions, given the lack of detailed information about buildings. A summary of the input parameters of BEM-TEB for this case study is presented in Table 3.3.

As it was previously done with the CS (section 2.4.4), electricity consumption, natural gas consumption, and anthropogenic heat fluxes from the CAPITOUL experiment are compared to BEM-TEB simulation results for two months in winter (Fig. 3.9). Electricity and natural gas consumption computed as MBE and RMSE between BEM and observations are presented in Table 3.2. The RMSE of electricity consumption is 5.1 W m^{-2} , averaged over the urban area, where the average electricity consumption calculated by the model is 30.8 W m^{-2} . A similar RMSE of gas consumption is obtained, 7.4 W m^{-2} . It can be seen that BEM-TEB slightly underpredicts electricity and gas consumption in this comparison, which can be due to internal heat gains not accounted for in the analysis, such as cooking and domestic hot water.

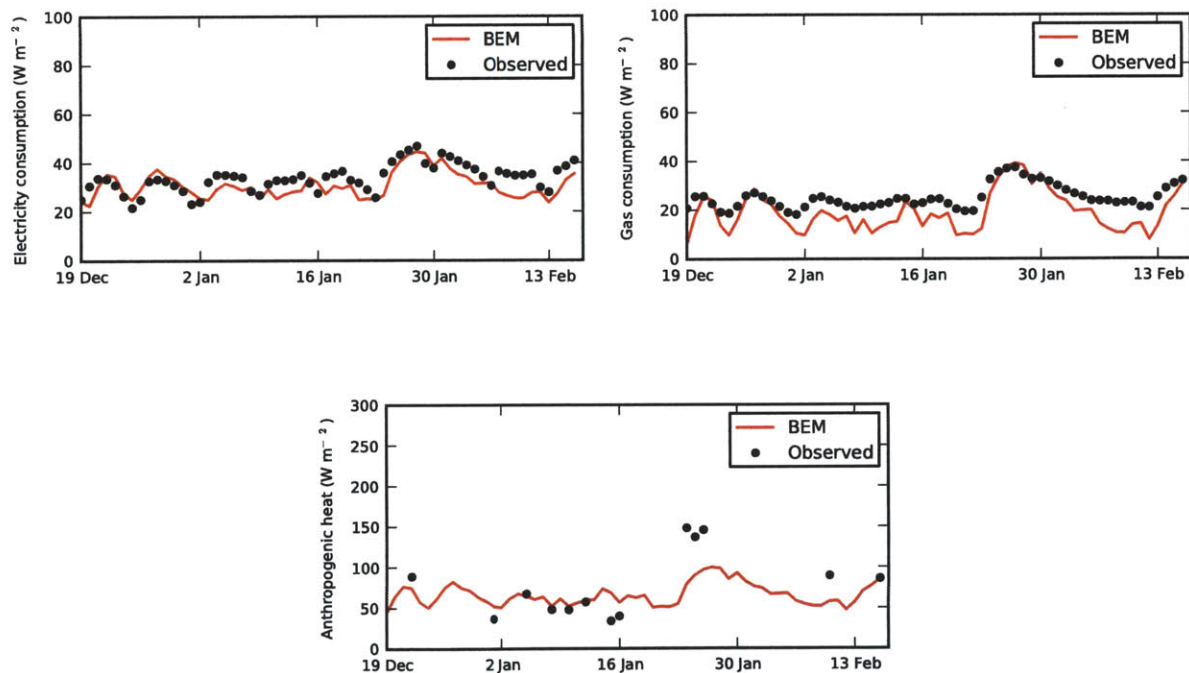


Figure 3.9 – Daily-average electricity consumption (top-left), natural gas consumption (top-right), and anthropogenic heat (bottom) per unit of urban area from observations and calculated by BEM-TEB in winter for the dense urban center of Toulouse.

3.3.4 Comparison with field data from Athens, Greece

Field data from a second experiment is used to evaluate BEM-TEB in summer. This experiment was carried out in Athens (Greece) between May and September 2009, framed in the European project BRIDGE [Synnefa et al., 2010, 2011]. Indoor air temperatures were measured in representative residential buildings of the Egaleo neighborhood. Sensors were placed in the center of the living room of an intermediate floor, at a height of about 1 m above the floor. Outdoor air temperatures were simultaneously monitored by a meteorological station located at the municipality of Egaleo. Three of the monitored buildings share similar input parameters in BEM-TEB (Table 3.4) and are used in this comparison.

The three analyzed buildings were built between 1945-1965 (Fig 3.10). They are made of reinforced concrete with no insulation and single-pane windows. In summer, buildings are naturally ventilated and provided with exterior window shades. The geometry and construction parameters of this case study were reported in the experiments. Typical values of internal heat gains and infiltration for residential buildings are assumed. Reasonable modeling assumptions are made in terms of shades and natural ventilation operation (Table 3.4). A low pressure coefficient difference is chosen to represent the impediment to air movement imposed by interior partitions.

The measured indoor air temperatures are compared to BEM simulation results for two months in summer (Fig. 3.11). Indoor air temperatures in naturally-ventilated buildings are very sensitive to occupant behavior (e.g. occupation schedules, shades and window operation); thus, even if the buildings have similar parameters in terms of the simulation, their performance can be significantly different. As can be seen, BEM is able to reproduce the daily-average evolution, as well as the daily cycle amplitude, of indoor air temperatures measured in building 1 with an RMSE of 1.1 K (Table 3.2), but it overestimates the indoor air temperatures measured in building 2 and, to a lesser extent, those measured in building 3. This can be explained by the fact that building 1 performs more in phase with the outdoor environment than building 2, which means that building 1 has less fluctuations of internal heat gains and human building operation and, therefore, can be better captured by the simulation. Compared to building 1, BEM slightly overestimates the indoor air temperature during daytime (positive MBE), probably because BEM does not consider occupation schedules, which would decrease internal heat gains during working hours.

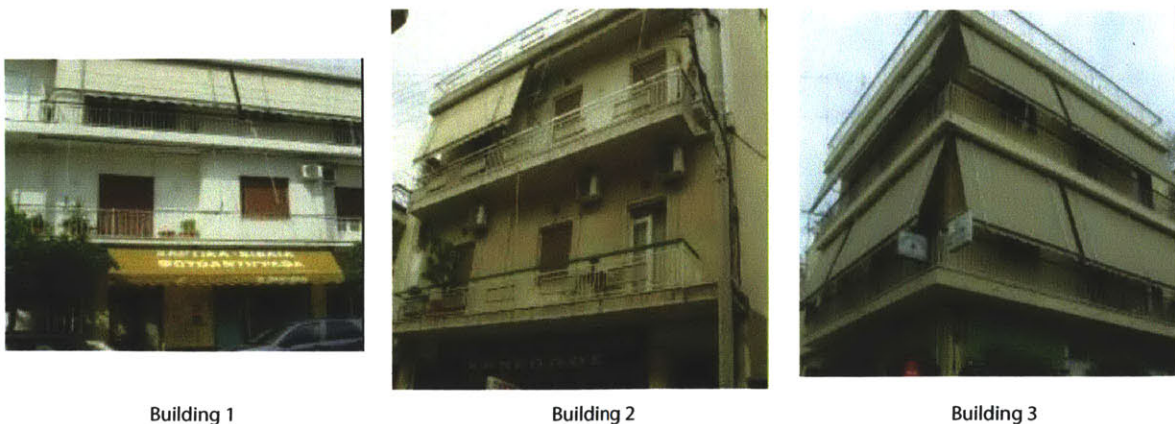


Figure 3.10 – Images of the buildings used in the comparison between BEM-TEB and the experiment carried out in the Egaleo neighborhood of Athens. *Source:* Synnefa et al. [2011].

Table 3.4 – Simulation parameters used in the comparison between BEM and observations. This configuration represents an urban area composed of residential buildings in the Egaleo neighborhood in Athens, Greece. The thermal properties of construction materials are indicated in Table 2.2.

Parameter	Settings
Location	Athens
Latitude	37.98°
Longitude	23.68°
Average building height	9.5 m
Building density	0.64
Vertical-to-horizontal urban area ratio	1.05
Roughness length	0.95
Wall and roof construction	Concrete - 30 cm No insulation
Wall and roof albedo	0.32
Building floor construction	Concrete - 20 cm
Glazing ratio	0.25
Window construction	Double-pane clear glass
Internal heat gains	Residential (see Table 2.1)
Infiltration/ventilation air flowrate	0.5 ACH
Cooling system	None
Natural ventilation	Activated; $\Delta C_p = 0.1$; $h_{win} = 1.5$ m (see appendix B)
Shading devices	Exterior shades; solar radiation on windows for which shades are ON: 250 W m ⁻² ; solar transmittance of shades: 0.3

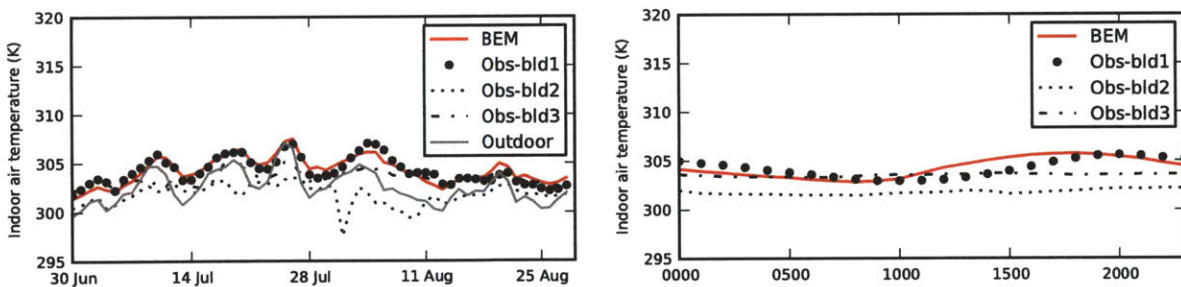


Figure 3.11 – Daily-average (left) and monthly-average diurnal cycle (right) of indoor air temperature from observations and calculated by BEM-TEB from June 30 to August 30, 2009, for the Egaleo neighborhood of Athens. Observations correspond to three different residential buildings. Daily-average outdoor air temperatures are also represented (left).

Chapter 4

The RC model for the analysis of the energy interactions between buildings and the urban climate

4.1 Overview

This chapter presents an urban canopy and building energy model based on a thermal network of constant resistances and capacitances. The benefits of the RC model with respect to the more detailed models previously presented (chapters 2 and 3) are its simplicity and computational efficiency. The model represents the fundamental physical mechanisms that govern the reciprocal energy interactions between buildings and the urban environment, retaining the sensitivity to the design parameters typically used in building energy and urban climate studies. The RC model is based on a state-space formulation that can be very efficiently solved by a numerical program. This allows for faster parametric analyses and makes it possible to easily evaluate modeling hypotheses.

In this chapter, the RC model is described and evaluated against the Coupled Scheme (CS) between EnergyPlus and TEB (chapter 2) for summer and winter and for different scenarios of waste heat emissions. The model is then used in a series of parametric analyses to investigate the impact of the UHI effect on the energy consumption of buildings for different building configurations. The model is also used to investigate the dominant mechanisms by which the indoor environment and the energy performance of buildings affect outdoor air temperatures. The conclusions of this study can be applied to a wide range of building and urban configurations.

4.2 Model description

Figure 4.1 shows the thermal network that represents the energy interactions within and between the indoor and outdoor environments. The indoor environment is defined as a single-zone building with an internal thermal mass. The outdoor environment is defined by an average-oriented urban canyon, composed of a generic façade and a generic road. Other urban canyon and building energy models, such as BEM-TEB (chapter 3), solve a very similar thermal network. The main difference is that, in the RC model, the state-space formulation solves the thermal network once for the whole simulation period instead of solving it at each time step.

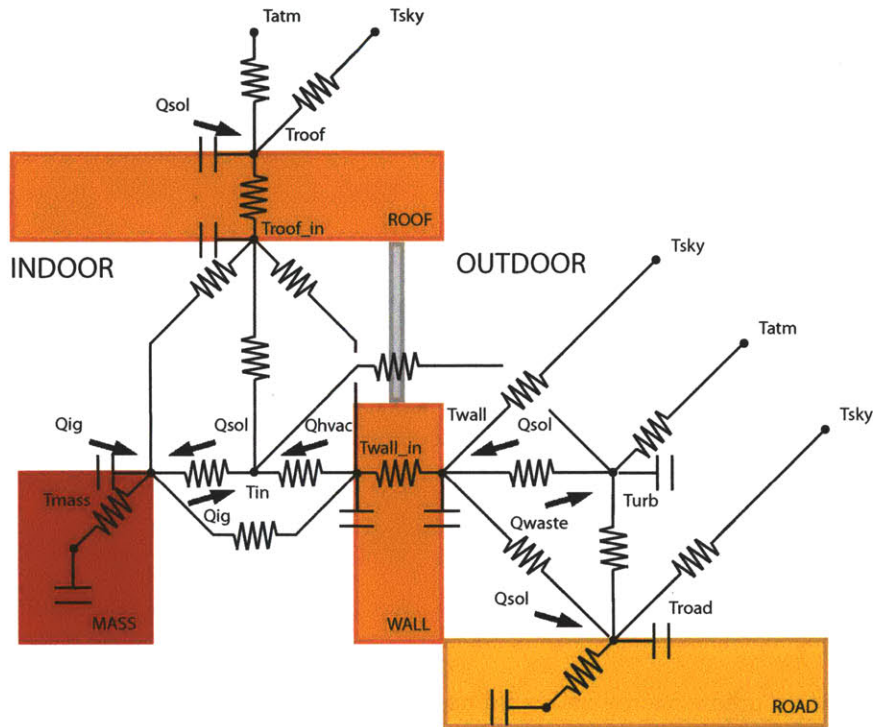


Figure 4.1 – Representation of an urban canopy and building energy model based on a thermal network of constant resistances and capacitances. A capacitance is associated with each temperature node. Nodes are connected by resistances. The heat sources of each node are represented by arrows. Four nodes are used to calculate the heat transfer through the wall, the roof and the road.

4.2.1 Physics

The RC model represents the following heat transfer phenomena and calculations:

- Transient heat conduction through building walls and roof.
- Steady state heat conduction through windows.
- Solar transmission through windows.
- Heat storage in intermediate floor constructions.
- Longwave radiant heat exchange among interior surfaces (wall, roof, and mass).
- Sensible heat balance of the indoor air, including the convective heat fluxes from walls, windows, roof, and intermediate floors, the convective fraction of internal heat gains, the heat fluxes due to infiltration and ventilation air, and the heat fluxes from the HVAC system.
- Sensible heat balance of the urban canyon air, including the convective heat fluxes from walls, windows and the road, the sensible heat exchange between the canyon air and the atmosphere, the heat fluxes due to exfiltration and exhaust air, and the waste heat from HVAC equipment.

- Solar radiation absorbed by walls, roof, and road assuming an average orientation of an urban canyon (see appendix D).
- Heat storage in the road soil.
- Wall-sky, road-sky, roof-sky, and wall-road longwave radiant heat exchanges, taking into account the view factors between each pair of elements. This represents the longwave trapping of urban canyons due to reduced sky view factors.

4.2.2 Assumptions

The objective of the RC model is to capture the fundamental physical mechanisms that govern the indoor and outdoor energy interactions, while keeping a state-space formulation that can be efficiently solved. This implies constant resistances in the thermal network represented in Fig. 4.1.

The rate of heat exchange between the urban canyon air and the atmosphere is usually characterized by an exchange velocity u_{ex} , which can be defined as:

$$u_{ex} = \frac{H_{urb}}{\rho c_p (T_{urb} - T_{atm})}, \quad (4.1)$$

where H_{urb} is the sensible heat exchange between the urban canyon and the atmosphere, T_{urb} is the urban canyon mean air temperature, and T_{atm} is the air temperature above the urban canopy layer. Preliminary results obtained with the RC model showed that urban canyon air temperatures are sensitive to the exchange velocity values. Different methods are proposed in the literature to calculate exchange velocities. In this version of the RC model, the correlations of Louis [1979] are used (Eq. C.13 in appendix C). In this method, exchange velocities depend on the Richardson number, which is a measure of the air stability inside the canyon and is a function of the canyon air temperature calculated by the RC model. Therefore, an iteration of the RC model is required to match the input and calculated exchange velocities.

As a consequence of the state-space formulation, the RC model assumes that the convection heat transfer coefficients (CHTC) and the exchange velocities remain invariant during the simulation. In detailed urban canopy and building energy models (e.g. CS and BEM-TEB), the CHTC can be calculated by correlations as a function of the wind speed and surface-air temperature difference. Exchange velocities usually depend on geometry, roughness length for momentum and heat, wind speed, and atmospheric stability. Even so, the RC model is able to reproduce the average diurnal cycle of the results of more sophisticated models by using the average exchange velocity calculated by correlations for the simulation period.

Other assumptions of the RC model include:

- Constant indoor air temperature.
- Constant infiltration and ventilation air flowrate.
- Constant internal heat gains.
- Single-zone building with intermediate floors represented as an internal thermal mass. The transmitted solar radiation and the radiant fraction of internal heat gains are perfectly absorbed by the internal thermal mass and then are released into the indoor environment.

- Adiabatic building floor. This condition is reasonable if the floor is well insulated.
- Ideal HVAC system: the energy supplied by the system equals the building energy demand, and the energy consumption is calculated from a constant efficiency. The dependence of the COP of cooling systems on outdoor air temperatures is included in BEM-TEB (chapter 3).
- Well-mixed air inside the urban canyon. This is a reasonable assumption for relatively homogenous urban canopies composed of low-rise to medium-rise buildings. Building, cars, and other heat sources keep a positive buoyancy level inside urban canyons, even at night, and enhance the mixing of air inside the urban canopy.
- Linearized radiation formulation and one-bounce approximation for indoor and outdoor longwave radiative heat exchanges.
- Air temperatures at the top of the urban canopy layer are boundary conditions of the model and therefore not affected by the heat fluxes from the canopy. This assumption is relaxed in chapters 5 and 6, and its effect is discussed.
- No sensible-to-latent conversion due to vegetation or other mechanisms. A simple urban vegetation model is presented in chapter 6.
- The water vapor of the urban canyon air does not participate in the radiant heat balance. This assumption is relaxed in chapter 6 to account for humid climates.

These assumptions have a small or no effect on the conclusions obtained with the RC model in this chapter. A systematic error will cancel when comparing different simulations with the RC model.

4.2.3 State-space formulation

The RC model is derived from energy conservation principles. For each capacitance node (Fig. 4.1), the rate of change of its internal energy is related to the heat fluxes reaching the node. This can be generally expressed as:

$$C_j \frac{dT_j}{dt} = \sum_k \frac{1}{R_k} (T_k - T_j) + \sum Q_j, \quad (4.2)$$

where C_j and T_j represent the capacitance and temperature of the node j , R_k and T_k represent the resistance and temperature of the nodes k that interact with the node j , and Q_j represents the heat fluxes acting on the node j .

Using these relations, a state-space formulation can be set up and efficiently solved by a numerical simulation tool. The general formulation can be written as:

$$\frac{dT_j(t)}{dt} = AT_j(t) + Bu_j(t), \quad (4.3)$$

where $T_j(t)$ is a vector of state variables that correspond to each of the temperature nodes associated with a capacitance, $u_j(t)$ is a vector of inputs that can be known temperatures or heat fluxes, and A and B are coefficient matrices.

4.2.4 Heat fluxes

The transmitted solar radiation is obtained by multiplying the solar radiation that reaches the average-oriented wall by a constant window transmittance provided by the user (see section 3.2.4).

In the case of a cooling situation, waste heat from the outdoor equipment is released into the outdoor environment (Q_{waste}). The waste heat is calculated as a function of the cooling energy demand of the building (Q_{dem}) and the energy consumed by the HVAC system to dehumidify the air that passes through the cooling coil (Q_{lat}):

$$Q_{waste} = f(Q_{dem} + Q_{lat}), \quad (4.4)$$

where the function f depends on the coefficient of performance (COP) of the cooling system, $f = (1 + 1/COP)$. The dehumidification energy (Q_{lat}) is obtained by assuming that the air enters the cooling coil at indoor conditions and leaves the cooling coil at supply temperature and at 90% relative humidity. Then,

$$Q_{lat} = m_{sys} l_v (q_{in} - q_{sys}), \quad (4.5)$$

where m_{sys} is the supply mass flowrate; l_v is the water condensation heat; q_{sys} is the supply specific humidity, calculated from the supply temperature (T_{sys}) and 90 % RH; and q_{in} is the indoor specific humidity, calculated from the set point of temperature and relative humidity provided by the user. To obtain the supply mass flowrate, the model requires the maximum sensible cooling load of the building, which is calculated through the simulation. Therefore, an iteration of the RC model is required in order to calculate waste heat emissions.

4.2.5 Boundary conditions, inputs and outputs

As boundary conditions, the RC model requires time-step values of air temperatures and wind speed at the top of the urban canyon (above the urban canopy layer), solar heat fluxes over the horizontal, and incoming longwave radiation or equivalent sky temperature. The inputs of the model are construction and geometric information, internal heat gains, indoor thermal and humidity set points, supply air temperature of the HVAC system, maximum sensible cooling load calculated through iteration of the model, CHTC of the different surfaces, and exchange velocity between the urban canyon and the atmosphere calculated through iteration of the model (see Table 4.1 for specific inputs). The outputs of the model are the average diurnal cycles of node temperatures, heat fluxes, building energy demand, and waste heat emissions for the simulation period.

4.3 Model evaluation

In this section, the RC model is compared with the EnergyPlus-TEB Coupled Scheme (CS) (chapter 2). The CS was evaluated with field data from the experiment CAPITOU conducted in Toulouse (France) from February 2004 to March 2005 [Masson et al., 2008]. The same case study is used for the evaluation of the RC model but assuming that AC systems are widely used in summer. Table 4.1 describes the inputs of the RC model used in this study.

Three different case studies are compared (Table 4.2). The first two cases are summertime simulations of a residential and a commercial building, respectively. The third case corresponds to a wintertime

Table 4.1 – Inputs of the RC model used in the comparison of the model with the CS. This configuration represents the dense urban center of Toulouse (France) assuming AC systems are used in summer. The thermal properties of construction materials are summarized in Table 2.2. The term fl indicates unit of floor area.

Parameter	Settings
Location	Toulouse
Latitude	43.48°
Longitude	1.3°
Simulation time-step	1800 s
Simulation period	Summer: 07/15 - 07/30 Winter: 02/01 - 02/16
Average building height	20 m
Building density	0.68
Vertical-to-horizontal urban area ratio	1.05
Floor height	3 m
Glazing ratio	0.3
COP of the cooling system	2.5
Fraction of waste heat mixed with the urban canyon air	1.0
Indoor air temperature	Summer: 25 °C Winter: 20 °C
Indoor relative humidity	50 %
Supply temperature of the cooling system	14 °C
Internal heat gains	Residential: 6.25 W m ⁻² fl Commercial: 31.75 W m ⁻² fl
Radiant fraction of internal heat gains	0.2
Latent fraction of internal heat gains	0.2
Indoor convective heat transfer coefficient (CHTC)	2.0 W m ⁻² K ⁻¹
Indoor radiative heat transfer coefficient	6.0 W m ⁻² K ⁻¹
CHTC road-air	15 W m ⁻² K ⁻¹
CHTC wall-air	25 W m ⁻² K ⁻¹
CHTC roof-air	20 W m ⁻² K ⁻¹
Indoor thermal mass construction	Concrete - 20 cm
Wall and roof construction	Inner layer: Insulation - 3 cm Outer layer: Brick - 30 cm
Wall and roof albedo	0.32
Road construction	Gravel and soil - 1.25 m
Road albedo	0.08
Window construction	Transmittance: 0.6 U-factor: 2.5 W m ⁻² K ⁻¹
Infiltration	0.5 ACH

simulation of a residential building. The average diurnal cycles calculated by the RC model and the CS for 15 days in summer and 15 days in winter are compared.

4.3.1 Building energy demand

Figure 4.2 compares the sensible cooling energy demand in summer and the heating energy demand in winter calculated by the RC model and the CS. The root-mean-square error (RMSE) and mean-bias error (MBE) of the comparison is presented in Table 4.3. As can be seen, the RC model is able to reproduce the average diurnal cycle of building energy performance predicted by the CS with RMSE between 0.3 and 1.8 W m⁻² of floor area. These values are much lower than the average building energy demand calculated by the CS for the simulation period, which is taken as the reference value (REF)

Table 4.2 – Case studies used in the comparison of the RC model with the CS, and inputs of the RC model obtained through iteration for each case study. In winter, the model assumes that there are no waste heat emissions from HVAC systems.

Parameter	Case 1	Case 2	Case 3
Season	Summer	Summer	Winter
Internal heat gains	Residential	Commercial	Residential
Parameters obtained through iteration			
Exchange velocity	0.29 m s ⁻¹	0.31 m s ⁻¹	0.30 m s ⁻¹
Maximum sensible cooling load	11.3 W m ⁻² fl	32.3 W m ⁻² fl	-

to which evaluate errors. The RMSE associated with the transmitted solar radiation calculated by both models ranges between 1.3 and 1.8 W m⁻² of floor area. Negative MBE values of transmitted solar radiation indicate that the RC model overestimates this parameter systematically. In addition, the solar transmission error is high compared to its reference value, which can be explained by the simplifications made in the RC model for its calculation. Interior wall and mass surface temperatures are well captured by the RC model with RMSE between 0.0 and 0.6 K.

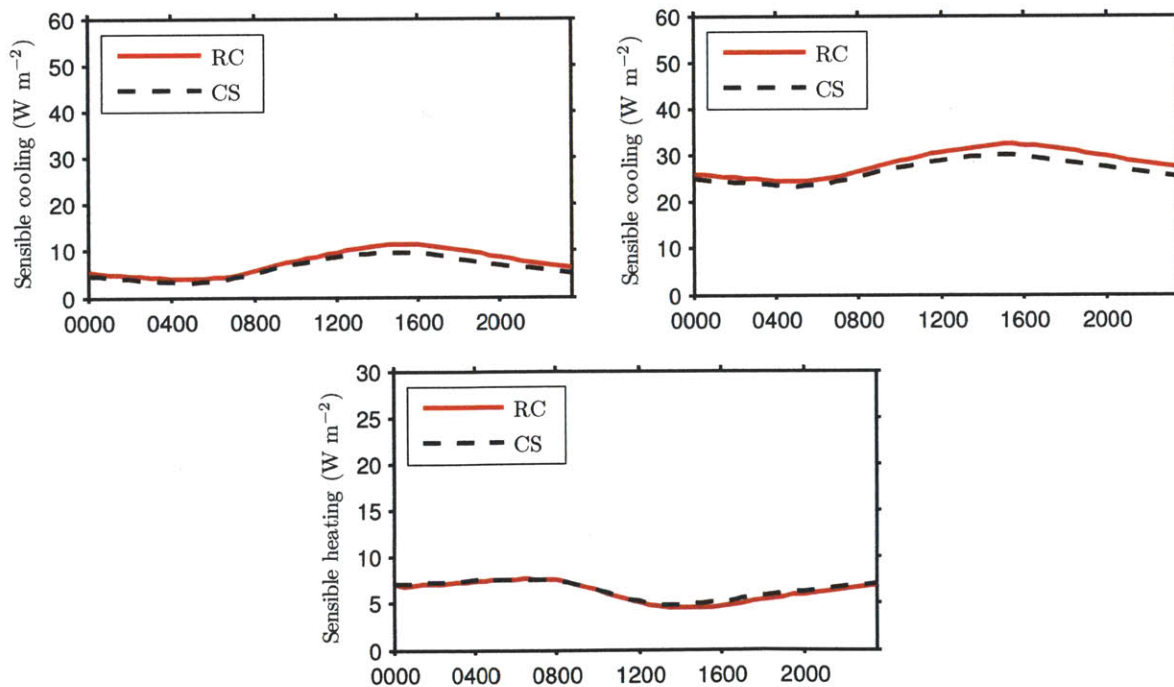


Figure 4.2 – Average diurnal cycle of sensible cooling energy demand of case 1 (top-left) and case 2 (top-right) for summer, July 15 - July 30, and average diurnal cycle of heating energy demand of case 3 (bottom) for winter, February 1 - February 16, calculated by the RC model and by the CS.

4.3.2 HVAC waste heat emissions

Figure 4.3 shows the average diurnal cycle of waste heat emissions in summer calculated by the RC model and the CS. As can be seen, the RC model is able to reproduce the waste heat emissions predicted by the CS with RMSE around 6.5 W m^{-2} of urban area, where the average waste heat flux calculated by the CS is 55 W m^{-2} for the residential case and 220 W m^{-2} for the commercial case.

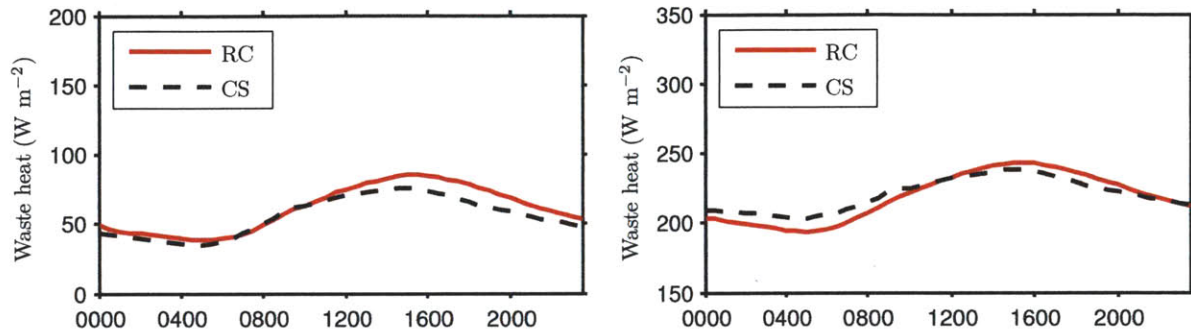


Figure 4.3 – Average diurnal cycle of HVAC waste heat emissions of case 1 (left) and case 2 (right) for summer, July 15 - July 30, calculated by the RC model and by the CS.

4.3.3 Urban air temperatures

Figure 4.4 represents the average diurnal cycle of air temperatures inside the urban canyon calculated by the RC model, the CS, and the TEB scheme. In case 1, in which waste heat emissions are around 55 W m^{-2} of urban area, the three models predict similar urban air temperatures. The RMSE between the RC model and the CS is 0.4 K , where the average temperature difference between the canyon and the atmosphere is 1.2 K . Case 2 presents waste heat emissions of around 220 W m^{-2} of urban area, and the urban air temperatures calculated by the RC model and the CS are around 1 K higher than those calculated by the TEB model, which does not account for waste heat emissions. The RMSE between the RC model and the CS is also 0.4 K , being the reference value 2.1 K . These relative errors are acceptable given the important uncertainties related to urban climate predictions.

In winter (case 3), the three models predict similar urban air temperatures. The RMSE between the RC model and the CS is 0.5 K , for which the reference canyon-atmosphere temperature difference is 0.7 K . Although the relative difference between the error and the reference value is higher in wintertime, the fact that for the three cases the error is very similar suggests that this is systematic and probably related to the different methods used to calculate exchange velocities. A systematic error will cancel when comparing different simulations with the RC model, as in the parametric analyses of the following sections.

In terms of wall and road surface temperatures, the RMSE between RC and CS ranges between 1.7 K and 0.6 K . The reference values for these parameters can be of the same magnitude or even lower, which can be explained by the generic values of CHTC used as inputs of the model. A better agreement of surface temperatures can be obtained by using the average CHTC calculated by the CS. However, these simulations show that these differences in surface temperatures do not have a significant effect on urban air temperatures.

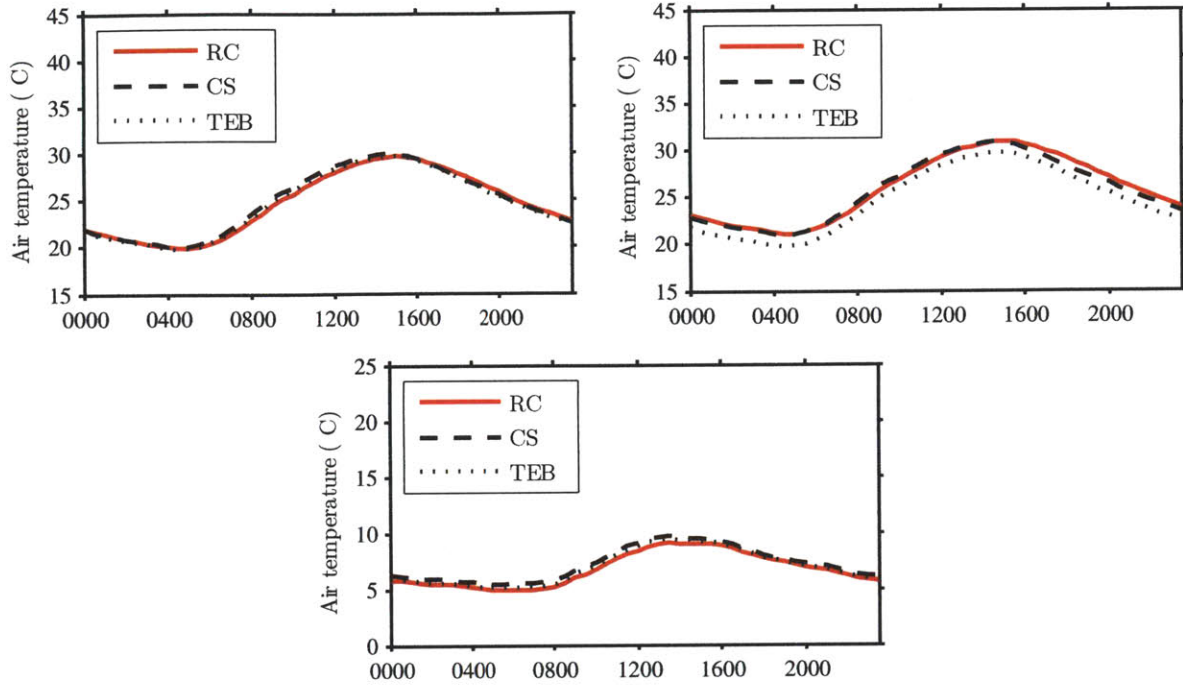


Figure 4.4 – Average diurnal cycle of urban air temperatures of case 1 (top-left) and case 2 (top-right) for summer, July 15 - July 30, and of case 3 (bottom) for winter, February 1 - February 15, calculated by the RC model, by the CS, and by the TEB scheme.

Table 4.3 – Root-mean-square error (RMSE), mean-bias error (MBE), and reference value (REF) of the comparison between the CS and the RC model. The reference value of outdoor air temperature is the average of the difference between the outdoor air temperature calculated by the CS and the atmospheric temperature. The reference value of indoor and outdoor surface temperatures is the average of the difference between the surface temperatures calculated by the CS and the indoor and outdoor air temperature, respectively. The reference value of energy and heat fluxes is the average of the energy and heat fluxes calculated by the CS. The terms urb and fl indicate unit of urban area and floor area, respectively.

Parameter	Case 1			Case 2			Case 3		
	RMSE	MBE	REF	RMSE	MBE	REF	RMSE	MBE	REF
Urban air temperature (K)	0.4	0.2	1.2	0.4	-0.1	2.1	0.5	0.5	0.7
Road surface temperature (K)	1.7	0.7	2.7	1.6	0.4	2.6	0.6	-0.4	-0.7
Exterior wall surface temperature (K)	1.2	-0.3	1.2	1.3	-0.6	1.1	1.5	1.4	0.6
Waste heat emissions (W m^{-2} urb)	6.8	-5.4	55.2	6.2	1.5	219.9	-	-	-
Interior wall surface temperature (K)	0	0	0.7	0.3	0.3	1.8	0.3	-0.3	-1.7
Mass surface temperature (K)	0	0	0.8	0.2	0.2	1.8	0.6	-0.6	-0.7
Transmitted solar radiation (W m^{-2} fl)	1.8	-1.7	2.6	1.8	-1.7	2.6	1.3	-1.2	0.9
Building energy demand (W m^{-2} fl)	1.2	-1.1	6.3	1.8	-1.7	26.6	0.3	0.2	6.4

4.4 Impact of the UHI effect on the energy performance of buildings

In this section, the RC model is used to analyze the impact of the UHI effect on the energy performance of buildings. A series of simulations is carried out imposing outdoor conditions (T_{urb}) to the RC model. This is achieved by using outdoor temperatures as boundary conditions at the top of the urban canyon and introducing a high exchange velocity between the urban canyon and the atmosphere. The outdoor conditions used in this analysis correspond to an UHI scenario measured during the CAPITOU L experiment (Table 4.4). The dependence of the building energy performance to other UHI scenarios is also tested.

Table 4.4 – Nighttime and daytime maximum urban-rural temperature differences that characterize the diurnal cycles of UHI effect used to analyze its impact on the energy performance of buildings.

		Summer	Winter
Design day		07/31/04	02/26/05
Maximum urban-rural temperature difference (K)	Night	4.1	5.3
	Day	0.3	0.9

Five case studies are analyzed (Table 4.5). The first three cases are simulated using summer outdoor conditions and the last two using winter outdoor conditions. Cases 1, 2, 4, and 5 correspond to a residential building with and without insulated walls. Case 3 corresponds to a commercial building with insulated walls.

Table 4.5 – Case studies used to analyze the interactions between buildings and the urban environment. In the insulated cases, the building wall is composed of 30 cm brick and an inner layer of 3 cm insulation. In the uninsulated cases, the building wall is composed of 30 cm brick. Internal heat gain values for the residential and commercial cases, as well as other building and urban parameters are defined in Table 4.1.

Cases	Insulation	Building use	Design day
1	Yes	Residential	Summer
2	No	Residential	Summer
3	Yes	Commercial	Summer
4	Yes	Residential	Winter
5	No	Residential	Winter

Figure 4.5(left) shows the daily-average change in sensible energy demand due to the UHI effect for different building glazing ratios. In Fig. 4.5(right), the energy demand change is divided by the actual energy demand of the building. The graphs show the absolute value of the change in energy demand, which is positive in summer and negative in winter. Fig. 4.5(left) shows that the UHI effect has a greater impact on the building energy performance for higher glazing ratios. As expected, the slope is lower for the cases in which walls are not insulated, and there is a convergence in energy demand change between insulated and uninsulated cases for higher glazing ratios. The fact that the ratio of energy demand change due to the UHI effect is decreasing in summer for higher glazing ratios is explained by the fact that the overall building energy demand increases faster than the energy demand change due to the UHI effect for higher glazing ratios. The results show a small influence of the glazing ratio and wall insulation on the ratio of energy demand change due to the UHI effect.

Figure 4.6 shows the daily-average ratio of energy demand change due to the UHI effect for different infiltration air flowrates and vertical-to-horizontal building area ratios. Infiltration heat gains can be an important fraction of the building energy demand, above all in winter when the temperature difference

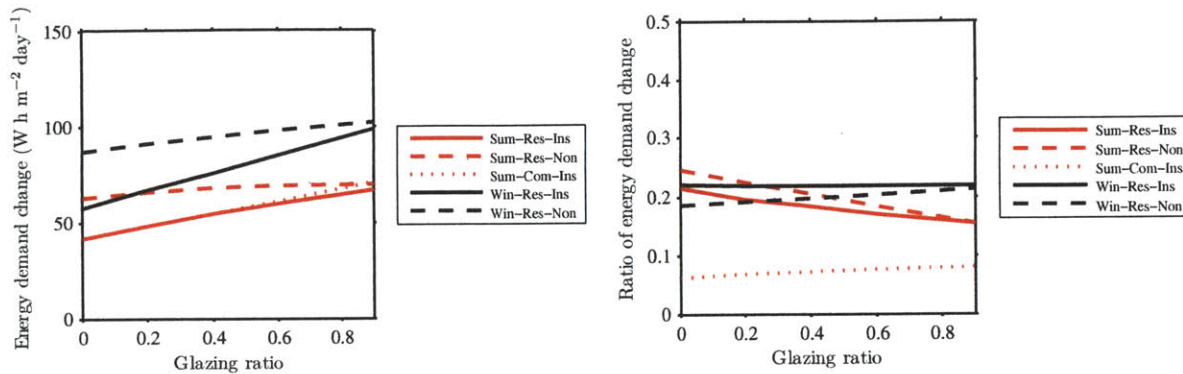


Figure 4.5 – Daily-average change in sensible energy demand due to the UHI effect for different building glazing ratios. The following cases are analyzed: 1. summer, residential, insulated walls; 2. summer, residential, uninsulated walls; 3. summer, commercial, insulated walls; 4. winter, residential, insulated walls; and 5. winter, residential, uninsulated walls. Results are given in absolute form (left) and relative form (right) divided by the overall sensible building energy demand. Other parameter settings are $T_{in} = 22\text{ }^{\circ}\text{C}$, $VH_{bid} = 2$, and $V_o = 0.5$ ACH.

between indoor and outdoor environments is high. The UHI effect modifies the heat gain due to infiltration, increasing the cooling energy demand in summer and decreasing the heating energy demand in winter. The vertical-to-horizontal building area ratio determines the relative amount of building surface area exposed to the outdoor environment and, therefore, affected by the UHI effect by means of heat transmission through walls and windows. The graphs show a significant influence of the infiltration level and weak dependence on the vertical-to-horizontal building area ratio. Having more building surface exposed to the outdoor environment usually implies more infiltration through opening cracks, but this effect is not taken into account in this analysis. The results suggest that the main mechanism by which the UHI effect influences the indoor environment is the outdoor air entering the building, which can be produced by infiltration but also by natural or forced ventilation. The UHI impact from the conductive heat transfer through the building enclosure is relatively small.

Different UHI effect scenarios are represented in Fig. 4.7. The ratio of energy demand change due to these UHI effect scenarios is indicated in Fig 4.8, which shows a linear relationship. For residential buildings in summer, the results show a 5% increase in cooling energy demand per 1 K increase in the maximum UHI effect at night. A similar order-of-magnitude decrease in heating energy demand is also produced by an equivalent wintertime UHI effect. The energy demand of commercial buildings, usually dominated by internal heat gains, are less influenced by the outdoor environment, and therefore not significantly affected by the UHI effect if they do not have building systems with a close interaction with the outdoor environment such as economizers or natural ventilation.

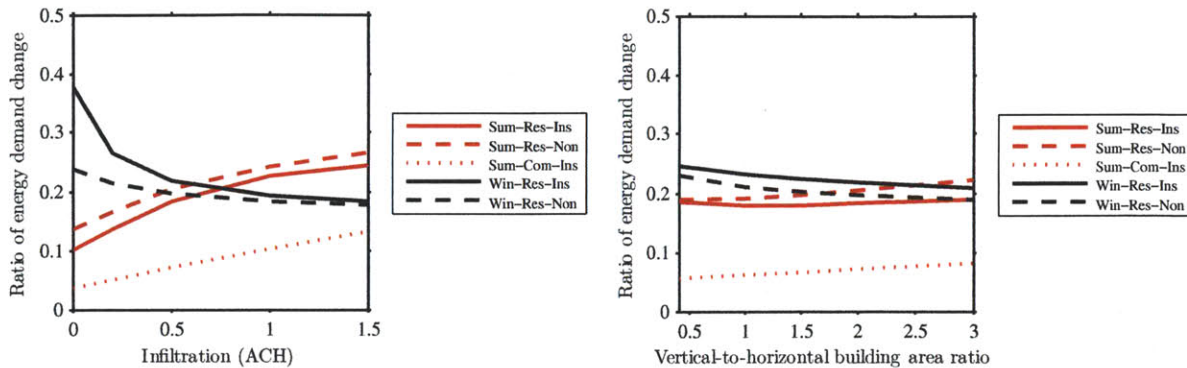


Figure 4.6 – Daily-average change in sensible energy demand due to the UHI effect divided by the overall sensible building energy demand for different infiltration air flowrates (left) and vertical-to-horizontal building area ratios (right). The following cases are analyzed: 1. summer, residential, insulated walls; 2. summer, residential, uninsulated walls; 3. summer, commercial, insulated walls; 4. winter, residential, insulated walls; and 5. winter, residential, uninsulated walls. Other parameter settings are $T_{in} = 22\text{ }^{\circ}\text{C}$, $GR = 0.4$, $VH_{bld} = 2$, and $V_o = 0.5$ ACH.

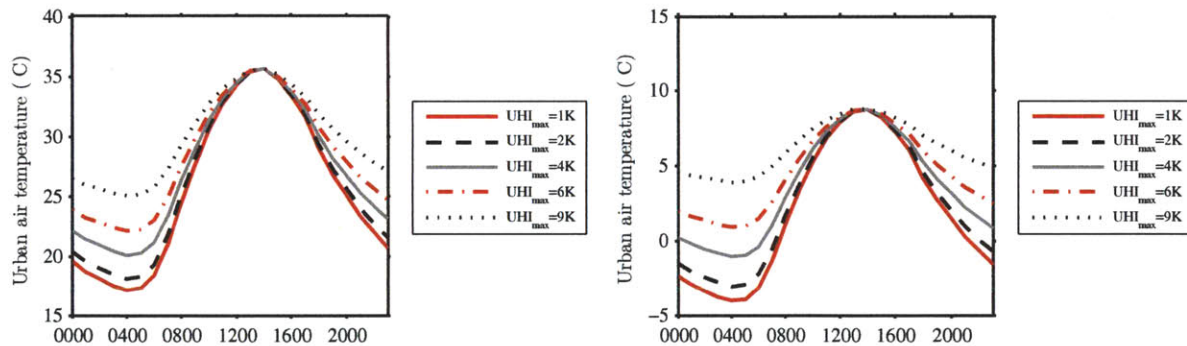


Figure 4.7 – Diurnal cycles of urban air temperature in summer (left) and in winter (right) for different maximum urban-rural air temperature difference.

4.5 Impact of the energy performance of buildings on the outdoor environment

In this section, a parametric analysis is carried out with the RC model to investigate the impact of the indoor energy performance on urban air temperatures. Table 4.6 summarizes the boundary conditions above the urban canyon used in this analysis. The summer and the winter design days correspond to a hot and a cold day, respectively, measured in Toulouse during the CAPITOUl experiment. The average wind speed above the urban canyon is set to 5 m s^{-1} . The dependence of outdoor temperatures to this parameter is also tested. The same five case studies presented in the previous section are analyzed (Table 4.5).

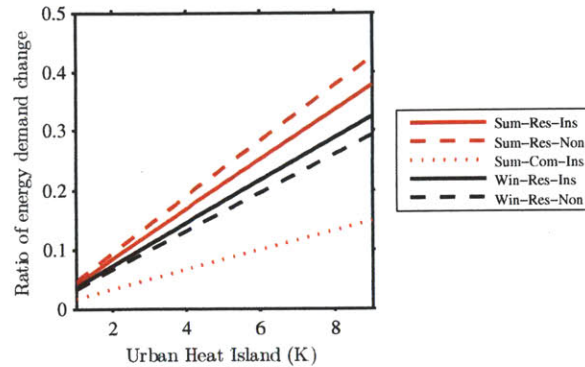


Figure 4.8 – Daily-average ratio of energy demand difference for different maximum urban-rural air temperature difference. The following cases are analyzed: 1. summer, residential, insulated walls; 2. summer, residential, uninsulated walls; 3. summer, commercial, insulated walls; 4. winter, residential, insulated walls; and 5. winter, residential, uninsulated walls. Other parameter settings are $T_{in} = 22\text{ }^{\circ}\text{C}$, $GR = 0.4$, $VH_{bid} = 2$, and $V_o = 0.5\text{ ACH}$.

Table 4.6 – Meteorological conditions above the urban canyon used to analyze the impact of the energy performance of buildings on the outdoor environment.

	Summer	Winter
Design day	07/31/04	01/26/05
Maximum air temperature	35.1 $^{\circ}\text{C}$	-0.2 $^{\circ}\text{C}$
Daily air temperature range	15.6 K	2.8 K
Average wind speed	5.0 m s^{-1}	5.0 m s^{-1}

4.5.1 Effect of the indoor environment without waste heat emissions

Without considering waste heat emissions, a change in the indoor thermal conditions can affect the outdoor environment by heat conduction through the building enclosure, which modifies outdoor surface temperatures and end up affecting outdoor air temperatures by convective heat transfer. A change in the indoor environment can also have an impact on outdoor air temperatures through exfiltration. Assuming that all the air that enters a building through infiltration leaves it at indoor air temperature, there is an exfiltration heat flux associated with the indoor-outdoor temperature difference, which is more important in winter than in summer.

Figure 4.9(left) shows the daily-average difference in outdoor air temperature due to an increase in the indoor air temperature of 5 K in summer and in winter for different building glazing ratios. As can be seen, indoor air temperatures have a small influence on the outdoor environment when there are no waste heat emissions from AC systems and no exfiltration heat.

Figure 4.9(right) shows the daily-average difference in outdoor air temperature due to a change in the exfiltration air flowrate from 0.0 to 0.5 ACH for different indoor air temperatures. As can be seen, exfiltration has an unimportant influence on the outdoor environment in summer, but it might be relevant in some winter situations. Due to the high indoor-outdoor temperature difference, the exfiltration heat flux can be compared to other urban fluxes in a cloudy day in winter.

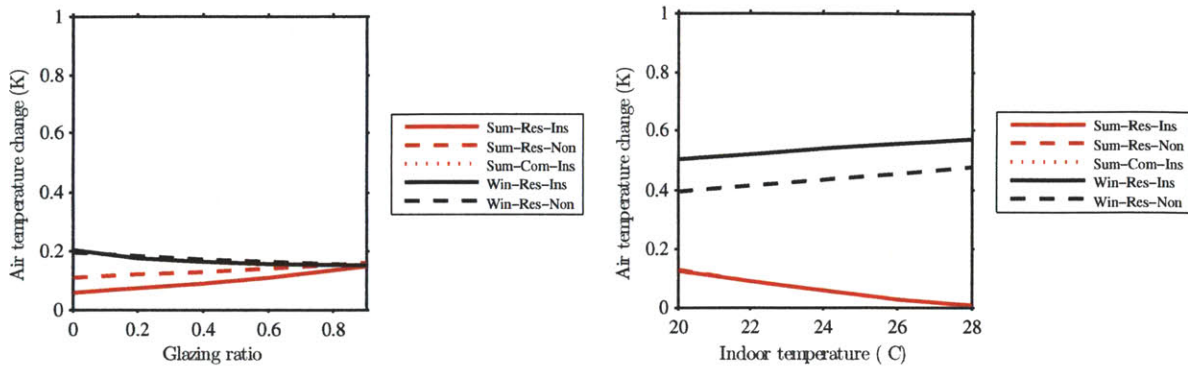


Figure 4.9 – Daily-average difference in outdoor air temperature due to a change in indoor air temperature from 22 °C to 27 °C in summer and from 17 °C to 22 °C in winter for different building glazing ratios (left). Daily-average outdoor air temperature difference due to a change in exfiltration air flowrate from 0.0 to 0.5 ACH for different indoor air temperatures in summer and in winter (right). The following cases are analyzed: 1. summer, residential, insulated walls; 2. summer, residential, uninsulated walls; 3. summer, commercial, insulated walls; 4. winter, residential, insulated walls; and 5. winter, residential, uninsulated walls. Other parameter settings are $\rho_{bld} = 0.5$, $VH_{urb} = 1$, $GR = 0.4$, $f_{waste} = 0.0$, and $V_o = 0.0$ ACH.

4.5.2 Effect of waste heat emissions

Waste heat emissions from HVAC systems are significant sources of heat in the energy balance of an urban canyon. Fig. 4.10(left) shows the daily-average difference in outdoor air temperature due to the waste heat from AC systems in summer for different indoor air temperature values. Daily-average waste heat emissions are represented in Fig. 4.10(right). Commercial buildings, due to their high internal heat gains, have a greater impact on the outdoor environment.

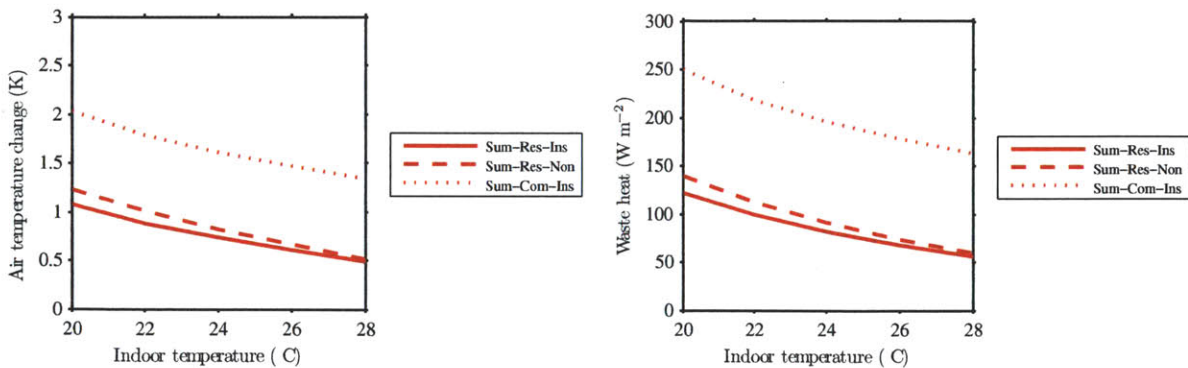


Figure 4.10 – Daily-average difference in outdoor air temperature due to waste heat emissions (left) and waste heat emissions in summer for different indoor air temperatures (right). The following cases are analyzed: 1. summer, residential, insulated walls; 2. summer, residential, uninsulated walls; and 3. summer, commercial, insulated walls. Other parameter settings are $\rho_{bld} = 0.5$, $VH_{urb} = 1$, $V_o = 0.5$ ACH, and $GR = 0.4$.

Figure 4.11 represents the daily-average difference in outdoor air temperature due to waste heat emissions for different building densities. This parameter, typically used in urban planning, has a significant impact on outdoor air temperatures. This can be seen by the fact that to condition bigger indoor spaces

in summer implies pumping more heat into a smaller outdoor environment, and therefore outdoor air temperatures soar.

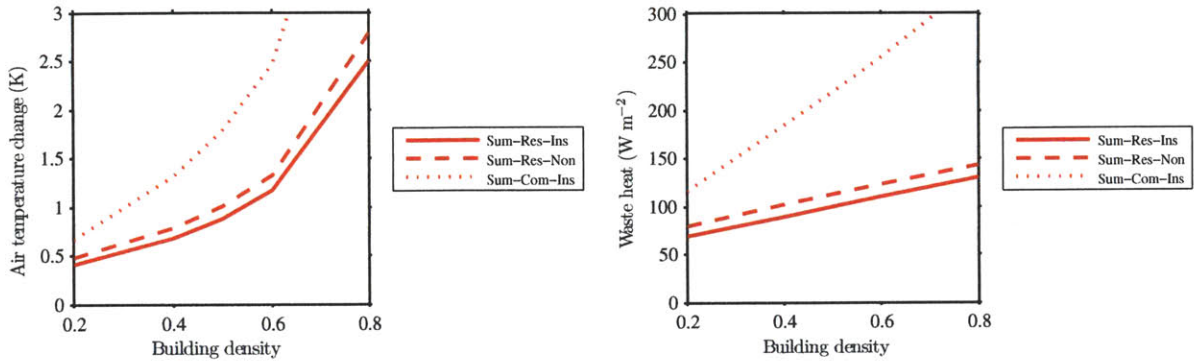


Figure 4.11 – Daily-average difference in outdoor air temperature due to waste heat emissions (left) and waste heat emissions (right) in summer for different building densities. The following cases are analyzed: 1. summer, residential, insulated walls; 2. summer, residential, uninsulated walls; and 3. summer, commercial, insulated walls. Other parameter settings are $VH_{urb} = 1$, $V_o = 0.5$ ACH, $GR = 0.4$, and $T_{in} = 22$ °C.

The wind speed above the urban canopy affects the heat exchange rate between the urban canyon and the atmosphere through the average exchange velocity used in the RC model. Fig. 4.12 shows the dependence of the urban canyon air temperature change due to waste heat emissions on the wind speed above the urban canopy. For the residential cases, in which waste heat emission are around 100 W m^{-2} of urban area, the increase in outdoor temperature ranges between 0.5 K for a wind speed of 10 m s^{-1} and 1 K for a wind speed of 2 m s^{-1} . For the commercial case, in which the average waste heat flux is 220 W m^{-2} of urban area, the increase in outdoor temperature ranges between 1.2 K for a wind speed of 10 m s^{-1} and 2.2 K for a wind speed of 2 m s^{-1} . It can be concluded that, for building densities lower than 0.6, the increase in outdoor air temperature is approximately proportional to the heat flux per unit of urban area released into the urban canyon with a relation of 1 K per 100 W m^{-2} for low wind speeds and 0.5 K per 100 W m^{-2} for high wind speeds.

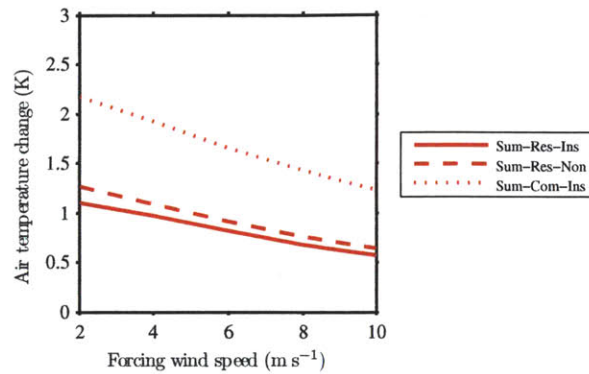


Figure 4.12 – Daily-average difference in outdoor air temperature due to waste heat emissions in summer for different wind speeds above the urban canopy layer. The following cases are analyzed: 1. summer, residential, insulated walls; 2. summer, residential, uninsulated walls; and 3. summer, commercial, insulated walls. Other parameter settings are $\rho_{bld} = 0.5$, $VH_{urb} = 1$, $V_o = 0.5$ ACH, $GR = 0.4$, and $T_{in} = 22$ °C.

Urban climate prediction tool

Chapter 5

The Urban Boundary-Layer model

5.1 Overview

Urban Canopy and Building Energy Models (UC-BEM), such as those presented in chapters 2, 3, and 4, require meteorological information above the urban canopy layer as boundary conditions for their calculations. This information can be provided on-line if the UC-BEM is dynamically coupled with a mesoscale atmospheric model, but can also be measured or simulated off-line (as done in previous chapters). The off-line approach takes advantage of the low computational cost of UC-BEMs in order to effectively perform parametric analyses of urban design criteria. However, this approach assumes that the urban boundary layer is not affected by changes in the urban surface, which is a restrictive assumption if one is interested in contrasted scenarios of urban heat fluxes. Furthermore, meteorological information above the urban canopy layer is only available through short-term experiments, a few permanent urban stations, and mesoscale atmospheric simulation results. This limits the use of UC-BEMs by other communities, such as building engineers and urban planners, who may be interested in urban climate prediction but do not have access to this type of information. On the other hand, meteorological information can be easily found in weather data files obtained from measurements at operational weather stations, usually located in open areas outside the city (e.g. airports).

This chapter presents a methodology to calculate air temperatures above the urban canopy from measurements at operational weather stations. The methodology is physically based and has a computational cost equivalent to UC-BEMs. At each time-step, an Urban Boundary-Layer (UBL) model calculates air temperatures above the urban canopy layer by solving an energy balance for a control volume inside the urban boundary layer. The model requires meteorological information measured at an operational weather station (air temperature at 2 m and wind speed at 10 m), surface sensible heat fluxes, and air temperatures at two different heights above the weather station provided by a Vertical Diffusion Model (VDM). The VDM calculates vertical profiles of air temperature by solving a one-dimensional transient heat diffusion equation. The VDM requires measurements at the operational weather station and rural sensible heat fluxes.

The chapter first describes the physics behind the UBL model and the VDM. Then, both models are evaluated separately by comparing them with three-dimensional high-resolution numerical simulations of an idealized city. These simulations are carried out by climatologists at the CNRM-GAME (France) with the Nonhydrostatic Mesoscale (MESO-NH) atmospheric model [Lafore et al., 1998]. Then, the coupled VDM-UBL scheme is evaluated against field data from two boundary-layer experiments, one

carried out in Basel, Switzerland, in 2002 [Rotach et al., 2005]; and another one carried out in Toulouse, France, during 2004 and 2005 [Masson et al., 2008].

5.2 Model description

The objective of this model is to describe the diurnal evolution of the UHI effect at mesoscale level based on an idealized conceptual model of rural and urban boundary layers as described in Hidalgo et al. [2009] (Fig. 5.1). At nighttime, the longwave radiation exchange between the rural surface and the sky keeps the boundary layer stratified. In contrast, due to the thermal inertia of urban areas and the anthropogenic sources of heat, the nighttime urban boundary layer is mixed. At daytime, the solar radiation heats the rural and urban surfaces and the atmosphere is well mixed up to a high altitude [Stull, 1988]. As a result, the UHI effect (urban-rural air temperature difference) presents a marked diurnal cycle with positive values at nighttime, negative values during the morning, and weak positive values during the afternoon [Oke, 1987].

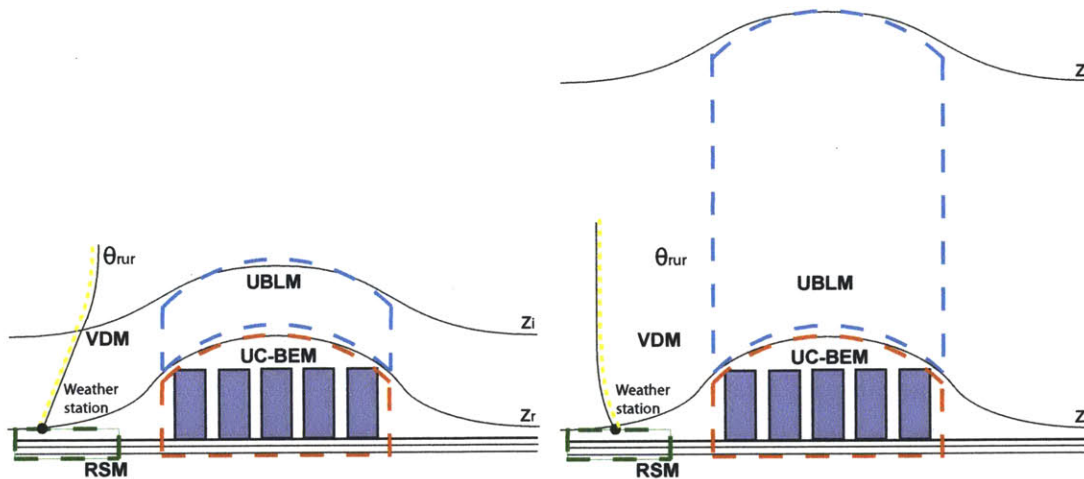


Figure 5.1 – Representation of a city and the physical domain of the four modules that compose the Urban Weather Generator (chapter 6): the Rural Station Model (RSM), the Vertical Diffusion Model (VDM), the Urban Boundary Layer (UBL) model, and the Urban Canopy and Building Energy Model (UC-BEM). The diagram represents nighttime (left) and daytime conditions (right) (not at scale). The VDM calculates vertical profiles of potential temperature (θ_{rur}) at the rural site. The UBL model solves an energy balance at the urban boundary layer between the blending height (z_r) and the boundary-layer height (z_i) to calculate air temperatures above the urban canopy layer.

This chapter uses the concept of potential temperature, which is a magnitude commonly used in meteorology to compare air temperatures at different heights without including the differences in pressure. Potential temperature is defined as the temperature that a parcel of fluid at a certain pressure would acquire if is brought adiabatically to a standard reference pressure.

5.2.1 Urban Boundary-Layer Model

The UBL model is based on an energy balance for a selected control volume inside the urban boundary layer delimited by the blending height (z_r), at which the influences of individual obstacles on vertical profiles or fluxes become horizontally blended, and the boundary-layer height (z_i) (Fig. 5.1). It differentiates between nighttime and daytime urban boundary layers, and between the advection effect driven by a geostrophic wind (forced problem) and by the urban breeze circulation (buoyancy-driven problem) [Hidalgo et al., 2008].

The energy balance of the UBL model is expressed as:

$$V_{CV} \rho c_v \frac{d\theta_{urb}}{dt} = H_{urb} + \int u_{ref} \rho c_p (\theta_{ref} - \theta_{urb}) dA_f, \quad (5.1)$$

where V_{CV} is the control volume, ρ is the air density, c_v is the air specific heat at constant volume, c_p is the air specific heat at constant pressure, θ_{urb} is the average potential temperature of the control volume, H_{urb} is the sensible heat flux at the surface of the control volume [W], θ_{ref} is a reference potential temperature outside the control volume, u_{ref} is a reference air velocity, and A_f is the lateral area of heat exchange between the control volume and its surroundings. In Eq. 5.1, the term on the LHS represents the thermal inertia of the control volume and the second term on the RHS represents the advection effect. The model assumes that the potential temperature is uniform inside the control volume and that there is no significant heat exchange at the top of it.

At daytime, a control volume of the size of the city and height $[z_i]_{day}$ is selected. The reference temperature of Eq. 5.1 is taken as the potential temperature outside the city at a height at which the vertical profile is considered uniform, $\theta_{rur}(z_{ref})$. This temperature is provided by the VDM.

In presence of geostrophic wind, the reference velocity is taken as the air velocity measured at the weather station, $u_{wind}(z_m)$ ($z_m = 10$ m), and the lateral area of heat exchange, A_f , includes the width of the city orthogonal to the wind direction, W . Under urban-breeze circulation at daytime, Hidalgo et al. [2009] proposed the following expression for the characteristic circulation velocity (u_{circ}):

$$u_{circ} = k_w \left(\beta z_i \frac{H_{urb} - H_{rur}}{\rho c_p} \right)^{1/3}, \quad (5.2)$$

where k_w is a constant ($k_w \sim 1$), β is the buoyancy coefficient ($\beta = g\theta^{-1}$), and H_{urb} and H_{rur} are the sensible heat fluxes [W m^{-2}] from the urban and the rural sites, respectively. The problem is assumed to be driven by buoyancy if the circulation velocity is greater than the air velocity measured at the weather station. For this situation, the circulation velocity (Eq. 5.2) is used in the energy balance and the lateral area of heat exchange includes its entire perimeter, P_{city} .

At night, in presence of geostrophic wind, the urban boundary layer is horizontally divided in various control volumes (Fig. 5.2). For the first control volume, the one upstream of the city, the reference potential temperature and wind velocity are assumed to have the following linear vertical profiles:

$$\theta_{rur}(z) = (\theta_{rur}(z_i) - \theta_{rur}(z_r)) \frac{z}{z_i} + \theta_{rur}(z_r), \quad (5.3)$$

and

$$u_{wind}(z) = u_{wind}(z_m) \frac{z}{z_m}, \quad (5.4)$$

where $\theta_{rur}(z_r)$ is the air temperature measured at the weather station ($z_r = 2$ m). $\theta_{rur}(z_i)$ is provided by the VDM, where the boundary-layer height (z_i) is an input of the model. For simplicity, Eq. 5.4

assumes that the air velocity is zero at z_r . For the control volumes downstream of the first one, the reference temperature is assumed to be uniform and given by the temperature of the control volume immediately upstream.

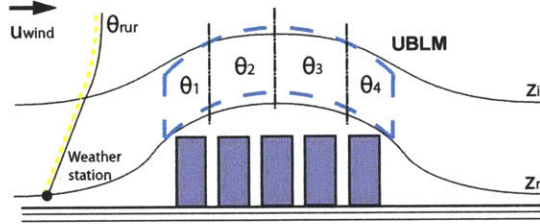


Figure 5.2 – Representation of the nighttime-forced scenario of the UBL model, in which the urban boundary layer is horizontally divided in various control volumes.

Under urban-breeze circulation at nighttime, the circulation velocity obtained by Eq. 5.2 is also used for the reference air velocity of Eq. 5.1, although this velocity scale was initially developed for daytime conditions (indeed, the circulation velocity scale proposed by Lu et al. [1997] for nighttime is equivalent to Eq. 5.2). The reference air temperature is assumed to have also a linear vertical profile (Eq. 5.3).

To simplify the mathematical formulation of the UBL model, the height reference is taken at z_r (e.g. $[z_i]_{model} = [z_i]_{real} - [z_r]_{real}$ and $[z_r]_{model} = 0$). The numerical method used to solve Eq. 5.1 is implicit Euler, in which $\frac{d\theta_{urb}}{dt} = \frac{\theta_{urb} - \theta_{urb}^-}{\delta}$, where δ is the simulation time-step. Then, Eq. 5.1 can be expressed as:

$$\theta_{urb} - \theta_{urb}^- = C_{surf} + C_{adv}\theta_{eq} - C_{adv}\theta_{urb}, \quad (5.5)$$

where C_{surf} , C_{adv} and θ_{eq} are calculated for each scenario according to Table 5.1.

Table 5.1 – Surface coefficient (C_{surf}), advection coefficient (C_{adv}), and equivalent temperature (θ_{eq}) used in Eq. 5.5 for each scenario. θ_{rur} is the potential temperature outside the city at different heights $\{z_r, z_i, \text{ and } z_{ref}\}$. θ_{n-1} is the average potential temperature of the control volume upstream of the one considered. H_{urb} is the urban sensible heat flux [W m^{-2}].

Night	C_{surf}	C_{adv}	θ_{eq}
Forced (first)	$\frac{H_{urb}\delta}{z_i\rho c_v}$	$\frac{u_{wind}(z_m)z_i\delta c_p}{2z_m d x c_v}$	$\frac{2}{3}\theta_{rur}(z_i) + \frac{1}{3}\theta_{rur}(z_r)$
Forced (rest)			θ_{n-1}
Buoyancy-driven	$\frac{H_{urb}\delta}{z_i\rho c_v}$	$\frac{P_{city}\mu_{circ}\delta c_p}{A_{city}c_v}$	$\frac{1}{2}\theta_{rur}(z_i) + \frac{1}{2}\theta_{rur}(z_r)$
Day			
Forced	$\frac{H_{urb}\delta}{z_i\rho c_v}$	$\frac{Wu_{wind}(z_m)\delta c_p}{A_{city}c_v}$	$\theta_{rur}(z_{ref})$
Buoyancy-driven	$\frac{H_{urb}\delta}{z_i\rho c_v}$	$\frac{P_{city}\mu_{circ}\delta c_p}{A_{city}c_v}$	$\theta_{rur}(z_{ref})$

5.2.2 Vertical Diffusion Model

The VDM calculates the vertical profiles of potential temperature above the weather station by solving the following heat diffusion equation:

$$\frac{\partial \theta(z)}{\partial t} = -\frac{1}{\rho(z)} \frac{\partial}{\partial z} \left(\rho(z) K_d(z) \frac{\partial \theta(z)}{\partial z} \right), \quad (5.6)$$

where z is the vertical space component, ρ is the air density, and K_d is a diffusion coefficient. The lower boundary condition of Eq. 5.6 is the temperature measured at the weather station $\theta(z_r)$. The upper boundary condition accounts for the fact that at a certain height ($z_{ref} \sim 200$ m), the profile of potential temperature is uniform and $\frac{\partial \theta}{\partial z}|_{z_{ref}} = 0$.

The difficulty of calculating vertical temperature profiles through a diffusion equation lies in the calculation of the diffusion coefficient K_d . In some atmospheric models, such as the MESO-NH model, this coefficient is related to the turbulent kinetic energy (TKE) at each vertical level [Bougeault and Lacarrere, 1989]:

$$K_d = C_k l_k E^{1/2}, \quad (5.7)$$

where E is the TKE, C_k is a model parameter set equal to 0.4, and l_k is a length scale. In these models, a prognostic equation for the TKE is then solved as a function of the temperature and velocity fields [Martilli et al., 2002], so coupled equations for the air velocity components have also to be computed. This approach adds excessive complexity and computational cost to this particular application, in which the uncertainties associated with urban climate prediction limit the reachable accuracy level. A simpler approach, proposed by Hong et al. [2006], calculates K_d based on correlations as a function of a mixed-layer velocity scale and the planetary boundary layer height, which has to be calculated iteratively.

The VDM proposes an alternative and robust solution, which combines the two approaches mentioned above. The diffusion coefficient is calculated by Eq. 5.7 and the TKE at each vertical level is approximated by:

$$E = \max(w_s^2, E_{min}), \quad (5.8)$$

where w_s is the mixed-layer velocity scale and E_{min} is set equal to $0.01 \text{ m}^2 \text{ s}^{-2}$. Atmospheric models usually establish a minimum TKE given the difficulties of predicting very stable boundary layers [Bravo et al., 2008]. A comprehensive description of the VDM is presented in appendix C.

5.3 Model evaluation

5.3.1 Comparison with mesoscale atmospheric simulations

This section presents a separate evaluation of the VDM and the UBL model through a comparison with idealized three-dimensional simulations carried out by J. Hidalgo from the CNRM-GAME (France) with the MESO-NH atmospheric model. The horizontal domain is $80 \text{ km} \times 80 \text{ km}$ with a circular city in the middle ($D = 10 \text{ km}$). The effects of the perturbations created by the city in the mean flow typically have a horizontal extent two to three times the size of the city [Hidalgo et al., 2008], so the horizontal domain was large enough to prevent interferences from the cyclic boundary conditions. The horizontal grid resolution was set to 500 m . The vertical coordinate was composed of 56 levels over a vertical

domain of 4 km. Vertical resolution varies from 4 m near the surface to 250 m on the top of the domain. The subgrid turbulence was parameterized following the scheme of Cuxart et al. [2000] and the mixing length of Bougeault and Lacarrere [1989].

Figure 5.3 represents the diurnal cycles of urban and rural surface heat fluxes imposed in the simulations. The integral of the difference between urban and rural sensible heat fluxes during one day of simulation (ΣH), the capping inversion height (z_{inv}), and the zonal wind force (u_{ref}) were used as external forcing parameters (the capping inversion height is the same as the boundary layer height at daytime). A set of these three parameters was chosen and fixed for each simulation. Simulations are carried out for $\Sigma H = \{1350 \text{ W h m}^{-2} \text{ and } 650 \text{ W h m}^{-2}\}$, $z_{inv} = \{1000 \text{ m and } 1500 \text{ m}\}$, and $u_{ref} = \{0 \text{ m s}^{-1}, 4 \text{ m s}^{-1}, \text{ and } 8 \text{ m s}^{-1}\}$. The roughness length was set to $z_{0r} = 0.01 \text{ m}$ for rural surfaces and $z_{0u} = 1.0 \text{ m}$ for urban surfaces. The meteorological context was an idealized anticyclonic summer situation representative of Southern France.

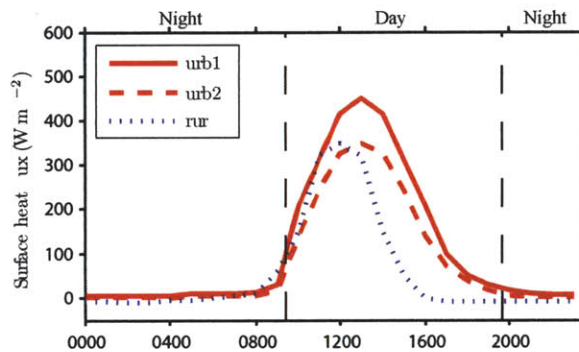


Figure 5.3 – Diurnal cycles of rural and urban sensible heat flux imposed in the mesoscale simulations for the cases of aggregated urban-rural difference $\Sigma H = \{1350 \text{ W h m}^{-2} \text{ (urb1) and } 650 \text{ W h m}^{-2} \text{ (urb2)}\}$. The model considers daytime when H_{urb} reaches 80 W m^{-2} in the morning and nighttime when H_{urb} drops below 30 W m^{-2} in the afternoon.

The simulation results used in this analysis correspond to a vertical plane passing through the city center. Rural conditions at different heights are taken as the horizontal average of the mesh points contained in a line of length D centered at a distance $D/2$ upwind of the city edge. Urban conditions are taken as the average of the mesh points contained in a plane of width D centered at the city center and height z_i .

Figure 5.4 shows the contours of potential temperature above and around the idealized city at nighttime. It can be seen that the urban boundary layer presents a horizontal distribution of air temperature due to the advection effect that could be captured by the discretization of the UBL model at nighttime (Fig. 5.2). Still, this feature is not tested in this comparison, and the average temperature above the city is used. It can also be noted that the effect of the city on the first atmospheric layers is almost restricted to its horizontal area. A rural boundary layer is formed soon after the edge of the city, affecting the region near the surface. The plume of the city may influence downstream rural areas but above the measurement height of air temperature. This means that, excluding micro-climate effects, a weather station located outside and downstream of the city would measure similar conditions as one located upstream of the city.

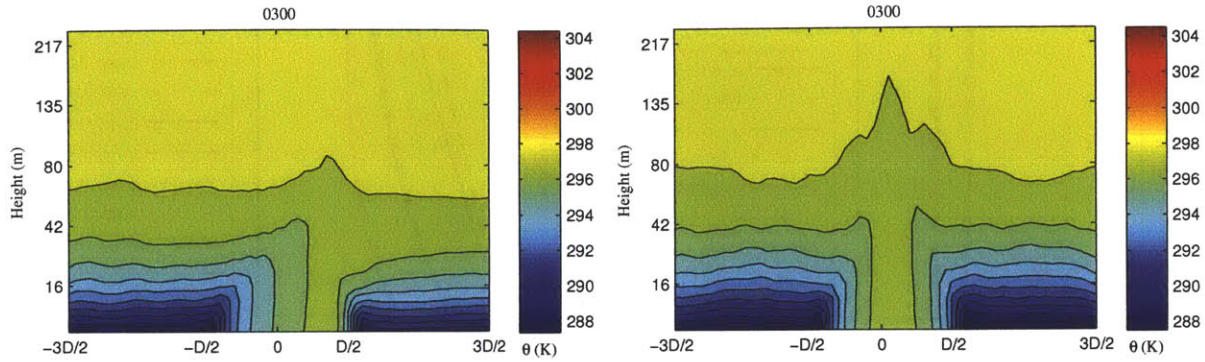


Figure 5.4 – Lower atmosphere nighttime contours of potential air temperature over a city of diameter D and its surroundings in the presence of a geostrophic wind ($u_{ref} = 4 \text{ m s}^{-1}$) (left) and under urban-breeze circulation ($u_{ref} = 0 \text{ m s}^{-1}$) (right) calculated by the mesoscale simulation for the case $\Sigma H = 1350 \text{ W h m}^{-2}$ and $z_{inv} = 1000 \text{ m}$.

Figures 5.5 and 5.6 compare the vertical profiles of potential temperature at the rural site for different zonal wind forces. It can be seen that the VDM is able to reproduce the daytime and nighttime vertical distribution of potential temperature calculated by the mesoscale simulations. Some differences appear in the night-day transition period, due to the different turbulence models used by the VDM and the Meso-NH model. The capacity of the VDM to predict $\theta([z_i]_{night})$ and $\theta([z_{ref}]_{day})$, which are the parameters required by the UBL model, is evaluated in Table 5.2. The root-mean-square error (RMSE) of $\theta([z_i]_{night})$ between the VDM and the mesoscale simulations ranges between 0.6 and 0.9 K, which is lower than the expected error of the UBL model ($\sim 1 \text{ K}$). The RMSE of $\theta([z_{ref}]_{day})$ ranges between 0.5 and 0.9 K. In this case, the mean-bias error (MBE) is always positive indicating a systematic overprediction of this temperature as compared to the mesoscale simulations. This can be explained by the fact that the VDM does not account for the longwave radiation exchange between the air and the upper atmosphere.

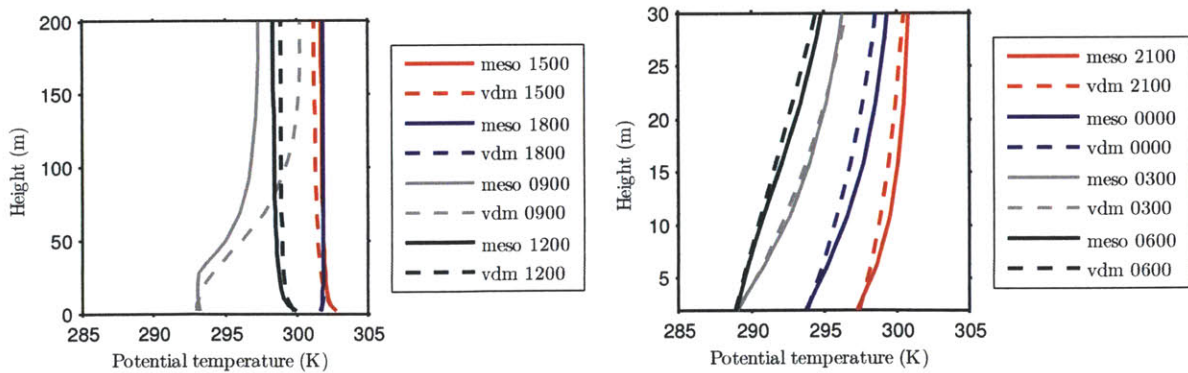


Figure 5.5 – Vertical profiles of potential temperature at daytime (left) and at nighttime (right) calculated by the VDM and by the mesoscale simulations for the case $\Sigma H = 1350 \text{ W h m}^{-2}$, $z_{inv} = 1000 \text{ m}$, and $u_{ref} = 0 \text{ m s}^{-1}$.

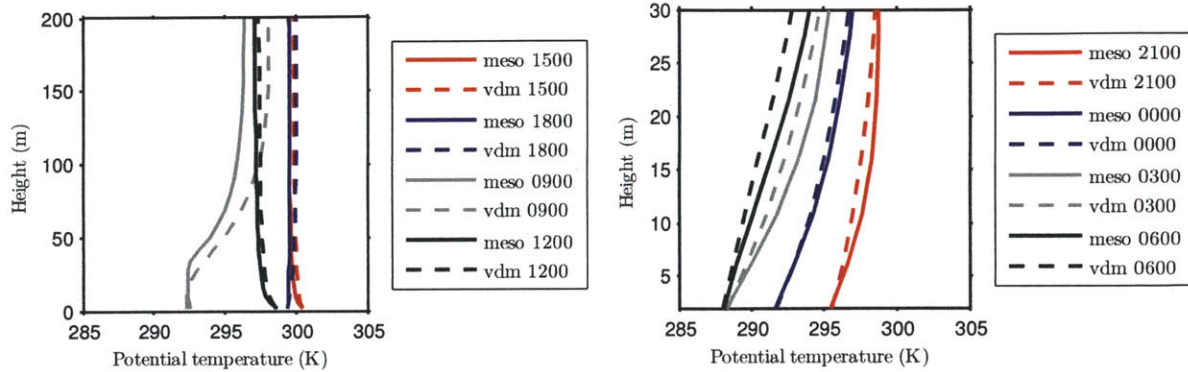


Figure 5.6 – Vertical profiles of potential temperature at daytime (left) and at nighttime (right) calculated by the VDM and by the mesoscale simulations for the case $\Sigma H = 650 \text{ W h m}^{-2}$, $z_{inv} = 1500 \text{ m}$, and $u_{ref} = 4 \text{ m s}^{-1}$.

Table 5.2 – Root-mean-square error (RMSE) and mean-bias error (MBE) between the potential temperature calculated by the VDM and by the mesoscale simulation at $[z_i]_{night}$ and $[z_{ref}]_{day}$ for different zonal wind forces (u_{ref}), aggregated surface heat fluxes (ΣH), and capping inversion heights (z_{inv}).

Mesoscale cases	$u_{ref} \text{ (m s}^{-1}\text{)}$	$z_{inv} = 1000 \text{ m}$ $\Sigma H = 1350 \text{ W h m}^{-2}$		$z_{inv} = 1500 \text{ m}$ $\Sigma H = 650 \text{ W h m}^{-2}$	
		RMSE (K)	MBE (K)	RMSE (K)	MBE (K)
$[z_i]_{night}$	0	0.6	0.0	0.6	0.5
	4	0.8	0.3	0.6	-0.3
	8	0.9	0.2	0.8	-0.4
$[z_{ref}]_{day}$	0	0.9	0.3	0.5	0.3
	4	0.7	0.5	0.5	0.4
	8	0.7	0.6	0.6	0.6

The input parameters used by the UBL model for the comparison with mesoscale simulations are detailed in Table 5.3. The model requires rural air temperatures at three different heights $\{\theta(z_r), \theta([z_i]_{night}), \theta([z_{ref}]_{day})\}$, which are provided by the mesoscale simulation results at the rural site (for the purpose of this comparison since they are normally provided by the VDM). The same diurnal cycles of surface heat fluxes imposed to the mesoscale simulations are used in the UBL model (Fig. 5.3).

Figures 5.7 and 5.8 compare the average potential temperatures of the urban boundary layer calculated by the UBL model with the average urban and rural boundary-layer temperatures calculated by the mesoscale simulation for different situations in terms of capping inversion height, surface heat flux and zonal wind force. Differences in air temperature, computed as RMSE and MBE between the model and the mesoscale simulations, are presented in Table 5.4. The RMSE ranges between 0.9 and 1.3 K, where the daily-maximum urban-rural temperature difference calculated by the mesoscale model ranges between 1.8 and 2.5 K. This error is acceptable given the important uncertainties associated with urban climate predictions. The MBE is generally low indicating that there are no systematic errors in the model. Note that the UHI effect calculated with the mesoscale model does not make use of the near-surface air temperature, which would come from an UC-BEM.

Figures 5.7 and 5.8 show that the difference in daytime urban sensible heat flux (Fig. 5.3) produces

Table 5.3 – Modeling inputs used in the comparison of the UBL model with mesoscale simulations. Other inputs of the model are rural air temperatures at three different heights $\{\theta(z_r), \theta([z_i]_{night}), \theta(z_{ref})\}$ and the wind speed at z_m calculated by the mesoscale simulation. The same diurnal cycles of rural and urban surface heat fluxes are imposed on the UBL model and to the mesoscale simulations.

Parameter	Settings
Simulation time-step	$\delta = 300$ s
Characteristic length of the city	$D, W = 10000$ m
Perimeter of the city	$P_{city} = 4D$
Horizontal area of the city	$A_{city} = D^2$
Horizontal discretization for scenario night-forced	$dx = D/4$
Nighttime boundary-layer height	$[z_i]_{night} - z_r = 30$ m
Daytime boundary-layer height	$[z_i]_{day} = 1000$ m
Reference height	$[z_{ref}]_{day} = 200$ m
Rural roughness length	$z_{0r} = 0.01$ m
Circulation velocity coefficient	$k_w = 1.2$

a relatively constant change in the air temperature of the urban boundary layer during the day. The wind speed does not have significant impact on the average urban boundary-layer temperature, a feature that is captured by both the mesoscale model and the UBL model.

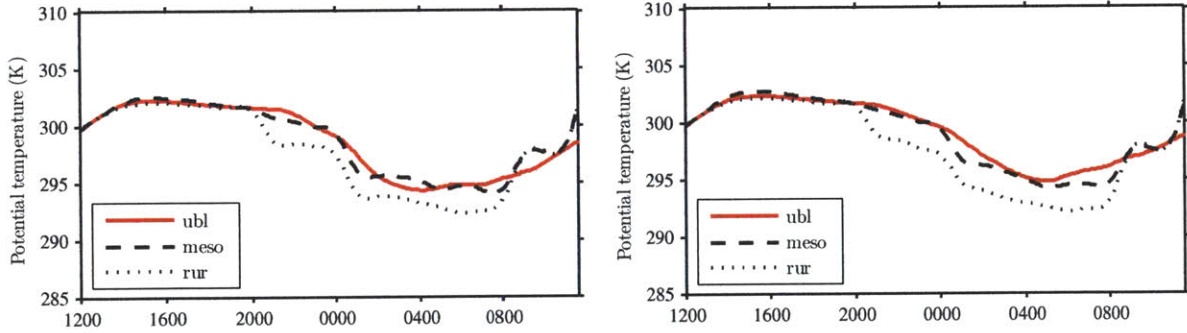


Figure 5.7 – Diurnal cycle of the average potential temperature over the urban boundary layer calculated by the UBL model and by the mesoscale simulation for the case $\Sigma H = 1350 \text{ W h m}^{-2}$, $z_{inv} = 1000$ m, and $u_{ref} = \{ 4 \text{ m s}^{-1}$ (left), 0 m s^{-1} (right) $\}$. The diurnal cycle of the average potential temperature over the rural boundary layer calculated by the mesoscale simulation is also represented (rur).

Table 5.4 – Root-mean-square error (RMSE) and mean-bias error (MBE) between the average potential temperature of the urban boundary layer calculated by the UBL model and by the mesoscale simulation for different aggregated surface heat fluxes (ΣH), capping inversion heights (z_{inv}), and zonal wind forces (u_{ref}). Errors are compared to the daily-maximum urban-rural temperature difference calculated by the mesoscale simulation (UHI_{max}).

Mesoscale cases	$z_{inv} = 1000$ m $\Sigma H = 1350 \text{ W h m}^{-2}$			$z_{inv} = 1500$ m $\Sigma H = 650 \text{ W h m}^{-2}$		
	u_{ref} (m s^{-1})	RMSE (K)	MBE (K)	UHI_{max} (K)	RMSE (K)	MBE (K)
0	0.9	0.1	2.4	1.3	-0.1	2.4
4	0.9	-0.2	2.5	1.2	-0.4	2.0
8	0.9	-0.1	2.1	1.0	-0.3	1.8

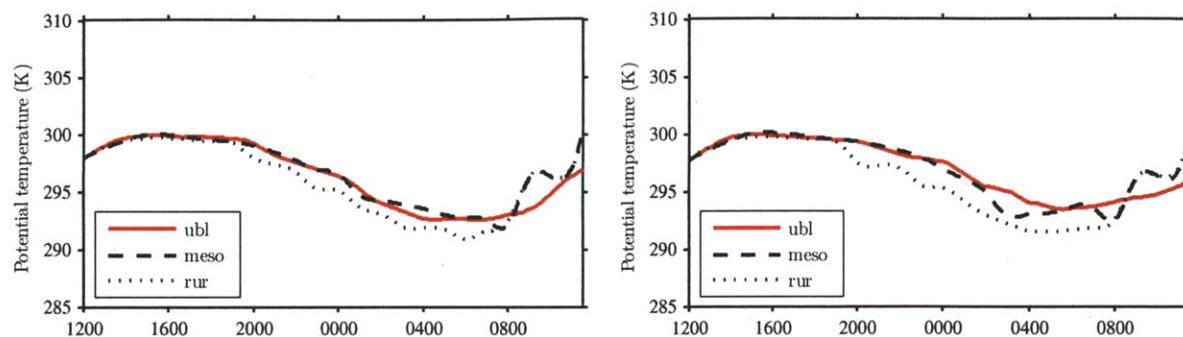


Figure 5.8 – Diurnal cycle of the average potential temperature over the urban boundary layer calculated by the UBL model and by the mesoscale simulation for the case $\Sigma H = 650 \text{ W h m}^{-2}$, $z_{inv} = 1500 \text{ m}$, and $u_{ref} = \{ 4 \text{ m s}^{-1} \text{ (left)}, 0 \text{ m s}^{-1} \text{ (right)} \}$. The diurnal cycle of the average potential temperature over the rural boundary layer calculated by the mesoscale simulation is also represented (rur).

5.3.2 Comparison with field data from Basel, Switzerland, and Toulouse, France

In this section, the VDM-UBL scheme is compared with field data from two boundary-layer experiments: the intensive observational period (IOP) of the BUBBLE experimental campaign, carried out in Basel (Switzerland) between June 10 and July 10, 2002 [Rotach et al., 2005]; and the CAPITOUL experimental campaign carried out in Toulouse (France) from February 2004 to March 2005 [Masson et al., 2008]. The climate information of both sites is characterized in Table 5.5.

Table 5.5 – Monthly normals of climate variables in Basel, Switzerland, and Toulouse, France. *Sources:* MeteoSwiss (www.meteoschweiz.ch), Info Climat (www.infoclimat.fr), and Climate Temp (www.climatetemp.info).

Variable	Site	Jan	Feb	Mar	Apr	May	Jun	Jul	Aug	Sep	Oct	Nov	Dec
Min Temperature (° C)	Basel	-2	-1	2	4	8	11	13	13	10	7	2	-1
	Toulouse	2	3	4	7	10	13	15	15	13	10	5	3
Max Temperature (° C)	Basel	4	6	10	14	18	22	24	23	20	15	8	4
	Toulouse	9	11	13	16	20	24	27	27	24	19	13	9
Mean Temperature (° C)	Basel	1	2	6	9	13	16	19	18	15	10	5	2
	Toulouse	5	7	9	11	15	18	21	21	19	14	9	6
Mean Wind Speed (m s ⁻¹)	Basel	3	3	3	2	2	2	2	2	2	3	3	3
	Toulouse	3	3	3	3	3	3	3	2	2	2	2	3
Mean Precipitation (mm)	Basel	53	40	48	55	76	93	86	94	79	60	56	44
	Toulouse	55	55	58	64	73	58	41	47	48	52	49	56

In both experiments, weather data is measured simultaneously at rural and urban sites from both in-canopy and above-canopy stations (Fig. 5.9). The evaluation of the VDM-UBL scheme consists of introducing 2-m rural weather data as inputs in the model and comparing the calculated and observed forcing air temperatures above the urban canopy layer.

In addition, during the CAPITOUL experiment, radiosondes (Vaisala RS92) were launched from various rural and urban locations. As the balloons ascended, meteorological data were recorded each second. This led to a vertical resolution of approximately 5 m. In this analysis, the measurements from radiosondes launched at a rural site 17 km Northwest from Toulouse are compared to the VDM.

From the network of weather stations of the CAPITOUL experiment (Fig. 6.5), the station located

at Mondouzil is assumed to be representative of rural conditions, and the station located next to the Monoprix building in the dense urban center of Toulouse is selected as representative of urban conditions.

The main urban experimental site in BUBBLE is Basel-Sperrstrasse. The site represents a heavily built-up part of the city center of Basel, mainly composed of residential buildings. The Grenzach weather station, inside the valley of the Rhine River, is used as the reference rural station.

Modeling input parameters are detailed in Table 5.6. City characteristic lengths of 7.5 km and 5 km for Toulouse and Basel, respectively, are estimated based on aerial views of the cities. Rural and urban sensible heat fluxes are obtained from the Rural Station Model (RSM) and the UC-BEM presented in chapter 6. Similar results are obtained by using the measurements of sensible heat fluxes from each experiment. A comparison of observed and calculated sensible heat fluxes is presented in section 6.3.4.



Figure 5.9 – Images of the weather stations of Sperrstrasse (top-left) and Grenzach (top-middle) in Basel, Switzerland, and of the weather stations of Monoprix (top-right) and Mondouzil (bottom) in Toulouse, France.

Vertical profiles of potential temperature obtained with the VDM are compared with measurements from the radiosondes. Fig. 5.10 compares calculated and measured vertical profiles for a day in winter and a day in summer, respectively. Given the simplicity of the VDM, the results show a reasonably good agreement with observations. The vertical shape of the profiles is reasonably well captured by the model, although the temperature values at the weather station, which are used as boundary conditions by the VDM, were not measured at the same location as where the radiosondes were launched.

The capacity of the VDM-UBL scheme to predict forcing air temperatures above the urban canopy layer is evaluated. Calculated monthly-average diurnal cycles are compared with observations at the urban site for summer, fall, and winter in CAPITOU (Fig. 5.11) and for summer in BUBBLE (Fig. 5.12). Air temperature measurements at 2 m at the rural site are also represented. As can be seen, the VDM-UBL scheme is able to capture both the UHI effect observed at night and the Urban Cool

Table 5.6 – Modeling inputs used in the comparison of the VDM-UBL scheme with field data from the experiments CAPITOU and BUBBLE. The scheme also requires $\theta(z_r)$ and $u(z_m)$ from measurements at the rural site. $\theta(z_i]_{night})$ and $\theta(z_{ref})$) are provided by the VDM to the UBL model. Rural and urban sensible heat fluxes are obtained from the RSM and the UC-BEM presented in chapter 6.

Parameter	Settings
Location	CAPITOU: Toulouse BUBBLE: Basel
Characteristic length of the city	CAPITOU: 7500 m BUBBLE: 5000 m
Simulation time-step	300 s
Weather data time-step	3600 s
Nighttime boundary-layer height	50 m
Daytime boundary-layer height	1000 m
Reference height	200 m
Rural roughness length	0.01 m
Circulation velocity coefficient	1.2

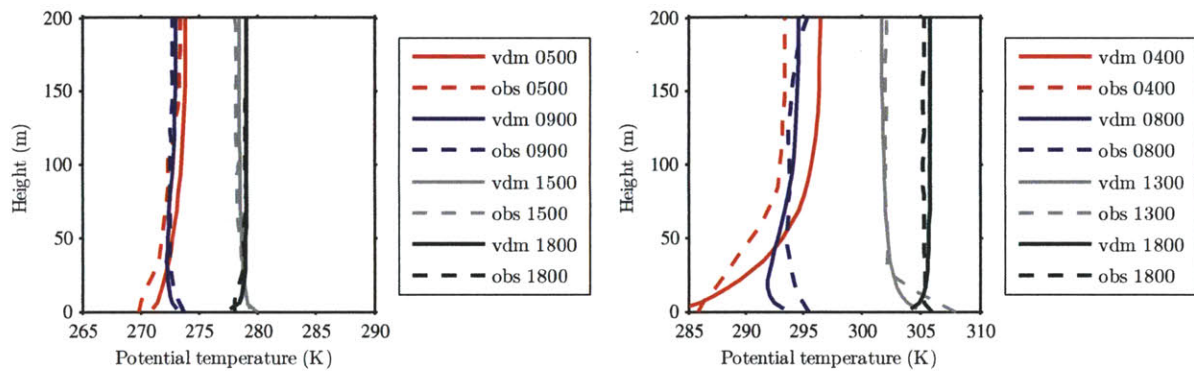


Figure 5.10 – Vertical profiles of potential temperature calculated by the VDM and observed during the CAPITOU experiment on March 2, 2005 (left), and on July 4, 2004 (right).

Island (UCI) effect observed in the morning. Here, the UHI and UCI effects are defined as the difference between the forcing air temperatures above the urban canopy layer and the rural air temperature measured at 2 m.

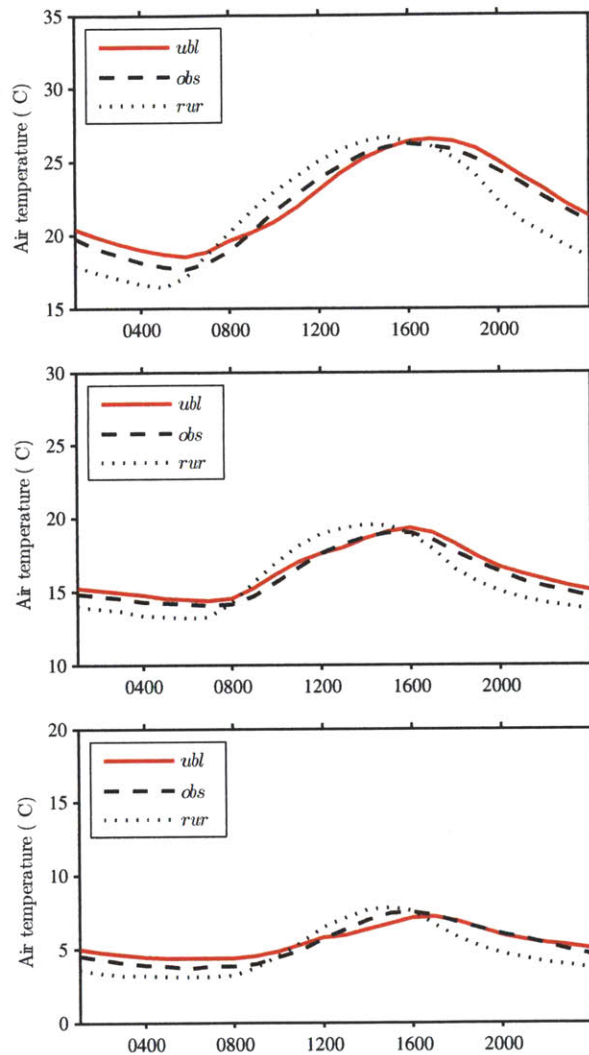


Figure 5.11 – Monthly-average diurnal cycle of forcing air temperatures above the urban canopy layer calculated by the VDM-UBL scheme and observed during the CAPITOUL experiment for July (top) and October (middle), 2004, and January (bottom), 2005, in the dense urban area of Toulouse. Monthly-average diurnal cycles of measured rural air temperatures (rur) for the same period are also represented.

Statistical results of this comparison are presented in Table 5.7. The RMSE between the model and observations ranges between 0.9 K and 1.2 K for both experiments, where the average daily-maximum UHI effect is 4.4 K in BUBBLE, 2.5 K in summer in CAPITOUL, and about 1.3 K in fall and winter in CAPITOUL. The MBE is small in all cases, which indicates that there are no systematic errors in the model.

A sensitivity analysis of the model indicates that values of $[z_i]_{night}$ between 30 m and 100 m have an impact of ± 0.1 K on the results. No significant variations are obtained for $[z_i]_{day}$ between 800 m and 2000 m. Chapter 6 extends the sensitivity analysis to other parameters of the model.

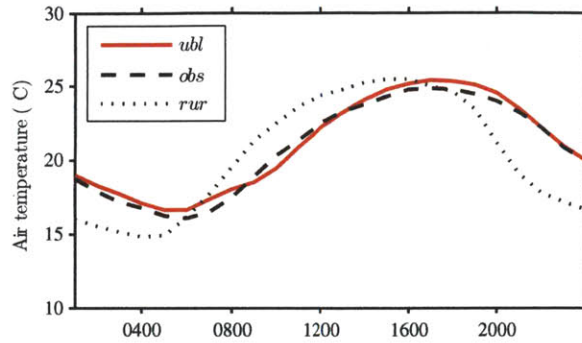


Figure 5.12 – Monthly-average diurnal cycle of forcing air temperatures above the urban canopy layer calculated by the VDM-UBL scheme and observed during the BUBBLE experiment between June 10 and July 10, 2002. Monthly-average diurnal cycle of measured rural air temperature (rur) for the same period is also represented.

Table 5.7 – Root-mean-square error (RMSE) and mean-bias error (MBE) between the forcing air temperatures above the urban canopy layer calculated by the UWG and observed during BUBBLE experiment between June 10 and July 10, 2002; and between the urban air temperatures calculated by the UWG and observed during CAPITOUL experiment in July and October, 2004, and January, 2005. Errors are compared with the average daily-maximum UHI effect ($\overline{UHI_{max}}$) observed during each period, defining the UHI effect as the difference between the forcing air temperatures above the urban canopy layer and the rural air temperature measured at 2 m.

Month	RMSE (K)	MBE (K)	$\overline{UHI_{max}}$ (K)
BUBBLE			
Summer	1.0	0.2	4.4
CAPITOUL			
Summer	1.0	0.3	2.5
Fall	0.9	0.3	1.3
Winter	1.2	0.2	1.4

Chapter 6

The Urban Weather Generator

6.1 Overview

This chapter combines models previously presented in this thesis to propose an integrated Urban Weather Generator (UWG) that calculates urban air temperature and humidity using meteorological information measured at an operational weather station located in an open area outside the city.

The UWG is a computationally efficient model based on energy conservation principles. It can be integrated into existing programs in order to account for site-specific urban weather files in building energy simulations. It can also be converted into a fully-operative program to predict building energy consumption at urban scale and the UHI effect, taking into account the energy interactions between buildings and the urban climate.

This chapter first describes the physics behind the UWG. Then, the model is evaluated against field data from the experiment BUBBLE (Basel, Switzerland) and the experiment CAPITOUL (Toulouse, France).

6.2 Model description

The UWG calculates hourly values of urban air temperature and humidity given the weather data measured at an operational weather station located outside a city. The model is composed of four coupled modules (Fig. 6.1): the Rural Station Model (RSM), which calculates sensible heat fluxes at the weather station; the Vertical Diffusion Model (VDM), which calculates vertical profiles of air temperature above the rural site; the Urban Boundary-Layer (UBL) model, which calculates air temperatures above the urban canopy layer (above urban canyons); and the Urban Canopy and Building Energy Model (UC-BEM), which calculates urban sensible heat fluxes and urban canyon air temperature and humidity. The interrelations between modules are illustrated in Fig. 6.2. The atmospheric component of the UWG, composed of the VDM and UBL model, is described in detail in chapter 5. This chapter describes the RSM and the UC-BEM.

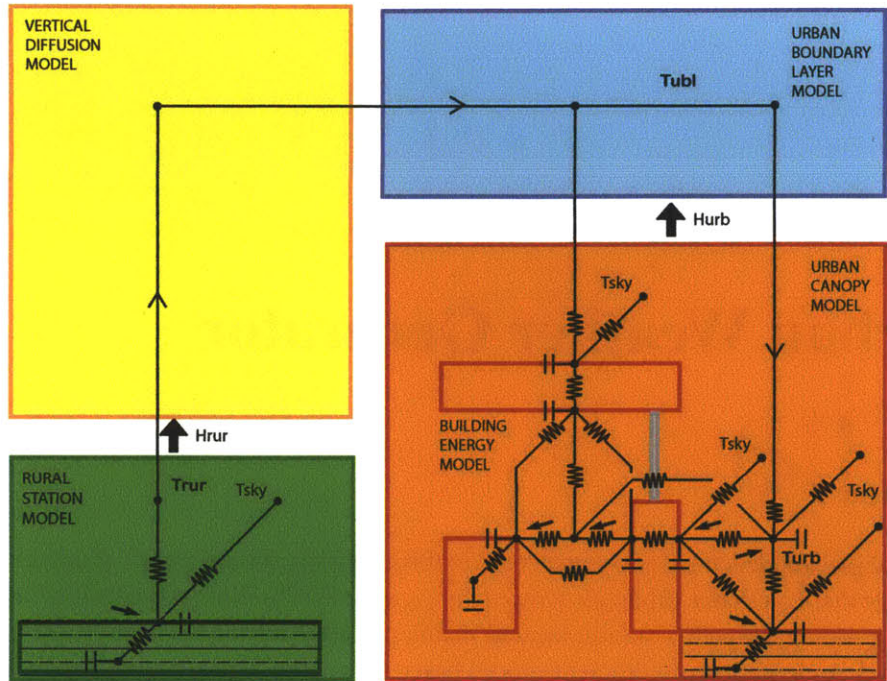


Figure 6.1 – Diagram of the Urban Weather Generator (UWG) scheme, which is composed of four modules: the Rural Station Model (RSM), the Vertical Diffusion Model (VDM), the Urban Boundary-Layer (UBL) model and the Urban Canopy and Building Energy Model (UC-BEM). Thermal networks indicate the main heat transfer processes included in the RSM and UC-BEM. T_{rur} , T_{ubl} and T_{urb} represent the air temperature measured at the weather station, calculated at the urban boundary layer, and calculated at the urban site. The RSM provides rural sensible heat fluxes (H_{rur}) to the VDM and the UBL model. The UC-BEM provides urban sensible heat fluxes (H_{urb}) to the UBL model.

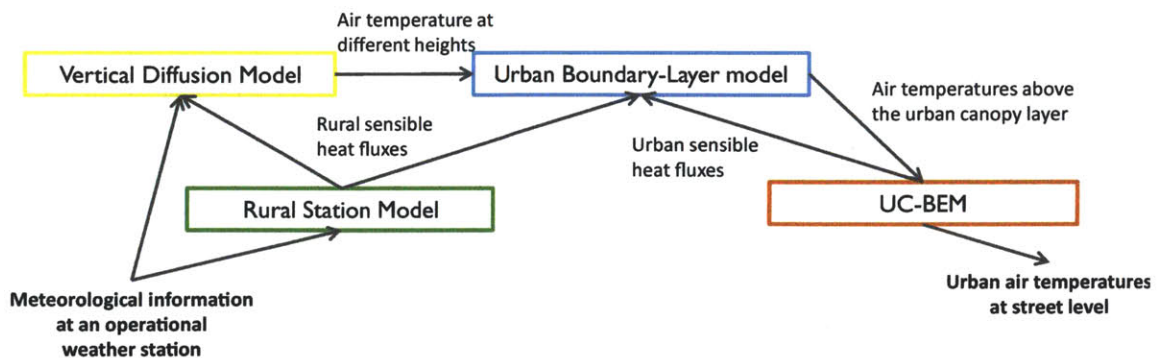


Figure 6.2 – Information exchanged among the different modules of the UWG.

6.2.1 Rural Station Model

The RSM is a rural canopy model that reads hourly values of meteorological fields measured at the rural site and calculates sensible heat fluxes, which are then provided to the VDM and the UBL model.

The model is based on an energy balance at the soil surface. A transient heat diffusion equation represents the storage and release of heat from the ground. Dividing the soil in discrete layers, the RSM solves the following system of equations:

$$d_1(\rho c)_1 \frac{\partial T_1}{\partial t} = C_{1,2}(T_2 - T_1) + Q_{surf} \quad (6.1)$$

for the first layer,

$$d_i(\rho c)_i \frac{\partial T_i}{\partial t} = C_{i,i+1}(T_{i+1} - T_i) + C_{i,i-1}(T_{i-1} - T_i) \quad (6.2)$$

for each intermediate layer, and

$$d_{n-1}(\rho c)_{n-1} \frac{\partial T_{n-1}}{\partial t} = C_{n-i,n}(T_{deep} - T_{n-1}) \quad (6.3)$$

for the deepest layer. In Eqs. [6.1-6.3], d_i , $(\rho c)_i$, and T_i represent the depth, the volumetric heat capacity [$\text{J m}^{-3} \text{K}^{-1}$], and the average temperature of the layer i , respectively; $C_{i,j}$ is the mean thermal conductance over the distance between two layers [$\text{W m}^{-2} \text{K}^{-1}$]; Q_{surf} is the sum of net-radiation, sensible, and latent heat fluxes at the surface; and T_{deep} is the annual-average air temperature of the site, used as boundary condition deep into the ground.

Surface sensible heat fluxes are computed by using convective heat transfer coefficients (CHTC) (see next section). Latent heat fluxes due to the evapotranspiration of vegetation (if present) are calculated as a fraction of the absorbed shortwave radiation. More sophisticated vegetation models, usually applied to numerical atmospheric models, can be found in the literature [Noilhan and Mahfouf, 1996]. However, they contain various empirical parameters for which it is difficult to find values if detailed information about the soil and plant composition is not available.

A suitable model for the accuracy requirements of the UWG takes advantage of the fact that the ratio between the latent heat flux and the net radiation is relatively constant during daytime. The net radiation is the sum of the net shortwave radiation (that which is absorbed) and the net longwave radiation, which typically presents small variations during the day. In the absence of light, plants' stomata are usually closed so that transpiration after sunset is virtually negligible. Roth [2007] shows this effect by comparing heat fluxes measured in different cities with different vegetation fractions. Other studies also indicate that the evapotranspiration from vegetation is mainly dependent on solar radiation [Shashua-Bar and Hoffman, 2002]. The difficulty is then to determine the fraction of absorbed solar radiation that is converted into latent heat by plants. As a first approximation, the current version of the model assumes 50% conversion.

6.2.2 Urban Canopy and Building Energy Model

Based on previous UC-BEMs (chapters 3 and 4), the UC-BEM of the UWG calculates urban canyon air temperature and humidity from radiation and precipitation data, air velocity and humidity measured at the weather station, and air temperature above the urban canopy layer calculated by the UBL model.

The UC-BEM assumes that the air inside the urban canopy layer is well mixed. Urban canyon air temperatures are obtained by the heat balance method, taking into account the heat capacity of the urban canyon air (Fig. 6.1). The urban canyon energy balance accounts for the heat fluxes from walls, windows and the road, the sensible heat exchange between the canyon air and the atmosphere, the heat fluxes due to exfiltration, the waste heat from HVAC equipment and other anthropogenic heat sources, and the radiant heat exchange between the canyon air and the sky. Thus, the urban canyon energy balance is given by:

$$\begin{aligned}
 V_{can}\rho C_v \frac{dT_{urb}}{dt} = & A_w h_w (T_w - T_{urb}) + \\
 & A_r h_r (T_r - T_{urb}) + A_r h_{rd,sky} (T_{sky} - T_{urb}) \\
 & A_{win} U_{win} (T_{in} - T_{urb}) + \dot{V}_{inf/vent} \rho C_p (T_{in} - T_{urb}) + \\
 & u_{ex} \rho C_p (T_{ubl} - T_{urb}) + H_{waste} + H_{traffic},
 \end{aligned} \tag{6.4}$$

where T_{urb} , T_{in} and T_{ubl} are the air temperature of the urban canyon, the indoor air temperature, and the air temperature of the urban boundary layer above the urban canyon, respectively; T_w and T_r are the surface temperatures of walls and road, respectively; T_{sky} is the effective sky temperature; V_{can} is the volume of the urban canyon air; U_{win} is the U-factor of windows including heat exchange coefficients at both sides; $\dot{V}_{inf/vent}$ is the exfiltration airflow rate; H_{waste} is the sensible component of waste heat flux released by HVAC systems into the urban canyon; $H_{traffic}$ represents other anthropogenic sources of heat; and u_{ex} is the exchange velocity between the in-canopy and above-canopy flows. An analogous latent heat balance is solved to calculate the humidity content of the urban canyon air by computing the latent heat fluxes from the atmosphere, buildings and road. The UWG assumes that the air humidity above urban canyons is the same as the one measured at the weather station for each time step.

The exchange velocity (u_{ex}) is obtained from an expression extracted from Bentham and Britter [2003]:

$$u_{ex} = \frac{u_*}{\frac{u_{atm}}{u_*} - \left(\frac{8}{\sqrt{H_{urb}}}\right)^{1/2}}, \tag{6.5}$$

where u_* is the friction velocity (see appendix C) and u_{atm} is a reference air velocity above the urban canopy assumed equal to the air velocity measured at the weather station.

In large spaces such as urban canyons, the water vapor present in the air participates in the radiant heat exchange. The air emissivity is calculated as a function of the humidity content and the size of the space [Siegel and Howell, 1981]. In Eq. 6.4, h_w and h_r are the heat transfer coefficients of walls and road, respectively, which combine convective and radiative effects ($h = h_{cv} + h_{rd}$); and $h_{rd,sky}$ is the radiant heat transfer coefficient between the urban canyon air and the sky (see appendix D).

External surface temperatures of walls, road, and roof are calculated by solving a similar surface energy balance to the one described for the rural soil (Eqs. [6.1-6.3]). The boundary conditions for the road are the same as for the rural soil. In the case of walls and roof, the indoor boundary condition is a heat flux calculated by the building energy model.

The outdoor surface heat flux is composed of shortwave radiation, longwave radiation, sensible and latent heat components. The solar radiation received by walls and road is calculated by assuming an average urban canyon orientation (see appendix D). The longwave radiation among walls, road, urban canyon air, and the sky is computed by linearization of the Stefan-Boltzmann equation accounting for

the transmittance of the urban canyon air and assuming only one bounce of radiative heat fluxes between surfaces (see appendix D). In terms of longwave radiation, window surfaces are assumed to have the same temperature as wall surfaces. Surface sensible heat fluxes are computed by using CHTC, which are calculated as a function of the air velocity above the urban canopy layer (u_{atm}) by using a correlation extracted from Palyvos [2008]:

$$h_{cv} = 5.8 + 3.7u_{atm}. \quad (6.6)$$

The air velocity inside the urban canyon (u_{can}) is used in Eq. 6.6 for the road. This is given by the following equation [Bentham and Britter, 2003]:

$$u_{can} = u_* \left(\frac{8}{VH_{urb}} \right)^{1/2}. \quad (6.7)$$

Urban sensible heat fluxes (required by the UBL model) are calculated as the sum of the heat exchange between the canyon air and the atmosphere and the convective heat flux from building roofs, including the fraction of waste heat emissions from outdoor HVAC equipment located there.

For horizontal surfaces (road and roof), the UC-BEM calculates the latent heat flux associated with a thin layer of water (max 1 mm) which remains after the precipitation water is run off. The mass balance to the film of water is given by:

$$\frac{dw_g}{dt} = (P_g - E_g), \quad (6.8)$$

where P_g and E_g are the precipitation and evaporation mass fluxes, respectively [$m s^{-1}$]. The water evaporation is calculated as:

$$E_g = \frac{1}{\rho_w R} (q_{sat}(T_{surf}) - q_a), \quad (6.9)$$

where R is an aerodynamic resistance [$s m^{-1}$] obtained from the CHTC (Eq. 6.6), ρ_w is the water density, q_{sat} is the saturation specific humidity [$kg kg^{-1}$] at surface temperature, and q_a is the specific humidity of the air above the surface. Whenever the depth of the layer of water is greater than zero, the latent heat flux is calculated as $LE = E_g \rho_w l_v$, where l_v is the latent heat of vaporization [$J kg^{-1}$].

The vegetation model of the UC-BEM follows the shade-convection approach [Shashua-Bar and Hoffman, 2002]. The solar radiation that reaches urban canyons is partially blocked by the tree canopy according to the horizontal vegetation density of the site. The solar radiation absorbed by the trees is split into sensible and latent heat fluxes as indicated in section 6.2.1. These fluxes then participate in the energy balance of the urban canyon. Although the tree canopy reduces the sky view factor of the urban canyon and consequently may reduce the net outgoing longwave radiation, the model assumes that the temperature of urban surfaces is close enough to the one of the tree canopy so that the overall effect of trees on the longwave radiation balance is negligible.

The building energy model is based on the one developed in chapter 3. The physical and geometric definition of buildings is kept as simple as possible, while maintaining the required features of a comprehensive building energy model. The model considers a single thermal zone, where the thermal inertia of building materials associated with multiple levels is represented by a generic thermal mass. The model accounts for heat gains due to transmitted solar radiation, heat conduction through the enclosure, infiltration, ventilation, and internal heat gains, as well as for the dynamical evolution of indoor air temperature (between thermal set points) and humidity.

To calculate cooling energy consumption, the model solves the dehumidification of the air passing through the cooling system by assuming that the air leaves the cooling coil at 90% relative humidity. The model includes the mixture of recirculated air and outdoor air according to the ventilation air flowrate.

Waste heat fluxes are calculated as a function of the building energy consumption (Q_{HVAC}) and building energy demand (Q_{dem}). For example, for a cooling system the waste heat flux is given by:

$$Q_{waste} = Q_{HVAC} + Q_{dem}. \quad (6.10)$$

6.3 Model evaluation

The UWG scheme is compared with field data from two boundary-layer experiments: the intensive observational period (IOP) of the BUBBLE experimental campaign, carried out in Basel (Switzerland) between June 10 and July 10, 2002 [Rotach et al., 2005]; and the CAPITOUL experimental campaign carried out in Toulouse (France) from February 2004 to March 2005 [Masson et al., 2008]. The climate information of both sites is characterized in Table 5.5.

Chapter 5 compares calculated and observed air temperatures above the urban canopy layer for these two case studies. This chapter evaluates the UWG by comparing calculated and observed urban canyon air temperatures.

The system parameters of the UWG used in this comparison are summarized in Table 6.1. The parameters of the VDM-UBL scheme are the daytime and nighttime boundary layer heights (z_i), the reference height (z_{ref}), and the urban-breeze scaling coefficient (k_w) (see chapter 5). In addition, the sensible-latent heat split of vegetation is assumed to be 0.5 and the vegetation albedo is taken as 0.25, which is the average value reported in the experiments. Finally, the model accounts for the effect of vegetation from May to November (deciduous vegetation).

Table 6.1 – System parameters of the UWG used in the model comparison with field data from Basel, Switzerland, and Toulouse, France.

Parameter	Setting
Daytime boundary-layer height	1000 m
Nighttime boundary-layer height	50 m
Reference height at which the vertical profile of potential temperature is assumed uniform	200 m
Urban-breeze scaling coefficient	1.2
Latent fraction of vegetation	0.5
Albedo of vegetation	0.25
Begin month for vegetation participation	May
End month for vegetation participation	November

6.3.1 Comparison with field data from Basel, Switzerland

The main urban experimental site in BUBBLE is Basel-Sperrstrasse. The site represents a heavily built-up part of the city center of Basel, mainly composed of residential buildings. Table 6.2 shows the inputs parameters used in the evaluation of the UWG, based on a characterization of the urban site carried out by Hamdi and Masson [2008]. A sensitivity analysis of input parameters is presented in section 6.3.3.

The Grenzach weather station, inside the valley of the Rhine River, is used as the reference rural station.

Figure 6.3 compares hourly values of urban air temperatures calculated by the UWG with the air temperatures measured at the urban and rural sites for a week in June. The monthly-average diurnal cycle for the IOP of the BUBBLE campaign is represented in Fig. 6.4. As can be seen, the UWG is able to capture both the UHI effect observed at night and the Urban Cool Island (UCI) effect observed during the day, although it overpredicts the later partly due to the simplifying assumptions of the vegetation model.

Statistical results of this comparison are presented in Table 6.3. The root-mean-square error (RMSE) between the model and observations is 1.1 K, where the average daily-maximum UHI effect is 5.2 K. Errors of about 1 K are acceptable given the important uncertainties associated with urban climate predictions (see next section). The mean-bias error (MBE) is -0.5 K, which reproduces the overprediction of the UCI effect observed in Fig. 6.3.

Table 6.2 – Inputs of the UWG used in the model comparison with field data from Basel, Switzerland, and Toulouse, France. Both parametrizations represent densely populated residential areas and rural areas covered by grass. The thermal properties of construction materials are indicated in Table 2.2.

Parameter	BUBBLE	CAPITOU
Urban parameters		
Location	Basel	Toulouse
Latitude	47.33°	43.48°
Longitude	7.35°	1.3°
City diameter	5000 m	7500 m
Average building height	14.6 m	20 m
Horizontal building density	0.54	0.68
Vertical-to-horizontal urban area ratio	0.48	1.1
Horizontal vegetation density (trees)	0.16	0.08
Wall construction	Concrete - 20 cm Insulation - 3 cm	Brick - 30 cm Insulation - 3 cm
Wall albedo	0.15	0.25
Roof construction	Tiles - 6 cm Concrete - 20 cm Insulation - 3 cm	Tiles - 6 cm Wood - 20 cm Insulation - 3 cm
Roof albedo	0.15	0.25
Road construction	Asphalt - 5 cm Stones - 20 cm Gravel and soil	Asphalt - 5 cm Stones - 20 cm Gravel and soil
Road albedo	0.08	0.08
Building parameters		
Building floor construction	Concrete - 20 cm	Concrete - 20 cm
Glazing ratio	0.3	0.3
Window construction	Double-pane clear glass	Double-pane clear glass
Internal heat gains	Residential	Residential (see Table 2.1)
Infiltration/ventilation	0.5 ACH	0.5 ACH
Cooling system	None	None
Heating system	Furnace	Furnace
Weather station parameters		
Construction	Soil	Soil
Albedo of the surface without vegetation	0.15	0.15
Vegetation fraction	0.8	0.8

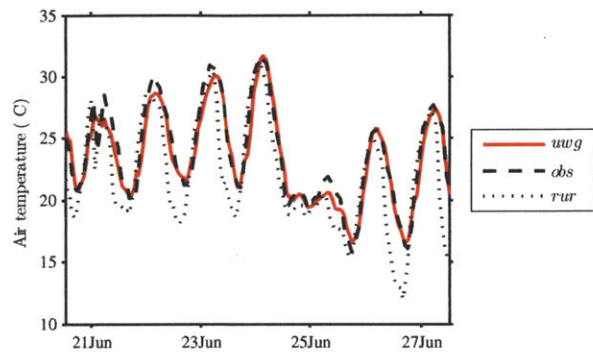


Figure 6.3 – Hourly values of urban canyon air temperature calculated by the UWG and observed during the BUBBLE experiment between June 21 and June 28, 2002. Hourly values of measured rural air temperature (rur) for the same period are also represented.

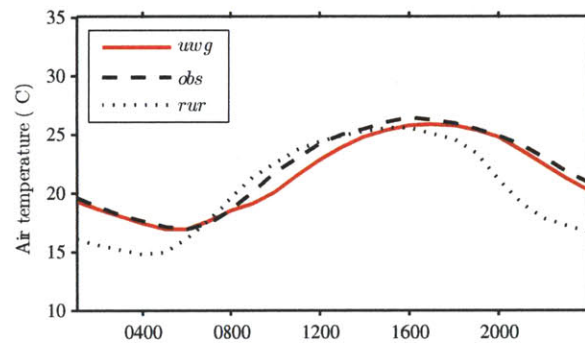


Figure 6.4 – Monthly-average diurnal cycle of urban canyon air temperature calculated by the UWG and observed during the BUBBLE experiment between June 10 and July 10, 2002. Monthly-average diurnal cycle of measured rural air temperature (rur) for the same period is also represented.

6.3.2 Comparison with field data from Toulouse, France

The CAPITOUL campaign is an extensive boundary-layer experiment, which includes (among other types of measurements) a network of weather stations inside and at the periphery of Toulouse (Fig. 6.5). In this analysis, the station located at the central location of the city, next to the Monoprix building (MNP), is selected as representative of urban conditions. Five of the surrounding urban stations are also included in the analysis (MIC, CIT, MIN, ILE, and CYP) to show the variability of air temperatures within the same urban area. The characterization of the site is presented in section 2.4.2. Similar input parameters are used here (Table 6.2). The reference weather station is located at Mondouzil (MON), an agricultural rural area at the North-East periphery of the city.

Figure 6.6 compares hourly values of urban air temperatures calculated by the UWG with the air temperatures measured at the urban and rural sites for a week in July. The monthly-average diurnal cycles for July and October, 2004, and January, 2005, are represented in Fig. 6.7. The error bar represents the root-mean-square difference between the air temperatures observed in the five urban stations surrounding the MNP station and the air temperature measured at the MNP station (Fig. 6.5). The results show the capacity of the UWG to reproduce the UHI effect for different seasons. The observed variability of air temperature around the MNP weather station is about 1 K. This justifies the statement that the error associated with UWG's predictions is acceptable and within the air temperature range observed in different locations of the same urban area.

Statistical results of this comparison are presented in Table 6.3 for the three months. The RMSE between the model and observations ranges between 0.8 K and 1.2 K, where the average daily-maximum UHI effect ranges between 2.4 K and 3.6 K. The MBE is generally low, which indicates that there are no systematic errors in the model.

Observations show that the UHI effect at mesoscale level (due to the aggregate effects of the whole city) cannot be neglected. From the daily-maximum UHI effect observed inside urban canyons (e.g. 3.6 K in summer in Toulouse, Table 6.3), more than half (e.g. 2.5 K, Table 5.7) is due to the mesoscale effect.

Table 6.3 – Root-mean-square error (RMSE) and mean-bias error (MBE) between the urban air temperatures calculated by the UWG and observed during BUBBLE experiment between June 10 and July 10, 2002; and between the urban air temperatures calculated by the UWG and observed during CAPITOUL experiment in July and October, 2004, and January, 2005. Errors are compared to the average daily-maximum UHI effect (\overline{UHI}_{max}) observed during each period.

Month	RMSE (K)	MBE (K)	\overline{UHI}_{max} (K)
BUBBLE			
Summer	1.1	-0.5	5.2
CAPITOUL			
Summer	0.8	0.3	3.6
Fall	0.9	-0.1	2.5
Winter	1.2	-0.1	2.4

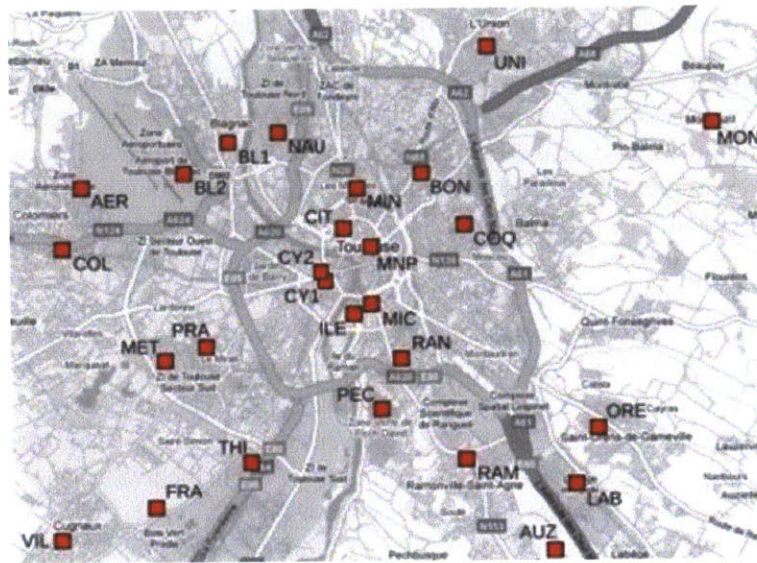


Figure 6.5 – Map of the weather station network during the CAPITOUL experiment carried out in Toulouse, France, from February 2004 to March 2005.

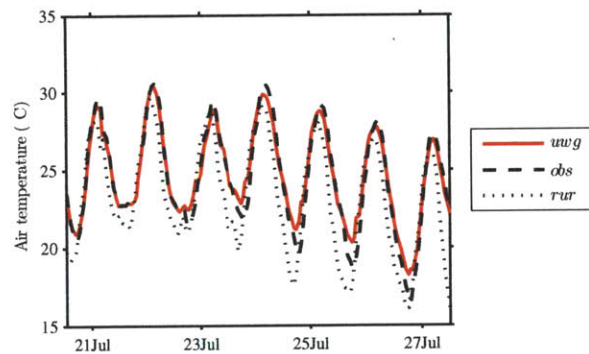


Figure 6.6 – Hourly values of urban canyon air temperature calculated by the UWG and observed during the CAPITOUL experiment between July 21 and July 28, 2004. Hourly values of measured rural air temperature (rur) for the same period are also represented.

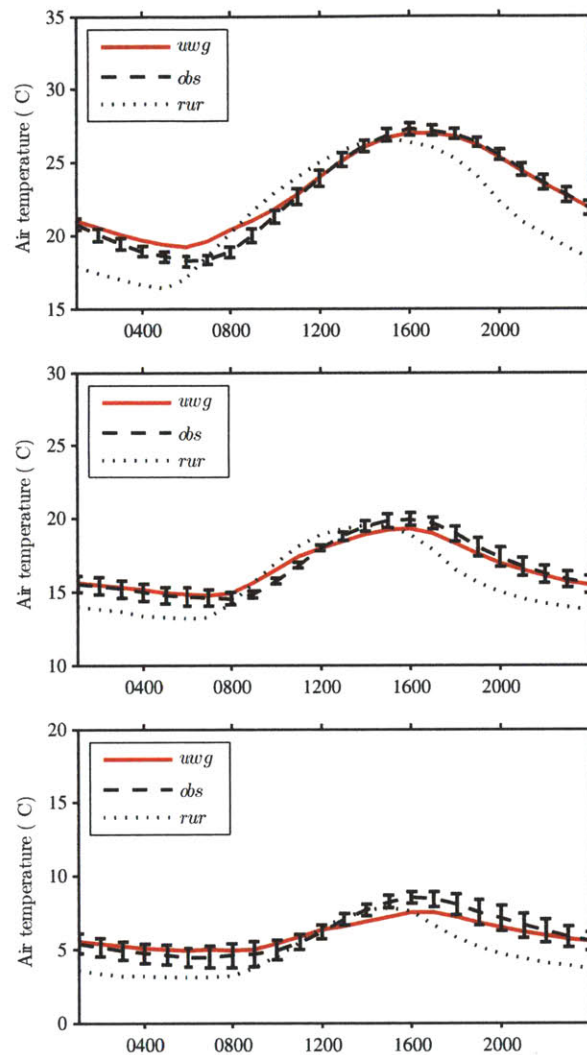


Figure 6.7 – Monthly-average diurnal cycles of urban canyon air temperature calculated by the UWG and observed during the CAPITOUL experiment in July (top) and October (middle), 2004, and in January (bottom), 2005. Monthly-average diurnal cycles of measured rural air temperature (*rur*) for the same periods are also represented. The error bar represents the root-mean-square difference between the air temperature observed in the five urban stations surrounding the MNP station and the air temperature measured at the MNP station.

6.3.3 Sensitivity analysis

A sensitivity analysis is carried out for some of the model parameters. Table 6.4 shows the variation of the error obtained in the comparison between the UWG and observations in summer when model parameters range between -25% and +25% of the reference value indicated in Tables 6.1 and 6.2. It can be seen that, although all parameters have an effect, the most critical ones are the morphological parameters; in particular, the horizontal building density and the vertical-to-horizontal urban area ratio. Values for these parameters are available for numerous cities around the world and can be obtained from

geographic information systems.

Another parameter that has a noticeable effect on the results is the reference height of the VDM at which the vertical profile of potential temperature is assumed uniform. The value used in this analysis gives reasonably good results and was obtained from comparison with mesoscale atmospheric simulations (chapter 5), but further investigation might be required.

The case study of BUBBLE is sensitive to some vegetation parameters for which it is difficult to find exact values. This indicates another area for model improvement. It is also sensitive of the thermal mass of the road (it has a lower building density than the case of CAPITOU).

Table 6.4 – Maximum variation of the RMSE or the MBE obtained in the comparison between the urban air temperatures calculated by the UWG and observed during the experiments in summer when model parameters range between -25% and +25% of the reference value indicated in Tables 6.1 and 6.2. Units are K.

Parameter	BUBBLE	CAPITOU
City diameter	0.1	0.1
Average building height	0.1	0.1
Horizontal building density	0.4	0.4
Vertical-to-horizontal urban area ratio	0.8	0.3
Horizontal vegetation density (trees)	0.1	0.1
Wall albedo	0.1	0.1
Roof albedo	0.1	0.1
Road albedo	0.1	0.1
Volumetric heat capacity of concrete/brick in walls	0.1	0.1
Volumetric heat capacity of asphalt in road	0.2	0.1
Internal heat gains	0.1	0.1
Rural vegetation fraction	0.3	0.1
Daytime mixing height	0.1	0.1
Nighttime boundary-layer height	0.1	0.1
Reference height at which the vertical profile of potential temperature is assumed uniform	0.3	0.4
Urban-breeze scaling coefficient	0.1	0.1
Latent fraction of vegetation	0.4	0.1

6.3.4 Heat flux comparison

An additional evaluation of the UWG (in particular, of the RSM and the UC-BEM) is carried out by comparing the sensible and latent heat fluxes leaving the rural and urban canopies. The rural and urban sensible heat fluxes are exchanged between the canopy models and the VDM-UBL scheme (Fig. 6.1). The latent heat flux comparison allows testing the proposed vegetation model. Fig. 6.8 compares the monthly-average diurnal cycle of sensible and latent heat fluxes calculated by the UWG and observed during the BUBBLE and CAPITOUL experiments in summer. The sensible-latent split factor of the vegetation model (section 6.2.1) may cause the overprediction of the latent heat flux at the rural site. The oscillation of latent heat flux at the urban site can be explained by the intermittent precipitation recorded for some days in summer. Still, the agreement between simulated and observed heat fluxes is acceptable for the sensitivity of the UWG to these variables.

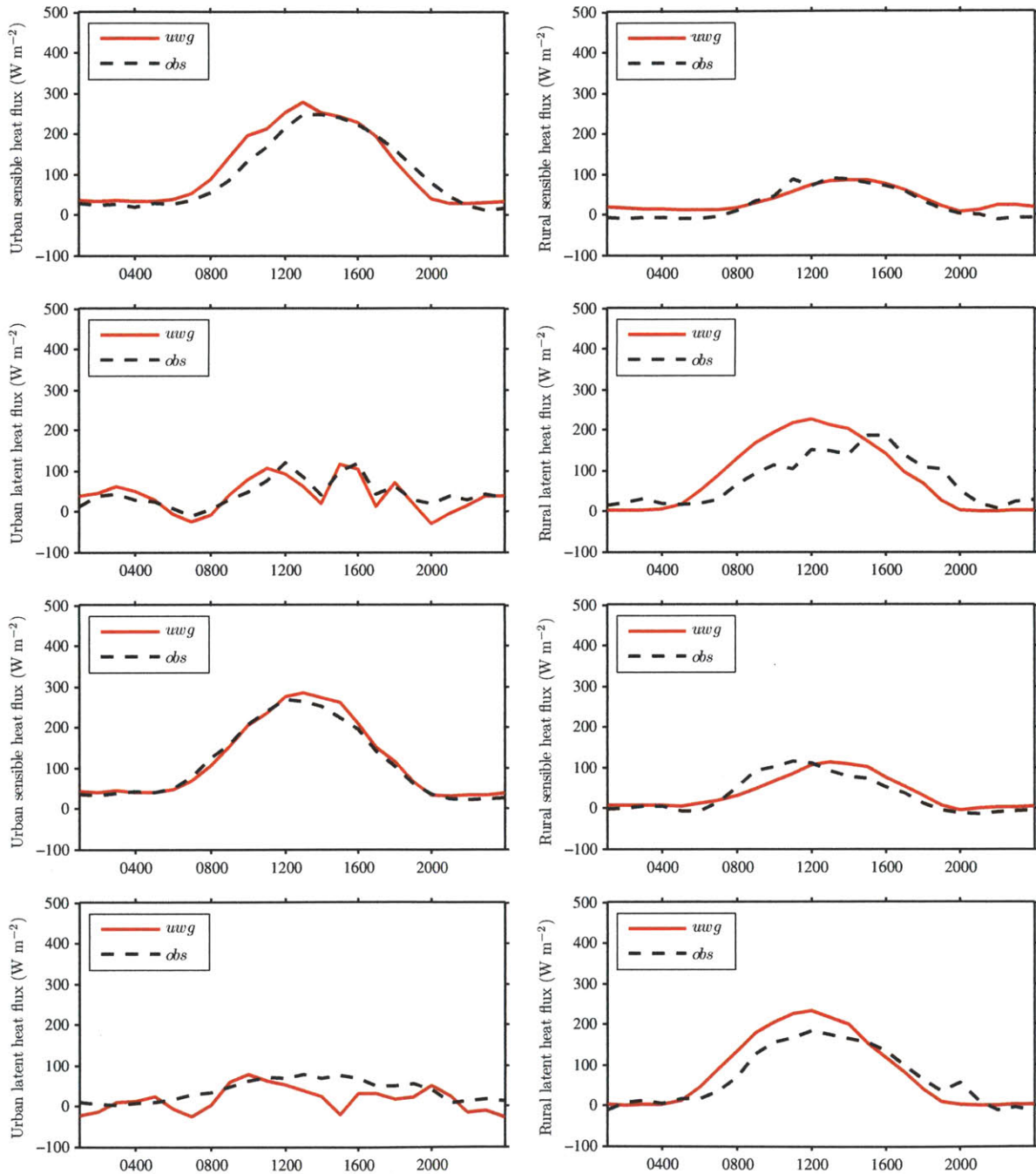


Figure 6.8 – Monthly-average diurnal cycles of surface heat fluxes calculated by the UWG and observed during the BUBBLE and CAPITOUL experiments in summer. The following scenarios are represented: (top-left) Basel-urban sensible, (top-right) Basel-rural sensible, (middle-top-left) Basel-urban latent, (middle-top-right) Basel-rural latent, (middle-bottom-left) Toulouse-urban sensible, (middle-bottom-right) Toulouse-rural sensible, (bottom-left) Toulouse-urban latent, (bottom-right) Toulouse-rural latent.

Conclusions

Chapter 7

Summary of contributions and future work

This thesis presents a study of the energy interactions between buildings and the urban climate through the development and evaluation of a set of models. Chapters 2, 3 and 4 are devoted to three different urban canopy and building energy models (UC-BEMs) with different levels of detail and applications. Chapters 5 and 6 present the different components of a novel urban climate prediction tool.

7.1 Urban canopy and building energy models

Chapter 2 presents a Coupled Scheme (CS) between a detailed building energy simulation model, EnergyPlus, and an urban canopy model, the Town Energy Balance (TEB) scheme [Masson, 2000]. The CS combines models that have already been extensively used and evaluated within their respective scientific communities, building engineering and urban climatology. This makes the CS a very useful tool to evaluate other UC-BEMs. It also allows an analysis of the effect on climate of sophisticated building and building system configurations (those included in EnergyPlus), as well as an evaluation of their sensitivity to urban climate conditions. Apart from the respective evaluations of EnergyPlus and the TEB model that can be found in the literature, this thesis presents a comparison of the CS with the original TEB model and field data from the urban center of Toulouse, France. This comparison verifies that the iterative coupling process between the two models is solved correctly and shows the capacity of the CS to predict heating energy consumption at urban scale. Chapter 2 also presents some examples of application of the CS. The scheme is used to evaluate the effect on the energy consumption and waste heat emissions of three different energy efficiency strategies for Toulouse: shading devices, economizers, and heat recovery.

Before this thesis, only the last two of the three most popular urban canopy models, Masson [2000], Kusaka et al. [2001], and Martilli et al. [2002], had integrated building energy models [Kikegawa et al., 2003; Salamanca et al., 2010]. The building energy model of the TEB scheme is developed as a part of this research and is presented in chapter 3. Its objective is to represent the building effects on urban climate and to estimate the energy consumption of buildings at city or neighborhood scale. In contrast to previous building energy models integrated in urban canopy models, BEM-TEB is developed in collaboration between the urban climatology community represented by the CNRM-GAME (France) and the building engineering community represented by the Building Technology Program at MIT. Further-

more, it includes specific models for active and passive building systems, which allows a performance assessment of different energy efficiency strategies in an urban context. An evaluation of the model is presented in three steps: modeling assumptions, verification, and comparison with field data. The CS, which already incorporates a detailed building simulation model, is used in the verification process. BEM-TEB, and the possibility of coupling it with mesoscale atmospheric simulations, allows for a multi-scale simulation platform from the atmosphere down to buildings that can be used to study the implications for urban climate and building energy consumption of future climate change scenarios. Further developments of BEM-TEB include extending the evaluation to other building configurations and climates, introducing new HVAC configurations, such as heat-pumps or variable-air-volume systems, and improving the current models of shadowing devices and natural ventilation systems.

Chapter 4 presents a simple and fast UC-BEM, the resistance-capacitance (RC) model, specifically designed to investigate the energy interactions between buildings and the urban climate. The RC model is built on a state-space formulation of the thermal network that represents the fundamental physical relations between buildings and their urban environment. This allows for faster parametric analyses and makes it possible to easily test modeling hypotheses. The RC model is evaluated against the CS for summer and winter conditions and for different building configurations. The model is then used in a series of parametric analyses to investigate the impact of the UHI effect on the energy consumption of buildings. The resulting relationship is linear. For residential buildings in summer, a 5% increase in cooling energy demand can be expected per 1 K increase in the maximum UHI effect (usually at night). A similar order-of-magnitude decrease in heating energy demand of a residential building can be expected from an equivalent wintertime UHI effect. The energy demand of commercial buildings is not significantly affected by the UHI effect if they are not naturally ventilated. Although not included in the analysis carried out with the RC model, the UHI effect can have an impact on the energy consumption of commercial buildings through the dependence of the system efficiency on outdoor air temperatures.

Depending on the proportion of cooling and heating days of each particular climate and the type of system used to meet building energy demands, the UHI effect can have a positive or negative impact on the overall energy consumption of cities. The main mechanism by which the UHI effect influences the indoor energy performance is infiltration and ventilation; the impact from the conductive heat transfer through the building enclosure is relatively small. This result highlights the importance of considering the UHI effect in the design and analysis of building systems, such as natural ventilation or economizers, in which the outdoor air entering the building plays a critical role.

The RC model is also used to investigate the dominant mechanisms by which the indoor environment affects outdoor air temperatures. In wintertime, exfiltration heat fluxes can have a noticeable effect on outdoor air temperatures. Waste heat emissions from AC systems are the main mechanism by which the energy performance of buildings affects outdoor thermal conditions, the impact from heat conduction through the building enclosure again being relatively small. This analysis shows that, for building densities lower than 0.6, the increase in outdoor air temperature is approximately proportional to the heat flux per unit of urban area released into the urban canyon with a relation of 1 K per 100 W m^{-2} for low wind speeds ($\sim 2 \text{ m s}^{-1}$) and 0.5 K per 100 W m^{-2} for high wind speeds ($\sim 10 \text{ m s}^{-1}$). This analysis can be seen as a lower limit of the impact of waste heat on urban air temperatures because it assumes that the boundary conditions at the top of urban canyons are invariant to the changes in the canopy heat fluxes. Future work could relax this assumption by using the coupled effect between the urban boundary layer and the urban canopy layer captured by the Urban Weather Generator (UWG).

The UC-BEMs developed in this thesis have been evaluated with field data from urban areas in which the use of AC systems is negligible. The Center for Environmental Sensing and Modeling (CENSAM)

in Singapore is carrying out urban climate experiments that could be adapted to simultaneously record building energy consumption. Future work will consist of participating in such experiments and further evaluating the capacity of UC-BEMs to predict cooling energy consumption of urban areas and the effect of waste heat emissions on the urban climate.

7.2 Urban climate prediction tool

Chapters 5 and 6 present different components of the UWG scheme, a physically based and computationally fast model to predict the UHI effect in a city, both at mesoscale and at canopy-scale (Fig. 1.2), given meteorological information measured in an operational weather station outside the city.

The atmospheric component of the UWG is presented in chapter 5. The Vertical Diffusion Model (VDM) calculates vertical profiles of potential temperature at the rural site by solving a one-dimensional heat diffusion equation. The diffusion coefficient is calculated dynamically as a function of a mixed-layer velocity scale for which correlations can be found in the literature. Values of potential temperature at different heights calculated by the VDM are used in the Urban Boundary Layer (UBL) model, which calculates air temperatures above the urban canopy layer by applying an energy balance to the urban boundary layer (or sub-divisions). The VDM-UBL scheme requires the rural and urban sensible heat fluxes calculated by the canopy models.

The VDM-UBL scheme has been satisfactorily evaluated against three-dimensional mesoscale atmospheric simulations and against field data from Basel, Switzerland, and Toulouse, France. The comparison shows a reasonably good agreement, given the important uncertainties associated with urban climate predictions. The UBL model is being incorporated into the off-line model of the SURFEX scheme [Martin et al., 2007] in the context of a French project studying climate change impact on urban energy consumption [CNRM-GAME, 2010]. This makes it possible to carry out long-term analyses of future climate scenarios without having to run computationally expensive mesoscale simulations.

The canopy components of the UWG are presented in chapter 6. The Rural Station Model (RSM) reads hourly values of meteorological fields measured at the rural site and calculates sensible heat fluxes, which are then provided to the VDM and the UBL model. The UC-BEM calculates urban canyon air temperature and humidity from radiation and precipitation data, air velocity and humidity measured at the weather station, and air temperature above the urban canopy layer calculated by the UBL model.

The UWG has also been compared with the data sets from Basel, Switzerland, and Toulouse, France. The expected error associated with UWG predictions is about 1 K, which stays within the range of air temperature variability observed in different locations of the same urban area. The comparison with field data highlights that the UHI effect cannot be computed only from the urban canyon effect (vertical component), but must also include the aggregate effect of the whole city (horizontal component). As a consequence, urban climate prediction tools cannot be limited to an urban canopy model, but must also consider the effect of the urban boundary layer. This can be achieved by using mesoscale atmospheric simulations or by using the simplified approach of the VDM-UBL scheme.

The comparison of the VDM-UBL scheme with field data shows a slightly better performance than that of the integrated UWG. This can be explained by the assumptions made by the UC-BEM to represent the heat exchange between the in-canopy and the above-canopy flows. The current version uses semi-empirical correlations based on exchange velocities. This method was developed to represent homogeneous rural canopies (crops, trees, etc.), and its application to urban canopies has not been formally tested. Future developments of the UC-BEM will improve this representation. One possible solution is

the multi-layer approach developed by Hamdi and Masson [2008].

The reference weather station for the UWG can be situated in any location on the periphery of the city as long as it is not surrounded by urbanization and is not affected by site-specific micro-climate conditions produced by the orography or by the presence of large bodies of water. For example, a weather station near the sea would not be appropriate for applying the UWG. The current version of the UWG has performed well in European-type cities in which the urban morphology is relatively homogeneous and the urban vegetation is scarce. Further developments of the model will address the heterogeneity of urban areas and the spatial distribution of the UHI effect within a city. They will also include a better treatment of latent heat fluxes, while maintaining the approach of keeping the model as simple as possible.

The UWG can be integrated into existing programs in order to account for site-specific urban weather files in building energy simulations. It can also be converted into a fully-operative program to predict building energy consumption at urban scale and the UHI effect, taking into account the energy interactions between buildings and the urban climate.

Appendices

Appendix A

Nomenclature

Table A.1 – Nomenclature.

Symbol	Designation	Unit
<i>A</i>	Area	m ²
<i>A_{city}</i>	City horizontal area	m ²
<i>A_f</i>	Lateral heat exchange area	m ²
<i>AC</i>	Air-conditioning	
<i>BEM</i>	Building energy model	
<i>C</i>	Capacitance/Conductance/Coefficients	W s K ⁻¹ /W m ⁻² K ⁻¹ /
<i>CHTC</i>	Convective heat transfer coefficient	W m ⁻² K ⁻¹
<i>COP</i>	Coefficient of performance of an HVAC system	–
<i>CS</i>	Coupled Scheme between EnergyPlus and TEB	
<i>c</i>	Specific heat	J kg ⁻¹ K ⁻¹
<i>c_p</i>	Air specific heat at constant pressure	J kg ⁻¹ K ⁻¹
<i>C_p</i>	Pressure coefficient	–
<i>c_v</i>	Air specific heat at constant volume	J kg ⁻¹ K ⁻¹
<i>C_{vk}</i>	Von-Karman constant	–
<i>d</i>	Layer thickness	m
<i>dx</i>	Length of the control volume parallel to the main wind direction	m
<i>D</i>	City characteristic length	m
<i>E</i>	Turbulent kinetic energy	m ² s ⁻²
<i>E_g</i>	Water evaporation flux	m s ⁻¹
<i>f</i>	Fraction	–
<i>F</i>	View factor	–
<i>g</i>	Gravity acceleration	m s ⁻²
<i>GR</i>	Glazing ratio	–
<i>h</i>	Heat transfer coefficient	W m ⁻² K ⁻¹
<i>h_{bid}</i>	Average building height	m
<i>h_{win}</i>	Opening height for natural ventilation	m
<i>H</i>	Sensible heat	W m ⁻²
<i>HVAC</i>	Heating, Ventilation, and Air-Conditioning	
<i>k</i>	Thermal conductivity	W m ⁻¹ K ⁻¹
<i>k_w</i>	Urban-breeze circulation scale constant	–
<i>K</i>	Solar radiation	W m ⁻²
<i>K_d</i>	Diffusion coefficient	m ² s ⁻¹
<i>K_{sol}</i>	Solar constant	W m ⁻²
<i>l_k</i>	Length scale	m
<i>l_v</i>	Water condensation heat	J kg ⁻¹

APPENDIX A. NOMENCLATURE

Table A.2 – Nomenclature (continued).

Symbol	Designation	Unit
L	Monin-Obukhov length	m
LE	Latent heat	$W m^{-2}$
LHS	Left hand side of an equation	
\dot{m}	Air mass flowrate	$kg^3 s^{-1}$
N_{fl}	Number of floors in a building	–
P	Electric power/Partial pressure	W/Pa
P_{can}	Canyon perimeter	m
P_{city}	City perimeter	m
P_g	Precipitation flux	$m s^{-1}$
PLR	Part-load ratio	–
q	Specific humidity	$kg kg^{-1}$
Q	Heat flux	$W m^{-2}$
R	Resistance	$K W^{-1}$
Ri	Richardson number	–
RHS	Right hand side of an equation	
S^\downarrow	Incoming solar radiation	$W m^{-2}$
SBL	Surface boundary layer	
$SHGC$	Solar Heat Gain Coefficient	–
t	Time	s
T	Temperature	$^\circ C, K$
u	Mean air velocity	$m s^{-1}$
u_{ex}	Exchange velocity	$m s^{-1}$
u_*	Friction velocity	$m s^{-1}$
$UC - BEM$	Urban canopy and building energy model	
UCM	Urban canopy model	
U_{win}	Window U-factor	$W m^{-2} K^{-1}$
V	Volume	m^3
\dot{V}	Air volume flowrate	$m^3 s^{-1}$
V_o	Infiltration/exfiltration air flowrate	ACH
VH_{bld}	Vertical-to-horizontal building area ratio, defined as exterior vertical building area divided by building plan area.	–
VH_{urb}	Vertical-to-horizontal urban area ratio, defined as exterior vertical building area divided by the plan area of the urban site.	–
w_s	Mixed-layer velocity scale	$m s^{-1}$
w_*	Convective velocity scale	$m s^{-1}$
W	Width of the city orthogonal to the wind direction	m
X_{mix}	Mixing ratio	–
z	Vertical space component	m
z_i	Boundary-layer height	m
z_{inv}	Capping inversion height	m
z_m	Air velocity measurement height	m
z_r	Blending height	m
z_{ref}	Reference height	m
z_0	Roughness length	m
Z	Solar zenith angle	rad
α	Solar absorptivity	–
β	Buoyancy coefficient	$m s^{-1} K^{-1}$
δ	Simulation time step	s

Table A.3 – Nomenclature (continued).

Symbol	Designation	Unit
ε	Emissivity	–
η	Efficiency	–
θ	Potential temperature	K
θ_o	Critical canyon orientation	–
λ	Solar zenith angle	–
ρ	Density	kg m^{-3}
ρ_{bld}	Building density, defined as building plan area divided by the plan area of the urban site.	–
ρ_r	Road reflectivity	–
ρ_w	Wall reflectivity/water density	$-\text{kg m}^{-3}$
σ	Stefan-Boltzmann constant	$\text{W m}^{-2} \text{K}^{-4}$
ΣH	Difference between urban and rural sensible heat fluxes during one day of simulation	W h m^{-2}
τ	Transmittance	–
φ	Performance curve of a cooling system	–
ϕ_m	Wind profile function	–

Table A.4 – Nomenclature (continued).

Subscript	Designation
a	Air
atm	Atmosphere
bld	Building
can	Urban canyon
cap	HVAC system capacity
cd	Conduction
circ	Urban-breeze circulation
cons	Consumption
cool	Cooling
cv	Convection
CV	Control volume
dem	Energy demand
dif	Diffuse
dir	Direct
exch	Energy exchanged between an HVAC system and a building
fl	Floor
heat	Heating
HVAC	HVAC system energy consumption
ig	Internal heat gains
in	Indoor air
inf	Infiltration
is	Interior surface
lat	Latent or dehumidification
m	Building internal thermal mass
mix	HVAC mixing conditions
nt	Natural ventilation
r	Road
rat	Rated conditions
rd	Radiation
ref	Reference
rur	Rural
sat	Saturation
sens	Sensible heat
sol	Solar radiation
supply	HVAC system supply conditions
sys	HVAC system
ubl	Urban boundary layer
urb	Urban
vent	Ventilation
w	Walls
waste	Waste heat from HVAC systems
wi	Inner layer of wall
win	Windows
wind	Wind

Appendix B

Building Energy Model in TEB

B.1 Heat balance method

The convection term of Eq. (3.1) is calculated from:

$$Q_{cv} = h_{cv} (T_{is} - T_{in}), \quad (\text{B.1})$$

where T_{is} and T_{in} are the temperature of an interior surface and of the indoor air, respectively. The convective heat transfer coefficient has the following values obtained from EnergyPlus documentation [DOE, 2010a]: $h_{cv} = 3.076 \text{ W m}^{-2} \text{ K}^{-1}$ for a vertical surface; $h_{cv} = 0.948 \text{ W m}^{-2} \text{ K}^{-1}$ for a horizontal surface with reduced convection (floor surface with $T_{is} < T_{in}$ and ceiling surface with $T_{is} > T_{in}$); and $h_{cv} = 4.040 \text{ W m}^{-2} \text{ K}^{-1}$ for a horizontal surface with enhanced convection. The radiation term is calculated as:

$$Q_{rd,i-j} = h_{rd} F_{i-j} (T_{s,i} - T_{s,j}), \quad (\text{B.2})$$

where h_{rd} is a radiative heat transfer coefficient and F_{i-j} is the configuration factor between surfaces i and j . Radiative heat transfer coefficients are calculated as:

$$h_{rd} = 4\varepsilon^2 \sigma T_{rd}^3, \quad (\text{B.3})$$

where $\varepsilon = 0.9$ is the surface emissivity, σ is the Stefan-Boltzmann constant, and T_{rd} is an average surface temperature. View factors (F) between surfaces are based on those developed by Masson [2000] for a two-dimensional urban canyon:

$$F_{fl-m} = \left((h/w)_{fl}^2 + 1 \right)^{1/2} - (h/w)_{fl}, \quad (\text{B.4})$$

$$F_{fl-wi} = (1 - F_{fl-m})(1 - GR), \quad (\text{B.5})$$

$$F_{fl-win} = (1 - F_{fl-m}) GR, \quad (\text{B.6})$$

$$F_{aux} = \left((h/w)_{fl} + 1 - \left((h/w)_{fl}^2 + 1 \right)^{1/2} \right) / (h/w)_{fl}, \quad (\text{B.7})$$

$$F_{wi-m} = F_{win-m} = F_{aux} (2N_{fl} - 2) / (2N_{fl}), \quad (\text{B.8})$$

$$F_{wi-win} = (1 - F_{aux}) GR, \quad (\text{B.9})$$

$$F_{wi-fl} = F_{win-fl} = F_{aux} / 2N_{fl}, \quad (\text{B.10})$$

$$F_{win-wi} = (1 - F_{aux}) (1 - GR), \quad (\text{B.11})$$

$$F_{m-wi} = F_{wi-m} A_{wi} / A_m, \quad (\text{B.12})$$

$$F_{m-win} = F_{win-m} A_{win} / A_m, \quad (\text{B.13})$$

and

$$F_{m-fl} = F_{fl-m} / A_m, \quad (\text{B.14})$$

where the subscripts fl, m, wi, and win represent floor, internal mass, internal wall, and window, respectively; GR is the glazing ratio of the building; and $(h/w)_{fl}$ represents the aspect ratio of one building level.

B.2 Solar heat transmission

Generally, the solar heat transmitted through windows depends on the angle of incidence of the sun. However, based on simulations with EnergyPlus, it can be shown that the solar transmittance is proportional to the window SHGC for an average-oriented canyon. The Solar Transmittance Factor (STF) is defined as the ratio between the average of the solar transmittances for different window orientations and the SHGC.

A series of simulations was carried out with EnergyPlus for eight different orientations of a window in intervals of 45°. Three characteristic days in Toulouse, the two solstices and an equinox, were simulated for different values of the SHGC. Fig. A1 (top) represents the diurnal cycle of STF for windows with a SHGC=0.8. Fig. A1 (bottom) shows the dependence of the daytime STF on the SHGC. This analysis concludes that a constant STF of 0.75 ± 0.03 can be considered for an average-oriented window with a SHGC between 0.6 and 0.9.

B.3 Natural ventilation

The natural ventilation module first compares indoor and outdoor air temperatures. If $T_{in} > T_{urb} + 1$ K, the module estimates a natural ventilation potential, by calculating the indoor air temperature with and without natural ventilation, T_{open} and T_{close} , respectively.

The conditions are considered favorable for natural ventilation if $T_{open} < T_{cool,target}$, $T_{open} < T_{close}$, and $T_{open} > T_{heat,target} + 4$ K.

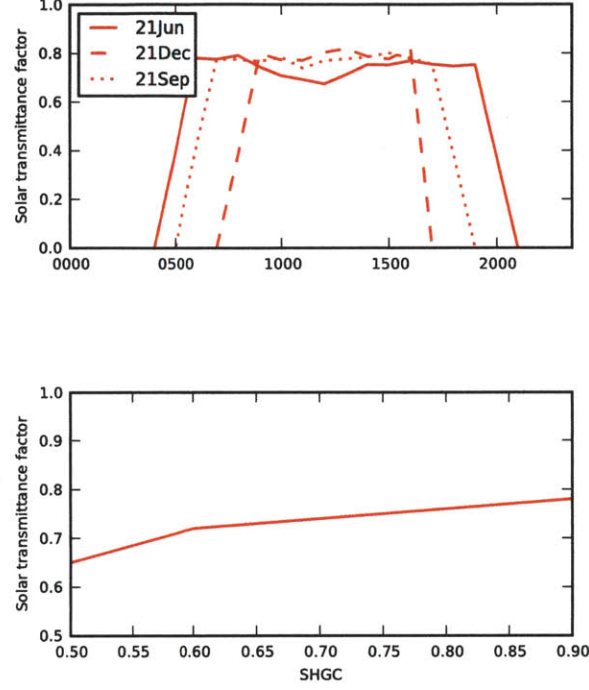


Figure B.1 – Diurnal cycle of the solar transmittance factor of a window with a SHGC=0.8 (top) and daytime-average solar transmittance factor for different SHGC (bottom). The solar transmittance factor is defined as the ratio between the average of the solar transmittances for different window orientations and the SHGC. In the first graph, three characteristic days of the year are represented, the two solstices and an equinox.

The natural ventilation air flowrate per unit width (\dot{V}_{nv}) is calculated from the following equation for a single opening with bidirectional flow [Truong, 2012]:

$$\dot{V}_{nv} = \frac{1}{3} \left[g \frac{T_{in} - T_{urb}}{T_{in}} \right]^{1/2} \left[h_{win} + \frac{T_{in}}{g(T_{in} - T_{urb})} \frac{1}{2} u_{ref}^2 \Delta C_p \right]^{3/2} \quad (B.15)$$

where h_{win} is the window height, ΔC_p is the pressure coefficient difference between the windward and the leeward sides of the building, and u_{ref} is the average air velocity where the pressure coefficients are measured.

B.4 Cooling system

BEM accounts for the dependence of a cooling system on outdoor and indoor conditions, through the definition of characteristic performance curves [DOE, 2010a]. The total cooling capacity is calculated from the rated capacity, modified by the following curve:

$$\varphi_Q = A_1 + B_1 T_{wb,i} + C_1 T_{wb,i}^2 + D_1 T_{c,i} + E_1 T_{c,i}^2 + F_1 T_{wb,i} T_{c,i}, \quad (B.16)$$

where $T_{wb,i}$ (°C) is the wet-bulb temperature of the air entering the cooling coil and $T_{c,i}$ (°C) is the dry-bulb outdoor air temperature for an air-cooled condenser (wet-bulb outdoor air temperature for an evaporative condenser). The actual COP of the system is calculated from the nominal COP, divided by the following curve:

$$\varphi_{COP} = A_2 + B_2 T_{wb,i} + C_2 T_{wb,i}^2 + D_2 T_{c,i} + E_2 T_{c,i}^2 + F_2 T_{wb,i} T_{c,i}. \quad (B.17)$$

The coefficients used in Eqs. B.16 and B.17 are the defaults used by EnergyPlus when a single-speed direct-expansion cooling system is defined: $A_1 = 0.942587793$, $B_1 = 0.009543347$, $C_1 = 0.00068377$, $D_1 = -0.011042676$, $E_1 = 0.000005249$, $F_1 = -0.00000972$, $A_2 = 0.342414409$, $B_2 = 0.034885008$, $C_2 = -0.0006237$, $D_2 = 0.004977216$, $E_2 = 0.000437951$, and $F_2 = -0.000728028$.

The coefficient f_{PLR} of Eq. (3.11) is given by:

$$f_{PLR} = 0.85 + 0.15PLR, \quad (B.18)$$

where PLR is the part-load ratio, calculated as the fraction between the energy supplied and the system capacity.

B.5 Autosize function

The rated cooling capacity is calculated by dynamically simulating the building with predefined diurnal cycles of outdoor air temperature and incoming solar radiation. The diurnal cycle of outdoor air temperature has a maximum defined by the user and an amplitude of 10.7 K. The time evolution is sinusoidal according to the following equation:

$$T_{can} = T_{size,max} - 5.35 + 5.35 \sin(2\pi(t + 57600)/86400). \quad (B.19)$$

The solar radiation at each time step is given by:

$$S^\downarrow = K_{sol} D_{corr} \cos(Z), \quad (B.20)$$

where $K_{sol} = 1367 \text{ W m}^{-2}$, $D_{corr} = 1 + 0.0334 \cos(0.01721 D_{julian} - 0.0552)$, and Z is the solar zenith angle; and where D_{julian} is the Julian day of the year.

Appendix C

Vertical Diffusion Model

The length scale (l_k) used in Eq. 5.7 is determined by solving the following set of equations [Bougeault and Lacarrere, 1989]:

$$\int_z^{z+l_{up}} \beta(\theta(z) - \theta(z')) dz' = E(z), \quad (C.1)$$

$$\int_{z-l_{down}}^z \beta(\theta(z') - \theta(z)) dz' = E(z), \quad (C.2)$$

and

$$l_k = \min(l_{up}, l_{down}), \quad (C.3)$$

where l_{up} and l_{down} are the distances that a parcel originating from level z , and having the turbulent kinetic energy $E(z)$, can travel upward and downward before coming to rest due to buoyancy effects. l_{down} cannot be greater than the height above the ground.

The mixed-layer velocity used in Eq. 5.8 is calculated according to [Hong et al., 2006]:

$$w_s = (u_*^3 + \phi_m C_{vk} w_*^3 z / z_i)^{1/3}, \quad (C.4)$$

where u_* is the friction velocity, $C_{vk} = 0.4$ is the Von-Karman constant, ϕ_m is a wind profile function, w_* is the convective velocity scale, and z_i is the boundary-layer height.

For unstable and neutral conditions ($H_{rur} > 0$), the wind profile function and the convective velocity scale are calculated as:

$$\phi_m = \left(1 - 8 \frac{0.1 z_i}{L}\right)^{-1/3}, \quad (C.5)$$

and

$$w_* = \left(\frac{g}{\theta(z_r)} \frac{H_{rur}}{\rho c_p} z_i\right)^{1/3}. \quad (C.6)$$

For stable conditions, $w_* = 0$ and

$$\phi_m = 1 + 5 \frac{0.1z_i}{L}, \quad (\text{C.7})$$

where L is the Monin-Obukhov length, calculated as:

$$L = \frac{u_*^3 \theta(z_r) \rho c_p}{C_{vk} H_{rur}}. \quad (\text{C.8})$$

The friction velocity, u_* is calculated according to Louis [1979]:

$$u_* = au(z_r) f_m^{1/2}, \quad (\text{C.9})$$

where $a = \frac{C_{vk}}{\log \frac{z_r}{z_0}}$ is a drag coefficient, $u(z_r)$ is calculated from $u(z_m)$ assuming a logarithmic profile, and f_m is a coefficient that accounts for the atmosphere stability and is given by:

$$f_m = \frac{1}{(1 + 4.7Ri)^2}, \quad (\text{C.10})$$

for stable and neutral conditions ($Ri \geq 0$) and

$$f_m = \frac{1 - 9.4Ri}{1 + c(-Ri)^2}, \quad (\text{C.11})$$

for unstable conditions $Ri < 0$. In Eq. C.11, the constant c is given by $c = 69.56a^2 \left(\frac{z_r}{z_0}\right)^{1/2}$, and the Richardson number is calculated as:

$$Ri = \frac{gz_r(\theta(z_r) - \theta_{soil})}{\theta(z_r)u(z_r)^2}. \quad (\text{C.12})$$

The exchange velocity used in the RC model (chapter 4) is given by:

$$u_{ex} = 1.35a^2 f_m u(z_r). \quad (\text{C.13})$$

Appendix D

Urban Weather Generator

D.1 Outdoor radiant heat transfer

The radiant heat transfer coefficients (RHTC) among walls, road, and sky are given by:

$$h_{rd,i-j} = 4(1 - \epsilon_{can})\epsilon_i\epsilon_j\sigma F_{i-j}\overline{T_{i-j}}^3, \quad (D.1)$$

where ϵ_{can} is the urban canyon air emissivity (Eq. D.3), ϵ is the emissivity of the surfaces $i, j = \{ \text{wall, road, sky } (\epsilon_{sky} = 1) \}$; $\sigma = 5.67e^{-8} \text{ W m}^{-2} \text{ K}^{-4}$ is the Stefan-Boltzmann constant; F_{i-j} is the view factor between surfaces i and j ; and $\overline{T_{i-j}}$ is average temperature over surfaces i and j .

The RHTC between walls, road, sky and the urban canyon air are given by:

$$h_{rd,can-j} = 4\epsilon_{can}\epsilon_j\sigma\overline{T_{can-j}}^3. \quad (D.2)$$

The air emissivity (ϵ_{can}) is calculated from the following expression as a function of the humidity content and the size of the space [Siegel and Howell, 1981]:

$$\epsilon_{can} = 0.683 \left(1 - \exp \left(-1.17X^{1/2} \right) \right), \quad (D.3)$$

where $X = P_w L_e \frac{300}{T_{urb}} (P_a + bP_w)$; and where P_w and P_a are the partial pressures of water and air, respectively; L_e is the mean beam length calculated as the ratio between the transversal area of the urban canyon and its perimeter, $L_e = 3.6A_{can}/P_{can}$; and the parameter $b = 5 \left(\frac{300}{T_{urb}} \right)^{1/2}$.

D.2 Solar radiation received by walls and roofs

This formulation has been extracted from Masson [2000] for an average urban canyon orientation. The first bounce of solar radiation is given by the following equations for walls and roof:

$$K_w = K_{dir} \left(\frac{w_r}{h_{bld}} \left(0.5 - \frac{\theta_o}{\pi} \right) + \frac{1}{\pi} \tan(\lambda)(1 - \cos(\theta_o)) \right) + F_w K_{dif}, \quad (D.4)$$

$$K_r = K_{dir} \left(\frac{2\theta_o}{\pi} + \frac{2}{\pi} \frac{h_{bld}}{w_r} \tan(\lambda)(1 - \cos(\theta_o)) \right) + F_r K_{dif}, \quad (D.5)$$

where K_{dir} is the direct solar radiation; K_{dif} is the diffuse solar radiation; h_{bld} is the average building height; w_r is the average road width, $w_r = \frac{2h_{bld}(1-\rho_{bld})}{VH_{urb}}$; ρ_{bld} is the horizontal building density; VH_{urb} is the vertical-to-horizontal urban area ratio; λ is the solar zenith angle; θ_o is the critical canyon orientation for which the road is no longer sunlit, $\theta_o = \arcsin\left(\min\left[\frac{w_r}{h_{bld}} \frac{1}{\tan(\lambda)}, 1\right]\right)$, F_w is the wall sky view factor, $F_w = \frac{1}{2} \left[\frac{h_{bld}}{w_r} + 1 - \left(\left(\frac{h_{bld}}{w_r} \right)^2 + 1 \right)^{1/2} \right] / \frac{h_{bld}}{w_r}$, and F_r is the road sky view factor, $F_r = \left(\left(\frac{h_{bld}}{w_r} \right)^2 + 1 \right)^{1/2} - \frac{h_{bld}}{w_r}$.

Solar reflections are then calculated by:

$$M_w = \frac{R_w + F_w \rho_w R_r}{1 - (1 - 2F_w) \rho_w + (1 - F_r) F_w \rho_r \rho_w}, \quad (D.6)$$

and

$$M_r = \frac{R_r + (1 - F_r) \rho_r (R_w + F_w \rho_w R_r)}{1 - (1 - 2F_w) \rho_w + (1 - F_r) F_w \rho_r \rho_w}, \quad (D.7)$$

where ρ_w and ρ_r are the wall and road surface reflectivities, $R_w = \rho_w K_w$, and $R_r = \rho_r K_r$. Then, the total solar radiation received by walls and road is given by:

$$S_w = K_w + (1 - 2F_w) M_w + F_w M_r, \quad (D.8)$$

and

$$S_r = K_r + (1 - F_r) M_w. \quad (D.9)$$

References

- Adnot, J. (2003). *Energy Efficiency and Certification of Central Air Conditioners (EECCAC)*. ARMINES, Paris, France. 14, 35
- Assimakopoulos, M., G. Mihalakakou, and H. Flocas (2007). Simulating the thermal behaviour of a building during summer period in the urban environment. *Renewable Energy* 32(11), 1805 – 1816. 14
- Bentham, T. and R. Britter (2003). Spatially averaged flow within obstacle arrays. *Atmospheric Environment* 37(15), 2037 – 2043. 18, 94, 95
- Bougeault, P. and P. Lacarrere (1989). Parameterization of orography-induced turbulence in a mesobeta-scale model. *Monthly Weather Review* 117, 1872–1890. 81, 82, 121
- Bravo, M., T. Mira, M. Soler, and J. Cuxart (2008). Intercomparison and evaluation of mm5 and meso-nh mesoscale models in the stable boundary layer. *Boundary-Layer Meteorology* 128, 77–101. 81
- Bueno, B., J. Hidalgo, G. Pigeon, and L. Norford (2012). Air temperatures above the urban canopy layer from measurements at a rural operational weather station. *Journal of Applied Meteorology and Climatology*. Accepted with minor revisions. 18
- Bueno, B., L. Norford, J. Hidalgo, and G. Pigeon (2012). The urban weather generator. *Journal of Building Performance Simulation*. Submitted. 18
- Bueno, B., L. Norford, G. Pigeon, and R. Britter (2011). Combining a detailed building energy model with a physically-based urban canopy model. *Boundary-Layer Meteorology* 140, 471–489. 18
- Bueno, B., L. Norford, G. Pigeon, and R. Britter (2012). A resistance-capacitance network model for the analysis of the interactions between the energy performance of buildings and the urban climate. *Building and Environment* 54, 116–125. 18
- Bueno, B., G. Pigeon, L. K. Norford, K. Zibouche, and C. Marchadier (2012). Development and evaluation of a building energy model integrated in the teb scheme. *Geoscientific Model Development* 5(2), 433–448. 18
- CNRM-GAME (2010). Muscade project. <http://www.cnrm.meteo.fr/ville.climat/spip.php?rubrique49>. 15, 19, 41, 109
- Crawley, D. B. (2008). Estimating the impacts of climate change and urbanization on building performance. *Journal of Building Performance Simulation* 1(2), 91–115. 15

REFERENCES

- Crawley, D. B., L. K. Lawrie, F. C. Winkelmann, W. F. Buhl, Y. J. Huang, C. O. Pedersen, R. K. Strand, R. J. Liesen, D. E. Fisher, M. J. Witte, and J. Glazer (2001). Energyplus: creating a new-generation building energy simulation program. *Energy and Buildings* 33(4), 319 – 331. 15, 18, 23, 24
- Cuxart, J., P. Bougeault, and J.-L. Redelsperger (2000). A turbulence scheme allowing for mesoscale and large-eddy simulations. *Quarterly Journal of the Royal Meteorological Society* 126, 1–30. 82
- DOE (2010a). *EnergyPlus Engineering Reference*. EnergyPlus. 24, 27, 35, 44, 47, 117, 119
- DOE (2010b). *EnergyPlus testing with building thermal envelope and fabric load tests from ANSI/ASHRAE Standard 140-2007*. GardAnalytics, Arlington HeightsGardAnalytics, Arlington Heights. 24
- DOE (2010c). *EnergyPlus testing with IEA BESTEST mechanical equipment & control strategies for a chilled water and a hot water system*. GardAnalytics, Arlington Heights. 24
- Erell, E. and T. Williamson (2006). Simulating air temperature in an urban street canyon in all weather conditions using measured data at a reference meteorological station. *International Journal of Climatology* 26(12), 1671–1694. 15
- Erell, E. and T. Williamson (2007). Intra-urban differences in canopy layer air temperature at a mid-latitude city. *International Journal of Climatology* 27(9), 1243–1255. 14
- Grimmond, C. S. B., M. Blackett, M. J. Best, J.-J. Baik, S. E. Belcher, J. Beringer, S. I. Bohnenstengel, I. Calmet, F. Chen, A. Coutts, A. Dandou, K. Fortuniak, M. L. Gouvea, R. Hamdi, M. Hendry, M. Kanda, T. Kawai, Y. Kawamoto, H. Kondo, E. S. Krayenhoff, S.-H. Lee, T. Loridan, A. Martilli, V. Masson, S. Miao, K. Oleson, R. Ooka, G. Pigeon, A. Porson, Y.-H. Ryu, F. Salamanca, G. Steeneveld, M. Tombrou, J. A. Voogt, D. T. Young, and N. Zhang (2011). Initial results from phase 2 of the international urban energy balance model comparison. *International Journal of Climatology* 31(2), 244–272. 52
- Grimmond, C. S. B. and T. R. Oke (2002). Turbulent heat fluxes in urban areas: Observations and a local-scale urban meteorological parameterization scheme (lumps). *Journal of Applied Meteorology* 41(7), 792–810. 15
- Hamdi, R. and V. Masson (2008). Inclusion of a drag approach in the town energy balance (teb) scheme: Offline 1d evaluation in a street canyon. *Journal of Applied Meteorology and Climatology* 47(10), 2627–2644. 16, 24, 42, 96, 110
- Hamilton, I. G., M. Davies, P. Steadman, A. Stone, I. Ridley, and S. Evans (2009). The significance of the anthropogenic heat emissions of london’s buildings: A comparison against captured shortwave solar radiation. *Building and Environment* 44(4), 807 – 817. 37
- Hicks, B. B., W. J. Callahan, and M. A. Hoekzema (2010). On the heat islands of washington, dc, and new york city, ny. *Boundary-Layer Meteorology* 135(2), 291–300. 13
- Hidalgo, J., V. Masson, and L. Gimeno (2009). Scaling the daytime urban heat island and urban-breeze circulation. *Journal of Applied Meteorology and Climatology* 49(5), 889–901. 17, 78, 79

- Hidalgo, J., V. Masson, and G. Pigeon (2008). Urban-breeze circulation during the capitoul experiment: numerical simulations. *Meteorology and Atmospheric Physics* 102, 243–262. 81
- Hidalgo, J., G. Pigeon, and V. Masson (2008). Urban-breeze circulation during the capitoul experiment: observational data analysis approach. *Meteorology and Atmospheric Physics* 102, 223–241. 79
- Hong, S.-Y., Y. Noh, and J. Dudhia (2006). A new vertical diffusion package with an explicit treatment of entrainment processes. *Monthly Weather Review* 134(9), 2318–2341. 81, 121
- Houet, T. and G. Pigeon (2011). Mapping urban climate zones and quantifying climate behaviors - an application on toulouse urban area (france). *Environmental Pollution* 159, 2180 – 2192. 13
- Ihara, T., Y. Kikegawa, K. Asahi, Y. Genchi, and H. Kondo (2008). Changes in year-round air temperature and annual energy consumption in office building areas by urban heat-island countermeasures and energy-saving measures. *Applied Energy* 85(1), 12 – 25. 16, 24
- Kavgic, M., A. Mavrogianni, D. Mumovic, A. Summerfield, Z. Stevanovic, and M. Djurovic-Petrovic (2010). A review of bottom-up building stock models for energy consumption in the residential sector. *Building and Environment* 45(7), 1683 – 1697. 15
- Kikegawa, Y., Y. Genchi, H. Kondo, and K. Hanaki (2006). Impacts of city-block-scale countermeasures against urban heat-island phenomena upon a building's energy-consumption for air-conditioning. *Applied Energy* 83(6), 649 – 668. 16
- Kikegawa, Y., Y. Genchi, H. Yoshikado, and H. Kondo (2003). Development of a numerical simulation system toward comprehensive assessments of urban warming countermeasures including their impacts upon the urban buildings' energy-demands. *Applied Energy* 76(4), 449 – 466. 16, 19, 24, 37, 41, 107
- Kondo, H. and Y. Kikegawa (2003). Temperature variation in the urban canopy with anthropogenic energy use. *Pure and Applied Geophysics* 160, 317–324. 16
- Kusaka, H., H. Kondo, Y. Kikegawa, and F. Kimura (2001). A simple single-layer urban canopy model for atmospheric models: Comparison with multi-layer and slab models. *Boundary-Layer Meteorology* 101, 329–358. 107
- Kuttler, W. (2008). The urban climate - basic and applied aspects. *Urban Ecology*, 233–248. 14
- Lafore, J. P., J. Stein, N. Asencio, P. Bougeault, V. Ducrocq, J. Duron, C. Fischer, P. Hérel, P. Mascart, V. Masson, J. P. Pinty, J. L. Redelsperger, E. Richard, and J. Vilà-Guerau de Arellano (1998). The meso-nh atmospheric simulation system. part i: adiabatic formulation and control simulations. *Annales Geophysicae* 16(1), 90–109. 18, 77
- Lee, S.-H. and J.-J. Baik (2010). Statistical and dynamical characteristics of the urban heat island intensity in seoul. *Theoretical and Applied Climatology* 100, 227–237. 13
- Lemonsu, A., C. S. B. Grimmond, and V. Masson (2004). Modeling the surface energy balance of the core of an old mediterranean city: Marseille. *Journal of Applied Meteorology* 43(2), 312–327. 16, 23
- Louis, J.-F. (1979). A parametric model of vertical eddy fluxes in the atmosphere. *Boundary-Layer Meteorology* 17, 187–202. 61, 122

REFERENCES

- Lu, J., S. P. Arya, W. H. Snyder, and R. E. Lawson (1997). A laboratory study of the urban heat island in a calm and stably stratified environment. part i: Temperature field. *Journal of Applied Meteorology* 36(10), 1377–1391. 17, 80
- Mackey, C. W., X. Lee, and R. B. Smith (2012). Remotely sensing the cooling effects of city scale efforts to reduce urban heat island. *Building and Environment* 49(0), 348 – 358. 14
- Martilli, A., A. Clappier, and M. W. Rotach (2002). An urban surface exchange parameterisation for mesoscale models. *Boundary-Layer Meteorology* 104, 261–304. 24, 81, 107
- Martin, E., P. Le Moigne, V. Masson, A. Boone, A. Bogatchev, A. Brut, F. Bouyssel, J.-C. Calvet, J.-L. Champeaux, K. Chancibault, B. Decharme, S. Donier, H. Douville, A. Dziedzic, D. Giard, S. Faroux, C. Fischer, A.-L. Gibelin, F. Habets, G. Hello, L. Jarlan, M. Jidane, L. Kraljevic, L. Kullmann, C. Lac, P. Lacarrère, C. Lebeaupin, J.-M. Mahfouf, S. Malardel, I. Mallet, P. Marquet, V. Masson, M. Mokthari, J. Payart, J. Noilhan, P. Quintana-Seguí, Y. Seity, P. Tulet, B. Vincendon, R. Zaaboul, and I. Zuurendonk (2007). Le code de surface externalisé surfex de météoFrance. *Atelier de modélisation de l’atmosphère*, 16–18. 109
- Masson, V. (2000). A physically-based scheme for the urban energy budget in atmospheric models. *Boundary-Layer Meteorology* 94, 357–397. 16, 18, 23, 26, 27, 41, 107, 117, 123
- Masson, V., L. Gomes, G. Pigeon, C. Lioussé, V. Pont, J.-P. Lagouarde, J. Voogt, J. Salmond, T. R. Oke, J. Hidalgo, D. Legain, O. Garrouste, C. Lac, O. Connan, X. Briottet, S. Lachéradé, and P. Tulet (2008). The canopy and aerosol particles interactions in toulouse urban layer (capitoul) experiment. *Meteorology and Atmospheric Physics* 102, 135–157. 18, 23, 28, 41, 63, 78, 86, 96
- Masson, V. and C. Grimmond (2002). Evaluation of the town energy balance (teb) scheme with direct measurements from dry districts in two cities. *Journal of Applied Meteorology* 41(10), 1011–1026. 16, 23, 28
- Masson, V. and Y. Seity (2009). Including atmospheric layers in vegetation and urban offline surface schemes. *Journal of Applied Meteorology and Climatology* 48(7), 1377–1397. 17
- Memon, R., D. Leung, C.-H. Liu, and M. Leung (2011). Urban heat island and its effect on the cooling and heating demands in urban and suburban areas of hong kong. *Theoretical and Applied Climatology* 103, 441–450. 14
- Mirzaei, P. A. and F. Haghighat (2010). Approaches to study urban heat island - abilities and limitations. *Building and Environment* 45(10), 2192 – 2201. 17
- Noilhan, J. and J.-F. Mahfouf (1996). The isba land surface parameterisation scheme. *Global and Planetary Change* 13, 145 – 159. 93
- Offerle, B., C. S. B. Grimmond, and K. Fortuniak (2005). Heat storage and anthropogenic heat flux in relation to the energy balance of a central european city centre. *International Journal of Climatology* 25(10), 1405–1419. 23
- Ohashi, Y., Y. Genchi, H. Kondo, Y. Kikegawa, H. Yoshikado, and Y. Hirano (2007). Influence of air-conditioning waste heat on air temperature in tokyo during summer: numerical experiments using

- an urban canopy model coupled with a building energy model. *Journal of Applied Meteorology and Climatology* 46, 66–81. 37
- Oke, T. (1987). *Boundary layer climates*. University Paperbacks. Methuen. 13, 78
- Oke, T. (2004). Urban observations, instruments and methods of observation programme, iom report. World Meteorological Organization, Geneva, in press. 28
- Oxizidis, S., A. Dudek, and A. Papadopoulos (2008). A computational method to assess the impact of urban climate on buildings using modeled climatic data. *Energy and Buildings* 40(3), 215 – 223. 15
- Palyvos, J. (2008). A survey of wind convection coefficient correlations for building envelope energy systems' modeling. *Applied Thermal Engineering* 28(8-9), 801 – 808. 27, 95
- Pigeon, G., D. Legain, P. Durand, and V. Masson (2007). Anthropogenic heat release in an old european agglomeration (toulouse, france). *International Journal of Climatology* 27(14), 1969–1981. 29, 31, 34
- Pigeon, G., M. A. Moscicki, J. A. Voogt, and V. Masson (2008). Simulation of fall and winter surface energy balance over a dense urban area using the teb scheme. *Meteorology and Atmospheric Physics* 102, 159–171. 16, 23, 24, 29, 30
- P.R.B. (2011). World population data sheet. <http://www.prb.org>. 13
- Rhodes, J. D., B. Stephens, and M. E. Webber (2011). Using energy audits to investigate the impacts of common air-conditioning design and installation issues on peak power demand and energy consumption in austin, texas. *Energy and Buildings* 43(11), 3271 – 3278. 14
- Rotach, M. W., R. Vogt, C. Bernhofer, E. Batchvarova, A. Christen, A. Clappier, B. Feddersen, S.-E. Gryning, G. Martucci, H. Mayer, V. Mitev, T. R. Oke, E. Parlow, H. Richner, M. Roth, Y.-A. Roulet, D. Ruffieux, J. A. Salmond, M. Schatzmann, and J. A. Voogt (2005). Bubble an urban boundary layer meteorology project. *Theoretical and Applied Climatology* 81, 231–261. 13, 18, 78, 86, 96
- Roth, M. (2007). Review of urban climate research in (sub)tropical regions. *International Journal of Climatology* 27(14), 1859–1873. 13, 93
- Sailor, D. J. (2011). A review of methods for estimating anthropogenic heat and moisture emissions in the urban environment. *International Journal of Climatology* 31(2), 189–199. 14
- Salamanca, F., A. Krpo, A. Martilli, and A. Clappier (2010). A new building energy model coupled with an urban canopy parameterization for urban climate simulations - part i. formulation, verification, and sensitivity analysis of the model. *Theoretical and Applied Climatology* 99, 331–344. 16, 19, 24, 41, 107
- Salamanca, F. and A. Martilli (2010). A new building energy model coupled with an urban canopy parameterization for urban climate simulations - part ii. validation with one dimension off-line simulations. *Theoretical and Applied Climatology* 99, 345–356. 16, 24, 35
- Santamouris, M., N. Papanikolaou, I. Livada, I. Koronakis, C. Georgakis, A. Argiriou, and D. Assimakopoulos (2001). On the impact of urban climate on the energy consumption of buildings. *Solar Energy* 70(3), 201 – 216. 14

REFERENCES

- Santiago, J. and A. Martilli (2010). A dynamic urban canopy parameterization for mesoscale models based on computational fluid dynamics reynolds-averaged navier-stokes microscale simulations. *Boundary-Layer Meteorology* 137, 417–439. 17
- Shashua-Bar, L. and M. E. Hoffman (2002). The green ctic model for predicting the air temperature in small urban wooded sites. *Building and Environment* 37(12), 1279 – 1288. 93, 95
- Siegel, R. and J. Howell (1981). *Thermal radiation heat transfer*. Series in thermal and fluids engineering. Hemisphere Publishing Corporation. 94, 123
- Stull, R. (1988). *An introduction to boundary layer meteorology*. Atmospheric sciences library. Kluwer Academic Publishers. 78
- Swaid, H. and M. E. Hoffman (1990). Prediction of urban air temperature variations using the analytical ctic model. *Energy and Buildings* 14(4), 313 – 324. 15
- Swan, L. G. and V. I. Ugursal (2009). Modeling of end-use energy consumption in the residential sector: A review of modeling techniques. *Renewable and Sustainable Energy Reviews* 13(8), 1819 – 1835. 15
- Synnefa, A., M. Laskari, A. Sakka, M. Saliari, and K. Giannopoulou (2011). Athens case study in situ measurements. Work document. Project BRIDGE D.3.4 Annex 2. 56
- Synnefa, A., M. Stathopoulou, A. Sakka, K. Katsiabani, M. Santamouris, N. Adaktylou, C. Cartalis, and N. Chrysoulakis (2010). Integrating sustainability aspects in urban planning: the case of athens. *International Conference on Passive and Low Energy Cooling for the Built Environment (PALENC 2010) ; 5th European Conference on Energy Performance; Indoor Climate in Buildings (EPIC 2010); 1st Cool Roofs Conference, Rhodes Island, Greece*. 18, 41, 56
- Truong, P. (2012). *Recommendations for the Analysis and Design of Naturally Ventilated Buildings in Urban Areas*, M.S. Massachusetts Institute of Technology, Cambridge MA, USA. 119
- Zhou, Y. and J. Shepherd (2010). Atlanta’s urban heat island under extreme heat conditions and potential mitigation strategies. *Natural Hazards* 52, 639–668. 13